UNIVERSITÀ
DEGLI STUDI
DI PADOVA

Sede Amministrativa: Università degli Studi di Padova
Dipartimento di Innovazione Meccanica e Gestionale

SCUOLA DI DOTTORATO DI RICERCA IN INGEGNERIA INDUSTRIALE
INDIRIZZO: INGEGNERIA DELLA PRODUZIONE INDUSTRIALE
CICLO XXIV

MOULD THERMAL CONTROL FOR PRODUCTION OF WELDLINE-FREE AND HIGH-GLOSS PARTS

Direttore della Scuola: Ch.mo Prof. Paolo Francesco Bariani
Coordinatore d'indirizzo: Ch.mo Prof. Enrico Savio
Supervisore: Ch.mo Prof. Paolo Francesco Bariani
Correlatore: Ing. Giovanni Lucchetta

Dottorando: Marco Fiorotto

UNIVERSITÀ
DEGLI STUDI
DI PADOVA

Sede Amministrativa: Università degli Studi di Padova
Dipartimento di Innovazione Meccanica e Gestionale

SCUOLA DI DOTTORATO DI RICERCA IN INGEGNERIA INDUSTRIALE
INDIRIZZO: INGEGNERIA DELLA PRODUZIONE INDUSTRIALE
CICLO XXIV

MOULD THERMAL CONTROL FOR PRODUCTION OF WELDLINE-FREE AND HIGH-GLOSS PARTS

Direttore della Scuola: Ch.mo Prof. Paolo Francesco Bariani
Coordinatore d'indirizzo: Ch.mo Prof. Enrico Savio
Supervisore: Ch.mo Prof. Paolo Francesco Bariani
Correlatore: Ing. Giovanni Lucchetta

Dottorando: Marco Fiorotto

A Amy

ABSTRACT

In recent years, the requirement for a much thinner, lighter and better mechanical performing product is more and more important for the company. Such development tendency causes great challenges for conventional injection moulding process (CIM) in mould design, polymeric materials and moulding process. These challenges are mainly caused by the cool cavity surface which freezes the polymer melt prematurely during filling stage. The resulting frozen layer has a number of adverse effects on the surface qualities and mechanical performances of plastic parts. A new rapid heat cycle moulding (RHCM) process has been developed to overcome the limits of the conventional injection moulding process. In this novel technique the cavity surface is heated to a temperature close to the glass transition temperature before melt injection. The elevated mould temperature allows to produce perfectly smooth, thin-walled, complex shaped, and micro structured plastic products with low molecular orientation and residual stress. In order to dynamically control the mould cavity temperature according to the RHCM process requirement, a special auxiliary system is required. Development of capable techniques for rapidly heating and cooling a mould with a relatively large mass is technically challenging because of the constraints set by the heat transfer process and the endurance limits set by the material properties. Most of available heat generation technologies allow to heat the mould efficiently, but still have a lot of shortcomings to be applied in mass production. In spite of its industrial relevance, there are several aspects of this novel process that need to be understood completely.

In this Ph.D. dissertation, an innovative heating and cooling system based on the use of metallic foams has been developed by means of both a numerical and an experimental approach. An open-cell metal foam is a kind of porous medium that is emerging as an effective method of heat transfer enhancement, due to its large surface area to volume ratio and high thermal conductivity. Instead of conventional channels, the entire space

below the cavity can be used for heating and/or cooling, while the metallic foam allows an efficient through flow of water. The metallic foam provides mechanical support and simultaneously generates a cavity structure.

The aims of this Ph.D. dissertation consist on developing a new heating/cooling system to overcome the limitations of the available technologies and increasing the scientific knowledge about the RHCM process. Several aspects of this new manufacturing process have been studied.

(i) The feasibility of using aluminum foams in the heating and cooling system of injection moulds has been evaluated. A prototype mould for double gated tensile specimens was designed.

(ii) The finite element method (FEM) was used to analyze the structural deflection of the metallic foam and cavity surface at elevated temperature. A 3D computational fluid dynamic (CFD) simulation was performed to evaluate the thermal behaviour of the mould during the heating and cooling phases.

(iii) The mould was manufactured and a test production was carried out. The accuracy of the numerical approach has been verified, comparing the numerical results with experimental data.

(iv) The performances of the new RHCM system based on the use of metal foams were compared with the ones of a ball filled mould by means of experimental results. A cover plate for aesthetical applications was used as test case.

(v) The effect of fast variation of the mould temperature on the surface appearance of plastic parts, micro structured surfaces replication and weld line strength has been experimentally investigated.

(vi) The weld line developing process in micro injection moulding have been investigated. The influence of the main injection moulding process parameters on the mechanical properties and surface finish in the weld line zone was experimentally studied according to the Design of Experiments method. A visualization unit was integrated in the tool in order to observe the development of a micro scale weld line.

The work presented in this thesis was carried out mainly at the Te.Si. Laboratory, University of Padua, Italy, from January 2009 to December 2011, under the supervision of prof. Paolo Bariani and of Ing. Giovanni Lucchetta. Part of the research activity was performed at the Centre for Polymer Micro and Nano Technology, University of Bradford, Bradford, UK.

SOMMARIO

La richiesta di prodotti più leggeri, sottili e dotati di elevate proprietà meccaniche sta diventando un'esigenza sempre più importante negli ultimi anni in ambito industriale. Questa nuova tendenza sta imponendo nuove sfide nel processo di stampaggio a iniezione tradizionale e, in particolare, nuovi cambiamenti nella progettazione degli stampi, nella scelta dei materiali polimerici e nell'esecuzione del processo. La necessità di cercare nuove soluzioni tecniche è principalmente dovuta all'elevata differenza di temperatura tra il polimero fuso e la superficie fredda della cavità durante la fase di riempimento. Lo strato di materiale solidificato influenza negativamente le proprietà estetiche e meccaniche delle parti plastiche. Per superare i limiti che si riscontrano nel processo di stampaggio tradizionale è stata sviluppata una nuova tecnologia di stampaggio a iniezione con variazione rapida della temperatura dello stampo. L'innovativa tecnologia prevede il riscaldamento della superficie della cavità dello stampo fino ad una temperatura prossima alla temperatura di transizione vetrosa prima dalla fase di iniezione del materiale plastificato. L'elevata temperatura dello stampo consente di ottenere delle parti in materiale plastico caratterizzate da forme complesse, superfici perfettamente lisce, spessori sottili, superfici micro strutturate, ridotte orientazioni molecolari e tensioni residue. Tuttavia è necessario utilizzare un sofisticato sistema ausiliario per il controllo dinamico della temperatura della cavità dello stampo. Lo sviluppo di sistemi in grado di riscaldare e raffreddare rapidamente uno stampo dotato di massa relativamente elevata presenta degli aspetti critici legati ai vincoli imposti dallo scambio termico e ai limiti di resistenza imposti dai materiali impiegati. La maggior parte delle tecnologie attualmente disponibili per generare calore consentono di riscaldare efficientemente lo stampo, ma presentano molte carenze che ne limitano l'impiego in applicazioni per produzioni di

massa. A dispetto della sua rilevanza industriale, ci sono diversi aspetti di questo processo produttivo che necessitano di essere compresi completamente.

In questo lavoro di tesi, è stato sviluppato un innovativo sistema di riscaldamento e raffreddamento rapido basato sull'impiego di schiume metalliche, seguendo un approccio sia numerico che sperimentale. Le schiume metalliche a celle aperte sono una nuova tipologia di mezzi porosi che si sta imponendo come un'effettiva soluzione da impiegare per incrementare lo scambio termico, grazie all'alto rapporto tra superficie e volume del materiale e l'elevata conducibilità termica. Rispetto ai canali di raffreddamento tradizionali, l'intero spazio sotto la cavità può essere impiegato per riscaldare e/o raffreddare, mentre la schiuma consente il passaggio del flusso di acqua di condizionamento al suo interno. La schiuma metallica fornisce il necessario supporto meccanico, generando contemporaneamente una cavità strutturata.

Gli scopi della presente tesi di dottorato consistono nello sviluppare un nuovo sistema di condizionamento dello stampo che consenta di superare i limiti delle attuali tecnologie e nell'approfondire la conoscenza scientifica del processo di stampaggio a iniezione con variazione ciclica della temperatura. Sono stati studiati diversi aspetti di questo nuovo processo produttivo.

(i) È stata esplorata la possibilità di applicare inserti in schiuma metallica nel sistema di condizionamento dello stampo. A tale scopo è stato progettato un nuovo prototipo di stampo per provini per prove di trazione dotati di due punti di iniezione.

(ii) Attraverso il metodo agli elementi finiti è stata analizzata la deflessione in corrispondenza della schiuma metallica e della superficie della cavità ad elevata temperatura. È stata eseguita una simulazione fluidodinamica per valutare l'evoluzione della temperatura dello stampo durante le fasi di riscaldamento e raffreddamento.

(iii) Dopo aver realizzato lo stampo è stato condotto un test di produzione. L'accuratezza della strategia di progettazione basata sull'impiego di simulazioni numeriche è stata verificata confrontando i risultati numerici con i dati sperimentali.

(iv) Le prestazioni sperimentali del nuovo sistema per la variazione rapida della temperatura dello stampo basato sull'impiego di inserti in schiuma metallica sono state confrontate con quelle di un sistema a letto di sfere. Una piastra per applicazioni estetiche è stata scelta come caso di prova.

(v) È stato studiato l'effetto della variazione rapida della temperatura dello stampo sulle proprietà estetiche delle parti stampate, la replicazione di superfici micro strutturate e la resistenza in corrispondenza della linea di giunzione.

(vi) Sono state analizzate le fasi di sviluppo della linea di giunzione nel processo di micro stampaggio a iniezione. Attraverso la metodologia del Design of Experiments (DOE) si è indagata sperimentalmente l'influenza dei parametri di processo sulle proprietà meccaniche in corrispondenza della linea di giunzione. Un sistema di visualizzazione è stato integrato nello stampo per consentire l'osservazione del processo di sviluppo di una linea di giunzione su scala micro.

Il lavoro presentato in questa tesi è stato svolto principalmente presso il laboratorio Te.Si. dell'Università di Padova, Italia, nel periodo compreso tra i mesi di gennaio 2009 e dicembre 2011, sotto la supervisione del prof. Paolo Bariani e dell'ing. Giovanni Lucchetta. Parte dell'attività di ricerca è stata condotta presso il Centre for Polymer Micro and Nano Technology (University of Bradford), Gran Bretagna.

PREFACE

This thesis is based on a research work carried out at the DIMEG Labs, University of Padova, Italy, from January 2009 until December 2011. Especially, I want to say thanks to Prof. Giovanni Lucchetta, as my doctoral supervisor, his priceless guidance, encouragement, and support throughout this work help me finally reach the goal. His constructive suggestion and careful correction are quite helpful for me to improve the dissertation finally to be able to be published.

I am also really appreciated for the invaluable helps and supports from all the scientific and technical coworkers at DIMEG. I am feeling so lucky that I have such a chance to be able to work together with wonderful persons. In particular, I gratefully acknowledge Anna, Paolo, Manuel, Matteo, Francesco, Stefano, Emil, Gianluca, Daniele, Pier Tommaso, Alessandro and Riccardo.

Last but not least, I express my deep sincere gratitude to Amy. This thesis has become a reality with her unique support and love. But this work would not have been achieved without the support and understanding of my family. I am as ever indebted to my parents for their love and support throughout my life.

TABLE OF CONTENTS

CHAPTER 1
INTRODUCTION

Recent demands in injection moulding for thin products with high-grade in appearance and quality reveal technical problems which have been lying unsolved for a long time. The standard injection moulding process with constant mould temperature control suffers from problems caused by the large temperature difference between the mould and the incoming polymer. The usage of rapid heat cycle moulding (RHCM) has gained increasing attention in improving the surface quality of moulded plastic products. In RHCM, the mould cavity surface is required to be heated to a high temperature before melt injection, usually above the glass transition temperature (T_g), then the high temperature is kept in the filling process, and finally the mould is rapidly cooled down to solidify the shaped resin melt in the post filling process for demoulding. A large number of innovative approaches for rapidly heating the surface portion or the entire mould have been developed in recent years. These innovative methods heat the mould efficiently, but still have a lot of shortcomings to be applied in mass production. In spite of its industrial relevance, there are several aspects of this novel process that need to be understood completely.

In this Ph.D. thesis, an innovative heating and cooling system based on the use of metallic foams to increase the efficiency of the conventional RHCM technique has been developed. An in-depth investigation on this new manufacturing process has been carried out by means of both numerical simulations and experimental tests.

1.1 The industrial problem

In recent years, with the development of 3Cs (computer, communication, and consumer electronic) industries, the requirements for performance of the plastic products, such as LCD TV panel, and auto center consoles, have become higher, including high mechanical strength, close dimensional tolerances, high shape accuracy, low residual stress, good appearance and excellent surface texture (Figure 1.1).

Figure 1.1 – Auto centre console with high gloss surface.

In order to facilitate the flow of the polymer melt and improve the replicability of the moulded product, it is better to maintain a high temperature during filling and packing phases. However, an increase in mould temperature results in a great increase in cooling time to solidify the molten polymer inside the mould. In order to meet these high requirements on performance, a rapid heat cycle moulding (RHCM) technology has been developed. RHCM offers many advantages over standard injection moulding:

- Better flow and flow length extension.
- Superior surface finish, giving high gloss parts and reducing coating costs.
- Reduced defects as jetting, flow marks, weld lines, etc. (Figure 1.2).
- Better recycling (if no coating has been applied).
- Deformations eliminated (warping, bending) by reducing stresses.
- Reduction in moulding pressures allowing for lower clamp tonnage.

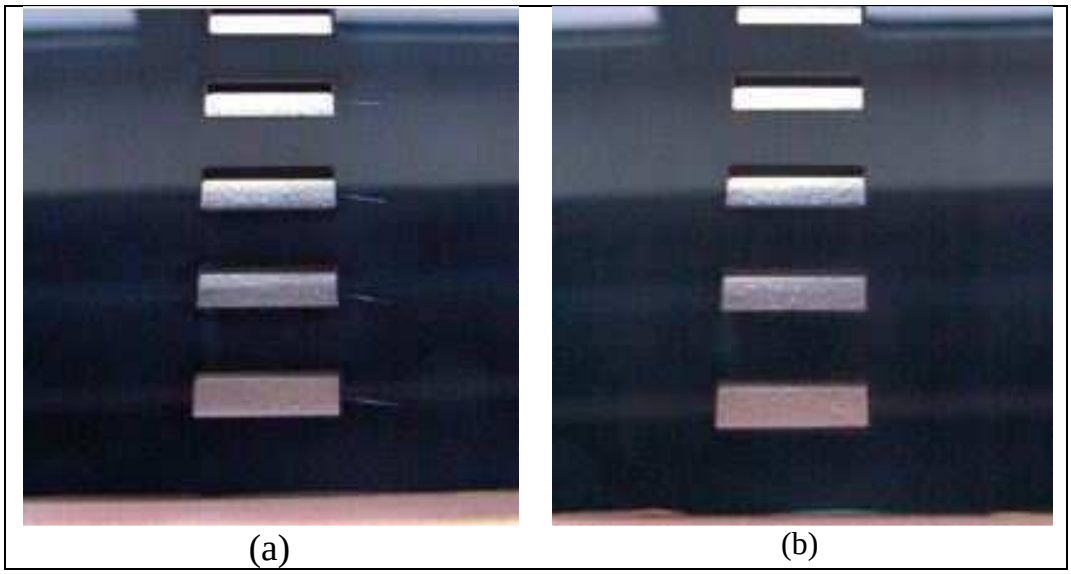

Figure 1.2 - Comparison of frames produced with (a) CIM and (b) RHCM.

However, maintaining high mould temperatures during the filling process while lowering the mould temperature to below deflection temperature during the postfilling process without a great increase in cycle time and energy consumption is complicated. In recent years, a number of innovative approaches for rapidly heating the surface of the mould have been developed, including methods such as resistive heating of a thin conductive layer, induction heating, high-frequency proximity heating, infrared heating, heating and cooling using a volume-controlled variable conductance heat pipe, heating and cooling using thermoelectric Peltier modules, passive heating by the incoming polymer, microwave heating, contact heating, convective heating using hot fluid or condensing vapour forced to flow through conformal channels or bearing ball filled niches, etc. Moreover the mould should have a low thermal mass and exhibit a low inertia to variation of thermal loads. Multilayer mould consisting of insulation layers with a resistance layer can efficiently shorten the moulding cycle time.

The aforementioned methods do heat the mould efficiently, but still have a lot of shortcomings to be applied in mass production. The drawback of the induction heating method is that the design of the induction coil is difficult for achieving a uniform cavity surface heating, especially for the parts with complex shapes. The mould structure using high-frequency proximity heating is very complex and needs to be carefully designed. The strength of the mould structure is relatively low due to the air pockets under the

cavity/core surfaces. Steam-assisted RHCM technique requires an external boiler to generate steam, which will increase the input and production costs, especially for small-scale users. The safety issue related to transmission of the high pressure steam in the workshop should be well considered and this will also increase the production cost. The ball filled mould technology can be applied only for parts with plane geometry. For the RHCM technique with multilayer mould, the low strength of the coating layers and the difficulty in coating the moulds with large and geometry-complicated cavity surfaces restricted its application in mass production.

In order to increase the process efficiency and to improve the quality of the final products, companies in the injection moulding industry are looking for other innovative RHCM technologies. Due to the higher precision and quality requirements of the new plastic parts produced with RHCM process than the ones produced with CIM, the development theory of the moulding problems, like reduced strength weld line, non uniform shrinkage, incomplete filling of micro structured surfaces etc., are needed to be understood completely. The effect of RHCM process parameters on surface finish and mechanical properties of plastic parts is also the subject of the present work.

1.2 The aim of the work

The present work comes from a project of the Department of Innovation in Mechanics and Management (DIMEG), at University of Padova. Part of this research work has been performed within a collaborative research activity program carried out between the DIMEG and the Centre for Polymer Micro and Nano Technology, University of Bradford (UK).

The final objective of this scientific project consists in developing an innovative rapid thermal cycling system, based on the use of open-cell aluminum foam, to increase part quality and process efficiency. Metal foams are low density, high strength porous media, which possesses such prominent features as light weight and high strength for structural applications and high convection coefficients with high area to volume ratios for heat transfer. Metallic foams can be integrated in the mould for a wide range of moulded parts to ensures extremely fast and energy-efficient heating and cooling processes.

The present work aims to developing a set of integrated tools that are able to provide designers of heating/cooling systems with a more in-depth scientific knowledge about the RHCM process. Several aspects of this novel technology need to be understood completely. In order to achieve this goal, the effect of RHCM on surface finish and mechanical properties for macro and micro moulded parts have been investigated. To fulfil this task the following goals have been outlined:

- Design and set-up of a novel injection mould, based on the use of metal foams, for the RCHM process.
- Development of a numerical environment to simulate the temperature evolution and the mechanical behaviour of the mould parts, approximating industrial operating conditions as closely as possible.
- Evaluation of the effect of fast variations of the mould temperature on the improvement of micro features replication and mouldings appearance.
- Evaluation of the effect of RHCM on mechanical properties in the weld line zone of tensile specimens.
- Design and set-up of a mould with an integrated visualization unit to observe the development of a micro scale weld line.
- Evaluation of the influence of the main injection moulding process parameters on the surface roughness and mechanical strength of micro tensile specimens produced with RHCM.

1.3 The organization of the work

The work is organized in ten chapters. Chapter 1 gives a general introduction to limits of traditional RHCM processes for production of weld line-free and high-gloss parts. In this chapter a new heating and cooling system, based on the use of open-cell aluminum foam, is then presented. The scientific relevance of the present work i explained.

Chapter 2 gives an overview of the state of the art in mould rapid heating and cooling, with the goal of explaining the working mechanisms and providing unbiased accounts of the pros and cons of existing technologies. The constituent elements and corresponding building blocks needed in a workable mould with a rapid heating and cooling capability will be described.

Chapter 3 describes the main characteristics of metal foams and the ways in which this new class of material is manufactured. A summary of the constitutive equations defining the mechanical and thermal behaviour of metal foams is then reported.

Chapter 4 presents the innovative heating and cooling system based on the use of metallic foams, which has been developed to increase the efficiency of the conventional RHCM technique. The implementation of a numerical environment suitable for analyzing the mechanical and thermal behaviour of the new heating and cooling system is reported. A structural simulation was carried out in order to evaluate the tension field and the deformation of the metallic foam during the polymer injection phase. A 3D thermal analysis was run simulating a cycle of rapid heating and cooling.

Chapter 5 describes the equipment used to experimentally investigate the innovative RHCM technology. A test production was performed and the surface finish of the plastic parts produced with the new mould was verified. The comparison between the numerical results and the experimental data regarding the cycle time is then reported.

Chapter 6 investigates the effect of fast variations of the mould temperature on the improvement of micro features replication. The manufacturing process of the micro channels and the procedure for the characterization of the moulded parts are described.

Chapter 7 focuses on the analysis of influence of the rapid heating and cooling on the mechanical properties of plastic parts. The result of the tensile test for filled and unfilled materials is reported.

Chapter 8 describes a comparison between the conditioning system based on the use of aluminum foam and the ball-filled niches technology. A plastic cover for aesthetic applications has been chosen as test case. The heating and cooling time of the different RHCM processes were analyzed to determine and compare their production costs.

Chapter 9 investigates the effect of the weld line developing process and its influence on surface finish and mechanical properties in micro injection moulding. A new mould with a variotherm system and an integrated visualization unit is described. Obtained results regarding the comparison between the conventional injection moulding process and RHCM for different materials and weld line types are then reported.

The last chapter, the tenth one, presents the conclusions of this work.

CHAPTER 2

BACKGROUND STUDY AND LITERATURE REVIEW

Injection moulding is one of the most widely used processing technologies in the plastics industry. In conventional injection moulding (CIM), polymer melt is injected into a closed cavity, held under pressure to compensate for thermal shrinkage until the gate freezes, and then ejected out of the cavity after the part has sufficiently cooled. A constant mould temperature is widely used in conventional injection moulding practice. The mould temperature is controlled by pumping fluid with constant temperature through the cooling channels of the mould and adjusting the rate and the temperature of the coolant. Mould temperature has a direct influence on the part quality and moulding cycle time and it has to be lower than the polymer phase transition temperature during the cooling stage. The standard injection moulding process suffers from problems caused by the large temperature difference between the mould and the incoming polymer. Upon contact with the mould surface, the polymer melt starts to solidify, almost instantaneously, at the mould surface. Because of this frozen layer, it is difficult to fill a part with a large length/thickness ratio. The premature freezing problem during the filling stage also results in weak weld lines because of the lack of molecular diffusion between the joining melt fronts. More important, the frozen outer layer deteriorates the optical and mechanical properties of the moulded part. The molecular orientations in the skin result in distributed birefringence and residual stresses, of which the latter is the primary driver for part warpage and dimensional instability. Often, the injection pressure in thin-wall moulding exceeds 100 MPa, a thousand times higher than the atmospheric pressure, resulting in high shear rates approaching 10^4 s^{-1}. Most of the aforementioned part defects may be alleviated or eliminated if an elevated mould temperature close to or even above the polymer transition temperature is used. This elevated mould temperature, however, substantially increases the cycle time, thus lowering the productivity to a great extent. The ideal moulding condition is to have a hot mould during the filling stage and a cold mould during the cooling stage. In reality, a single mould is used in injection moulding; therefore, means for rapid temperature change of the same mould are required to approximate this ideal moulding condition. Despite the advantages of the differential mould temperature setup, an injection mould typically presents a large thermal mass and is difficult to heat and cool rapidly within the normal injection moulding cycle.

Furthermore, any modified mould should possess similar mechanical performance as a standard mould.

Although most investigations on rapid heat cycle moulding (RHCM) appeared after 1990, some earlier endeavors date back to the early 1960s [1]. This very early study demonstrated the capability of improving the part quality but in a rather impractical way since it involved time-consuming heating and cooling of a large portion of the mould system. The number of studies on mould rapid heating and cooling has increased in recent years, especially after the 1990s. The primary driver comes from the growing need of precision parts, optical parts, and parts with microfeatures in the electronics and biomedical industries. Without an elevated mould temperature during the filling stage, it is difficult to mould a thin and long part without short shots, a precision part with minimal residual stress and thus acceptable warpage and dimensional stability and an optical part with a low level of birefringence. Recent works focused on selectively heating only the surface portion of the mould. Development of capable techniques for rapidly heating and cooling the mould surface portion is a difficult task because of the constraints and the endurance limits of the materials used for the mould. At present, rapidly heating and cooling a large surface area mould remains a major challenge in the polymer moulding industry.

This chapter presents an overview on the state of the art in mould rapid heating and cooling, aiming at explaining the working mechanisms and providing an unbiased account of the pros and cons of existing processes and techniques. Successful applications of existing processes are described and potential improvements to these processes are highlighted.

2.1 Process principle

The mould temperature control strategy of RHCM is quite different from that of CIM. CIM process consists of plastication of the polymer pellets in barrel, filling and packing of the resin melt in mould cavity, solidification of the shaped resin melt, and mould opening to eject out the moulded part. In RHCM, the mould is circularly heated and cooled and so the cavity surface temperature fluctuates significantly. As the temperature

of the cavity surface reaches the designated value, generally 10°C higher than T_g of the polymer, the resin melt in the barrel is injected into the cavity. When the thermal couple detects that the mould cavity surface has been heated up to the required temperature, the variothermal mould temperature control system sends a signal to the moulding machine immediately for melt injection. After filling and packing, the mould is cooled down quickly to solidify the shaped resin. Once the cavity surface temperature lowers to the required temperature, usually 10°C lower than the heat deflection temperature of the polymer, the moulding machine is given a signal to open the mould and the moulded part is ejected out. Then, the mould is reheated for the next moulding cycle. Figure 2.1 shows the comparison of the changes of the mould temperature during RCHM and CIM processes.

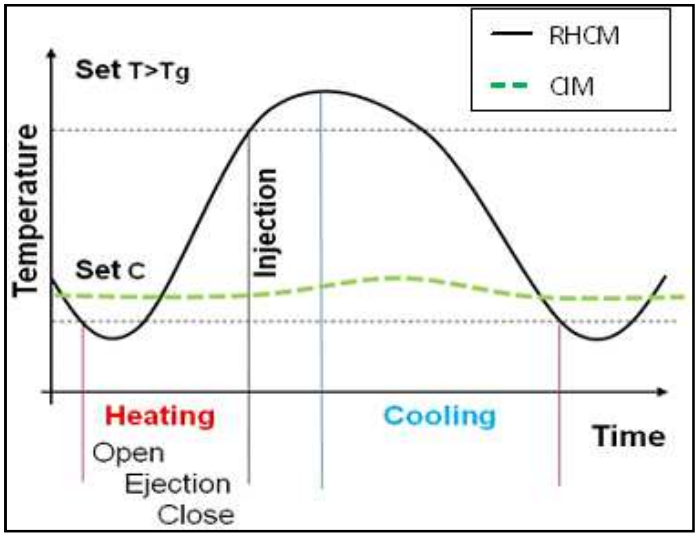

Figure 2.1 - Comparison of the changes of the mould temperature in RHCM and CIM processes.

As most of the shell plastic parts just fulfill the requirement of a good outer surface appearance, only one side of the mould, usually the cavity side, needs to be heated. According to the temperature feedback of a thermal couple, the variothermal mould temperature control system can coordinate the activities of the heating system, cooling system, and the moulding machine to achieve a continuous RHCM process.

The cycle time is one of the most important factors to be considered because it affects the production efficiency. In RCHM we expect to decrease the moulding cycle time by determining a reasonable starting time of the heating process to fully use ejecting time and mould closing time to heat the moulds. The heating process can start once the moulds are opened and the moulded part separates from the mould cavity. In this condition, the mould are heated during mould-opening, ejecting and taking out the part, and mould closing. The whole moulding cycle time, t_{cycle}, can be expressed as:

$$t_{cycle} = t_{filling} + t_{packing} + t_{cooling} + max\{(t_{opening} + t_{ejection} + t_{closing}), t_{heating}\} \quad (2.1)$$

where $t_{filling}$, $t_{packing}$, $t_{cooling}$, $t_{opening}$, $t_{ejecting}$, $t_{closing}$, and $t_{heating}$ denote the filling time, packing time, cooling time, mould-opening time, ejecting time, mould-closing time, and heating time, respectively. $max\{(t_{opening} + t_{ejecting} + t_{closing}), t_{heating})\}$ represents the maximum one of $t_{heating}$ and the sum of $t_{opening}$, $t_{ejecting}$, and $t_{closing}$. But if both the inner and outer surfaces of parts are required to have good aesthetics, the surfaces of the mould cavity and core sides all need to be heated. For this case, the heating process of the cavity and core can be started once the part is ejected out from the mould. The heating process of the cavity and core is performed simultaneously with the operations of ejecting and mould closing. In this condition, the whole moulding cycle time can be expressed as:

$$t_{cycle} = t_{filling} + t_{packing} + t_{cooling} + t_{opening} + max\{(t_{ejection} + t_{closing}), t_{heating}\} \quad (2.2)$$

2.2 Heat transfer process in injection moulding

There are three contributions to the heat in the thermoplastic melt during the injection stage: Q_1, convected heat from the melt; Q_2, heat conducted to the mold; and Q_3, heat generation inside the thermoplastic [2]. These contributions are quantitatively represented in the following equation:

$$\rho c_P \left(\frac{\partial T}{\partial t} + \boldsymbol{v} \cdot \nabla T\right) = \nabla \cdot (k \nabla T) + (\alpha \boldsymbol{\sigma} : \dot{\boldsymbol{\gamma}} + \dot{s}) \tag{2.3}$$

where ρ is density, c_p is specific heat, k is thermal conductivity, T is temperature, t is time, $\boldsymbol{v}$ is a velocity vector, $\boldsymbol{\sigma}$ is a total stress tensor, $\dot{\boldsymbol{\gamma}}$ is a strain rate tensor, α is the fraction of deformation energy converted into heat, and $\dot{s}$ is a heat generation source from a non deformation field. In Eq. (2.3), $\rho c_p v \cdot \nabla T$ represents the convective energy, that is, Q_1; $\nabla \cdot (k \nabla T)$ corresponds to the conduction loss to the mold, that is, Q_2; and $(\alpha \boldsymbol{\sigma} : \dot{\boldsymbol{\gamma}} + \dot{s})$ represents the total heat generation source, that is, Q_3. In Q_3, $\alpha \boldsymbol{\sigma} : \dot{\boldsymbol{\gamma}}$ denotes the heat generation due to permanent deformation, and in the filling stage, it is viscous heating, that is, $\eta \dot{\gamma}^2$, where $\dot{\gamma}$ is the equivalent strain rate. Figure 2.2 schematically illustrates the heat transfer process in thermoplastic injection moulding.

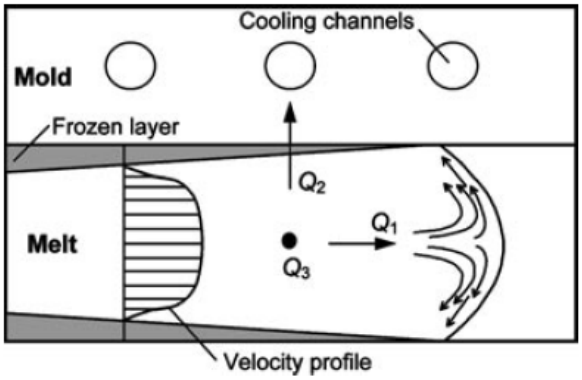

Figure 2.2 - Schematic of heat transfer process in injection moulding.

2.3 Mould design for rapid thermal cycling

The difficulty in designing a rapidly heatable and coolable mould arises from several specific functional requirements that a productive mould must satisfy. The typical injection pressure ranges from 10 MPa to more than 100 MPa. The high cavity pressure could cause a significant amount of shape change of the cavity. If soft organic materials are involved for insulation purposes, appropriate design schemes must be utilized to minimize the amount of mould deflection. The mould design should promote the generation of static pressure in the mould material rather than creating different normal

stresses in different directions and consequently a high level of shear stresses. For example, bending should be minimized. The mould must be mechanically capable of supporting an extremely high injection pressure and a large clamping force. This is important when stiff but brittle materials are used.

The mould should have a low thermal mass and exhibit a low inertia to variation of thermal loads [3,4]. Cycle time is as important as part quality in mass production and is directly related to the manufacturing cost. Even if the formidably high heating energy could be made affordable, it would still be difficult to cool a large thermal mass within the normal cycle time.

Finally, thermo mechanical durability during thermal cycling is critical in mass production of plastic parts. The design of a rapidly heatable and coolable moulding system must be considered carefully and must be economically and practically feasible. For a system with different materials used for insulation and heating purposes, the thermal mismatching problem could greatly reduce the life of the mould.

2.3.1 Constituent elements

An industrial process or machine can be decomposed into its constituent elements. These elements can then be recombined in a systematic way into either innovative solutions. Tadmor [2,7] proposed a framework for machine invention using elementary operations. Four constituent elements are needed for a rapidly heatable and coolable mould:

- low thermal mass;
- a stiff, strong, and durable mould;
- means for rapid heat generation in the mould surface portion;
- means for rapid heat removal in the mould surface portion.

Conventionally, mould cooling is achieved with fluid coolants, usually water and less frequently air or other fluid media. Although, in theory, cooling can be achieved by other mechanisms. But these methods are expensive and less effective than conventional water cooling. Compared with heating, cooling can be performed at a lower rate because, during cooling, the injection moulding machine needs additional time for plasticating a new shot

for the next cycle. Therefore, the thermal gradient developed in the cooling stage is lower than that in the heating stage and the mechanical requirements are almost solely designed for the heating means. In most studies [3,5,6] on mould rapid heating and cooling, although heating was carried out unconventionally, cooling was performed in the conventional way. Therefore, studies with unconventional cooling systems are uncommon.

2.4 Mould with low thermal mass

For RHCM, the required heating and cooling time of the mould mostly depends on the mass of the cavity/core to be heated and cooled. A mould with a low thermal mass exhibits a low thermal inertia and can be rapidly heated and cooled. As shown in Figure 2.3, the thermal performance of a rapidly heatable and coolable mould to three thermal rates: the initial heating rate, the secant heating rate and the initial cooling rate. Previous investigations [6,8,9] showed that a mould with a low thermal mass can deliver a rapid temperature rise of 100 °C/s with a heating power of the order of 100 W/cm^2. Since the heat used during heating needs to be removed during cooling, the low thermal mass is also critical for energy saving.

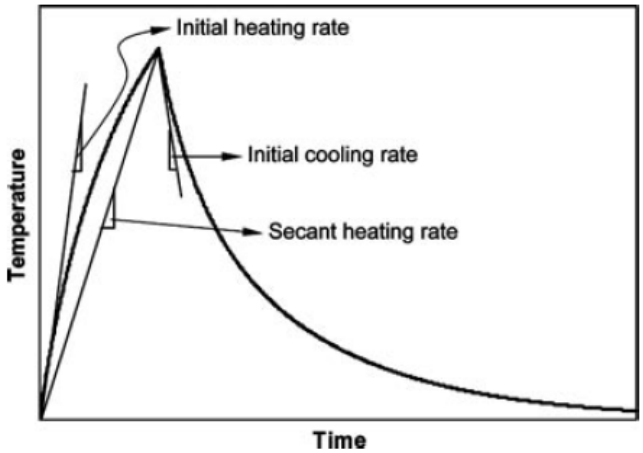

Figure 2.3 - Schematic heating and cooling response at the mold surface.

The thermal mass, *M*, can be defined as the product of mass and specific heat, as given in Eq. (2.4):

$$M = \rho V c_p \tag{2.4}$$

where V is the volume of the mass. Three basic building blocks for a low thermal mass are revealed from Eq. (2.4), that are density, specific heat and volume. The product of density and specific heat for most material, including metals, ceramics, and polymers, is of the level of 3×10^6 J/(m^{3}K). Density and specific heat are intrinsic material properties that cannot be modified. The first two building blocks are not useful in practice.

To reduce the thermal mass, the volume of the material being heated should be reduced. However, the extent of volume reduction is limited by some mould design constraints, particularly the required structural stiffness.

2.4.1 Mould with scaffolded structures

In the porous material building block, the mould comprises a significant percentage of voids. The actual volume of the mass is much smaller than the apparent volume of the mould, or to put it another way, the apparent density of the mould is much smaller than the density of the mould material. Technical approaches to this building block include scaffolded structures [10-12]. Figure 2.4 shows an example of scaffolded mould for lowering the thermal mass. Xu et al.[10,11] designed a scaffolded mould with beams as supporting elements arranged in a three-dimensional pattern, resulting in a fully open-pore mould insert. In general, to create such a mould, free-form additive manufacturing techniques are needed (e.g., selective laser sintering and three-dimensional printing). Figure 2.5 shows a demo insert with cooling channels and truss support made by 3D printing process. For a scaffolded mould, structural issues, particularly on the stiffness of the mould, need to be addressed in the design. This can be accomplished by a computer-aided structural analysis. In the case of simple internal hollow geometries combined machining and fusion techniques may be used. Yao et al. [9] created a thin plate with rectangular pockets on one side and welded this side to a thick mould base. The conformal pockets or channels near the mould surface create an opportunity for rapid cooling by passing a cooling medium in these spaces during the cooling stage [12-14].

Kimberling et al. [15] showed that a 50×25×25 mm mould insert with an air pocket design and the pulsed cooling method can be thermally cycled between 70 °C and 200 °C with a cycle time of only 5 s. Recently, Chen et al. [16] more quantitatively investigated the use of pulsed cooling for enhancing the thermal performance, proven to be effective even for a more conventional mould design. Any other stiff and strong porous materials may be used in low thermal mass moulds, for example, porous stainless steel produced by powder metallurgy.

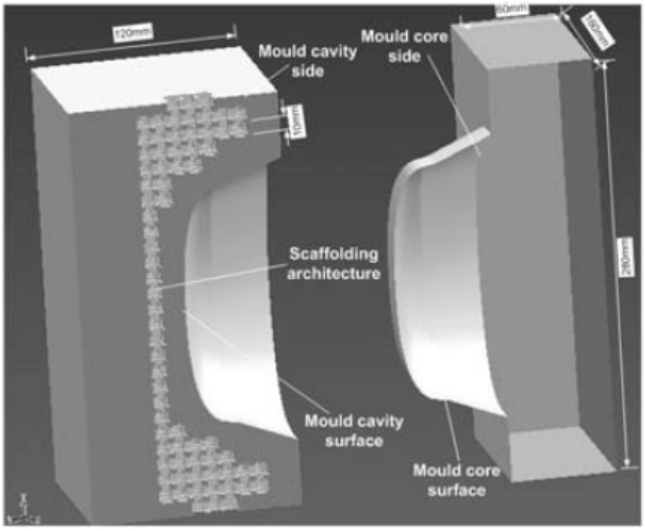

Figure 2.4 - Scaffolded mould design.

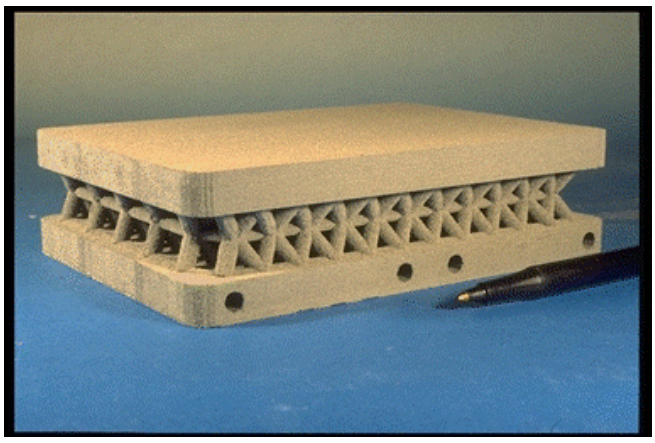

Figure 2.5 - An insert with cooling channels and truss support made by 3D printing process.

2.4.2 Multilayer mould

In an insulated mass building block, a thermal insulation is sandwiched between the bulk mould base and the cavity surface portion, resulting in a multilayer mould design [3,4,6,8,17-29, 30]. In this case, different materials are used in the mould. Because the thermal and mechanical properties are different between a typical conductor and an insulator, the main challenge arises from the high interfacial shear stress between the layers generated during the heating and cooling stages. Yao and Kim [8] simulated the thermal stress developed in a multilayer mould with a steel base, a metallic coating layer and an oxide insulation layer. Although most reported multiplayer moulds suffered from serious durability issues, the approach was found to be useful during passive heating [34].

Innovative technologies have been developed for creating many layers of thin materials near the surface, allowing gradual variation of properties between layers [31,32]. Similar techniques may be developed to improve the durability of a multilayer injection mould.

Orthotropic materials have been used for mould rapid heating applications. In particular, Yao and Kim [33] used pyrolytic graphite with orthotropic properties produced in a chemical vapor deposition (CVD) process. The material exhibited a factor of 200 in thermal conductivity difference and a factor of 1200 in electrical resistivity difference, and can be heated and cooled rapidly with a thermal rate over 100 °C/s. Although graphite is not a desired mould material, this approach could be extended to a more durable material.

2.5 Mould surface heating methods

The only two mechanisms relevant to mould rapid heating are heat generation and heat conduction. Among all possible internal heat generation mechanisms, electrical resistive heating is the most used mechanism for mould rapid heating. Electrical resistive heating can be accomplished by passing direct or alternating current in a thin electrical conductive layer or by skin effects from a high-frequency electromagnetic field. Two useful technical approaches for implementing this skin effect are induction heating and proximity heating. If the mould material is an insulator exhibiting reasonable dielectric

loss, it may be heated by high-frequency dielectric heating, including microwave heating. Heat generation using the Peltier effect has also been reported in mould heating, although the thermal rate was slow. The technical aspects for each technology will be described in detail in the following sections.

2.5.1 Electrical resistive heating

In electrical resistive heating, the heat is generated according to Joule's first law. For safety reasons, low voltage and high current are typically desired. Most good resistive heating materials either are brittle or require a specific geometry (e.g., resistive wires). In the case of mould rapid heating, a metallic heating layer is desired. However, metals are excellent electrical conductors and therefore high resistance is difficult to obtain unless the geometry is long and thin. A schematic setup of mould rapid heating by low frequency electrical resistive heating is illustrated in Figure 2.6.

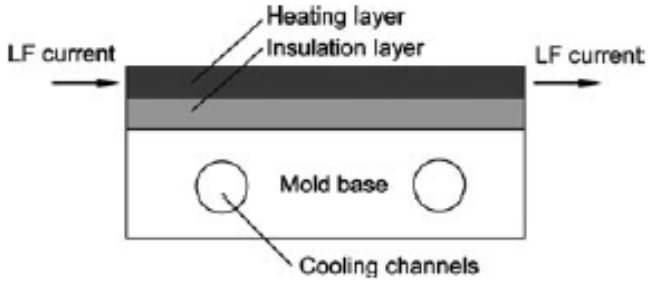

Figure 2.6 - A Electrical resistive heating with low-frequency electrical current.

Flexible, thin-film heaters are available commercially, typically made of a zigzag thin-film metallic pattern to increase the resistance, sandwiched between two insulation layers. For this method, an insulation layer is needed beneath the thin resistive heating layer (Figure 2.7). However, any tiny scratch on the surface could result in a catastrophic failure due to no uniform heating and local stress generated. Furthermore, the contact resistance at any connecting junctions could be significant, resulting in an additional failure mode. Significant efforts in multilayer resistive heating was directed to identify a identify stiff, strong, and durable materials with relatively high resistivity [1-3,17,19].

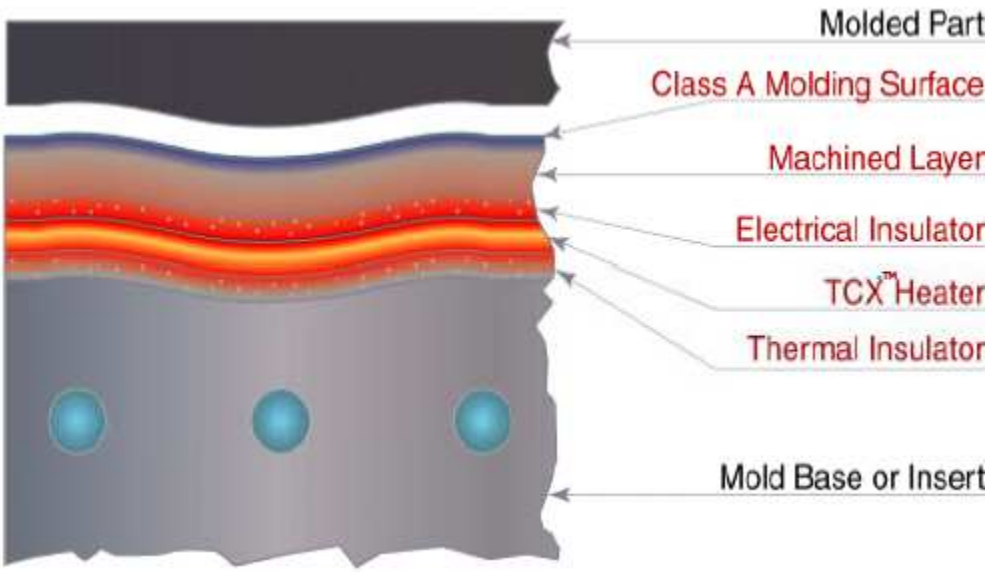

Figure 2.7 - A schematic setup of mould rapid heating by electrical resistive film (Thermoceramix® system).

2.5.2 Induction heating

Induction heating is the process of heating an electrically conducting object (usually a metal) by electromagnetic induction, where eddy currents are generated within the metal and resistance leads to Joule heating of the metal. An induction heater consists of an electromagnet, through which a high-frequency alternating current is passed. Induction heating is an efficient means to heat the mould surface in a non-contact procedure. Although Wada et al. [35] proposed the idea of using induction heating more than twenty years ago and a feasibility study on induction heating on mould heating was also reported recently, stable utilization of induction heating by the moulding industry will not be practical without a full understanding of induction heating from both the simulation and experimental point of view [36-41]. Chen et al. [42] applied induction heating to improve the surface appearance of weld lines. Kim et al. [43] used induction heating in a procedure that rapidly raises the surface temperature of a nickel stamp with nanoscale-grating structures. Park et al. [44] improved the mouldability of micro-features by applying high-frequency induction heating. This study applies induction heating to the elimination of weld lines in an injection-moulded mobile phone cover. A schematic setup of an induction heating system with an external elliptic coil is shown in Figure 2.8.

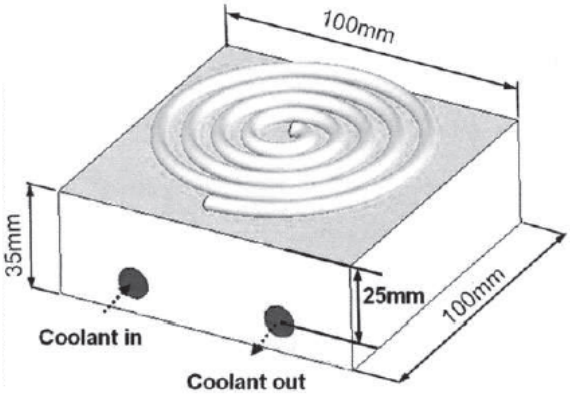

Figure 2.8 - A schematic setup for induction heating of mould inserts.

One benefit of this method, therefore, is that the electrical insulation right beneath the mould surface is not needed. But its use in mould surface heating requires solutions to several problems, including coil design, system operations, and parameter control. In general, direct embedment of the coil inside the mould is difficult and the common practice is to use a separate external coil. For this reason, the reported experiments were limited to mould preheating before the mould closes. Internal coils for induction heating [45,46] have been disclosed in patent applications (Figure 2.9). However, the effectiveness of this method cannot be assessed at this moment because of the lack of experimental data reported.

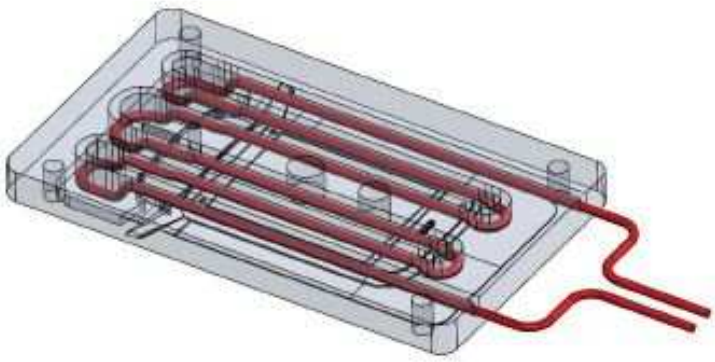

Figure 2.9 - A schematic setup for induction heating with internal coils (3iTech system developed by Roctool®).

2.5.3 High-frequency proximity heating

Another high-frequency resistive heating method is proximity heating [9,47]. The principle of this method is based on the proximity effect [48] between a pair of conductive blocks facing each other with a small gap in between and forming a high-frequency electric circuit, as shown in Figure 2.10. The high-frequency current flows at the inner sides of the facing pair, heating the mould surface portion. The proximity heating method does not need the presence of an electrical insulation layer beneath the mould surface. The main benefit of proximity mould heating over inductive mould heating is that the separate electrical coil is eliminated. This facilitates active heating to be performed even when the mould is closed. However, mould surfaces with complex shapes are difficult to heat.

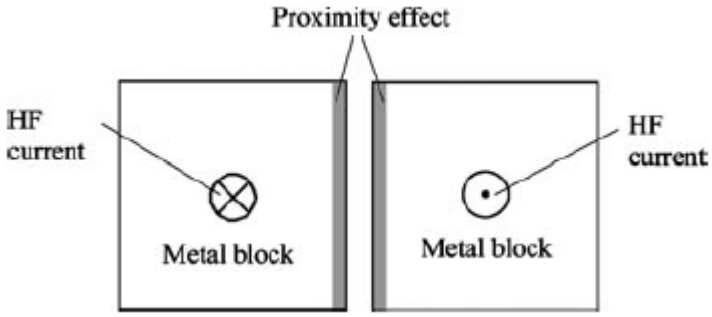

Figure 2.10 - Principle of high-frequency proximity heating.

2.5.4 Dielectric heating

Dielectric heating, also known as high-frequency heating, is the process in which a high-frequency alternating electric field, or radio wave or microwave electromagnetic radiation heats a dielectric material. The use of dielectric heating for mould rapid heating requires that the mould be a dielectric material and an electrical insulator. This method has limited applications in mould heating, and more often it is used for heating the polymer [49-51]. Dielectric heating of the polymer can be combined with induction heating for enhancing the mould heating performance [45]. In the case in which the mould is also made of a dielectric material, both the mould and the polymer can be actively heated [49] by the high-frequency energy. It should be noted that most polymers

are poor electromagnetic absorbers. Therefore, either a high power source or easily excitable additives are needed for the practical use of dielectric heating of the moulding polymer.

2.5.5 Thermoelectric heating

Thermoelectric cooling is based on the Peltier effect to create a heat flux between the junction of two different types of materials. A Peltier heater is a solid-state active heat pump which transfers heat from one side of the device to the other side against the temperature gradient with consumption of electrical energy. The direction of heat transfer can be reversed by switching the polarity of the power supply. Sequential heating and cooling can be performed by a single thermoelectric device. Kim and Wadhwa [52] used commercially thermoelectric devices for mould heating. The major limitation of such a thermoelectric heating device is that the heat generated on one junction is rapidly conducted to the other junction because of the small space involved and the moulding heating and cooling rate with thermoelectric heating is rather slow. Whiteside et al. [53] showed that the Peltier device did not have the power to adequately control the temperature of the cavity.

2.5.6 Radiation heating

The radiation heating building block implements a radiation boundary condition in the heat transfer process. The energy is transmitted from a remote body in a noncontact manner in the form of rays and waves. The use of radiation for mould rapid heating has been exclusively focused on infrared heating [54-61]. As is generally known, radiation energy propagating in a radiation absorbent is exponentially absorbed and attenuated. Its relation is described by Lambed-Beer's law.

$$I = I_0 \exp(-\beta x) \tag{1.3}$$

Absorbed radiation energy is converted into thermal energy, and then the absorbent temperature is increased. The extent of the radiation heating depends on the radiation absorption coefficient that is a function of the material components and radiation

wavelength. A characteristic point of the proposing technique is its non-contact, volumetric heating and good controllability for the heating extent. One part of the mould wall must be transparent to introduce the radiation energy from the outside of the mould blocks. Thus the moulded polymer is directly heated by radiation energy, and the temperature of the moulded polymer is easily controlled by radiation intensity. Many polymer materials have several absorption bands for infrared radiation.

Rapid thermal processing using radiation heat transfer is a widely used technique in semiconductor manufacturing processes such as chemical vapor deposition (CVD) on silicon substrates. Because of vacuum environment in the CVD chamber, radiation is a more efficient heat transfer mode to heat the silicon substrates rapidly. The short wavelength halogen lamps are used as the infrared source. The silicon substrate is insulated by quartz pillars and the temperature of silicon substrate can be raised from 300 K to 1300 K in 10 s. Some researchers have studied the temperature control of the RTPCVD system.

In injection moulding, multiple infrared lamps can be assembled on a lamp holder and used as a single external device that can be moved in and out of the space between the two mould plates [58-60]. A flat reflector with scattered lamps is shown in Figure 2.11.

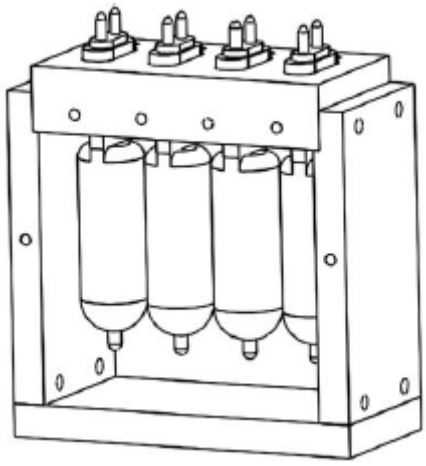

Figure 2.11 - Infrared heating system.

With the modification of the infrared rapid surface heating technique for injection moulding, e.g., increase power of bulbs, focus the energy at the area of mould insert and

lower the mould temperature, the cycle time can be kept within an affordable period of time. One difficulty in infrared heating is to achieve uniform heating temperature across the mould surface. Commercial optical analysis software can be used to simulate the infrared absorption of the mould surface for the first stage of analysis and to optimize the lamp pattern. Infrared lamps can be installed inside the mould plates in addition to external infrared sources [57]. In this case, infrared heat is available when the mould is closed, allowing active heating during the entire mould cycle. A schematic setup of a infrared heating system with external infrared lamps is shown in Figure 2.12.

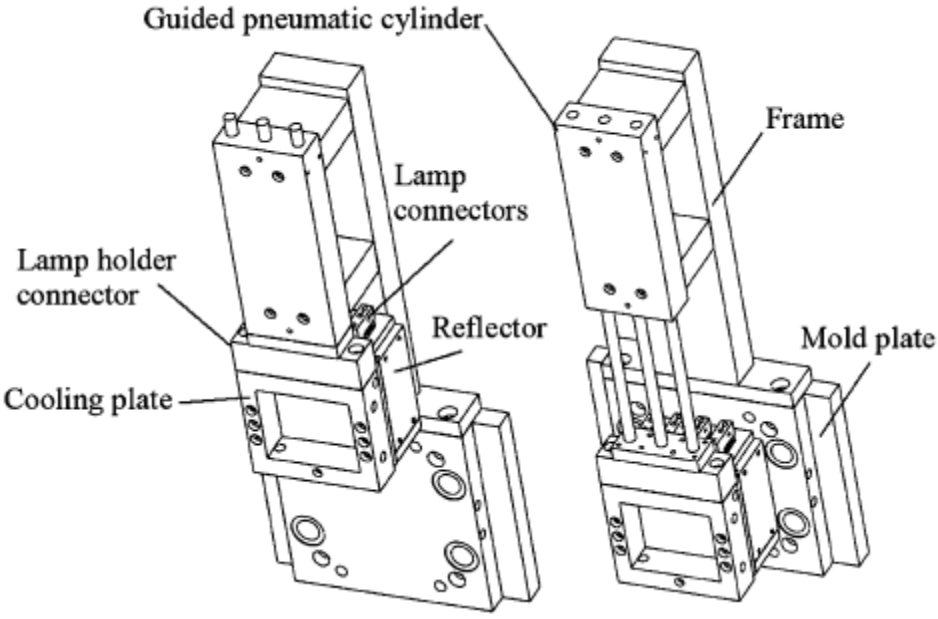

Figure 2.12 – Schematic of the infrared heating system assembled on the mould.

2.5.7 Contact heating

In contact heating or conduction heating, a low temperature body is conductively heated by contacting with a high-temperature body. Little effort [62,63] has been reported in mould rapid heating using contact heating. Stumpf and Schulte [62] disclosed a mould design in which a thin inner region of the mould adjacent to a hollow mould cavity is conductively heated by a more bulky outer region maintained at a higher temperature. After moulding, the thin inner mould region together with the moulded part is cooled independent of the outer region. Yao et al. [63] experimentally investigated the use of two

stations, one hot and the other cold, for rapidly heating and cooling flat shell moulds. They reported that aluminum shell moulds with a thickness of 1.4 mm could be rapidly heated from room temperature to 200 °C in about 3 s with a hot station at 250 °C. The use of contact heating between solid bodies for mould rapid heating is constrained by several physical limits of the heat conduction process. Since heat conduction is a diffusion process, penetration of heat into a thick section is a slow process. For complex shell geometry, additional concerns are on the uniform contact between the contacting bodies. For these reasons, contact heating is suitable for thin shell moulds with simple geometries and high thermal conductivity.

Passive heating of the mould surface by the incoming polymer melt may be considered as one special case of contact heating. In this case, the major mechanism for heat transfer is also heat conduction. A practical solution is to incorporate an insulation layer at the mould surface, as exemplified in the literature [4,26-29,64]. If a metallic surface is needed, as in compact disk moulding and micro moulding, a separate metallic stamp with microstructures can be placed over the insulation layer and heated by passive heating. In general, the mould surface temperature rise due to passive heating is moderate; however, a proper use of this effect can result in a significant delay of the frozen layer formation, thus improving the moulding quality. Iwami et al. [30] developed an injection mould system with an insulated thin metal cavity surface and a release-functioning core surface, as shown in Figure 2.13. Immediately after mould-filling under a low pressure such as one third of that in conventional moulding, the cavity surface rapidly increases in temperature to develop wettability and adhering, while the resin on the core side is released and migrates toward cavity side to compensate the surface shrinkage. Before deciding a proper ULPAC-cavity block, simulations for the thermal behaviour of ABS melt and metal surface was performed under variable parameters using a simulation software (Figure 2.14).

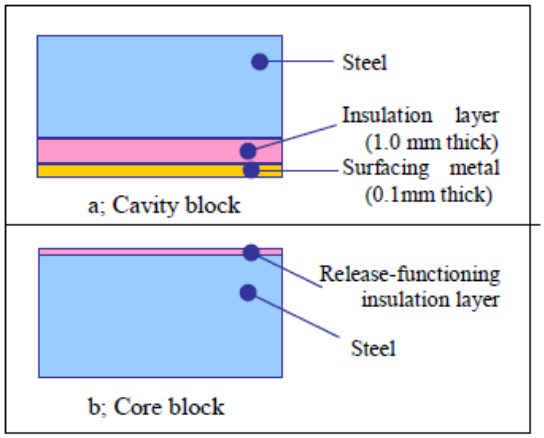

Figure 2.13 – The basic composition of ULPAC cavity and core block.

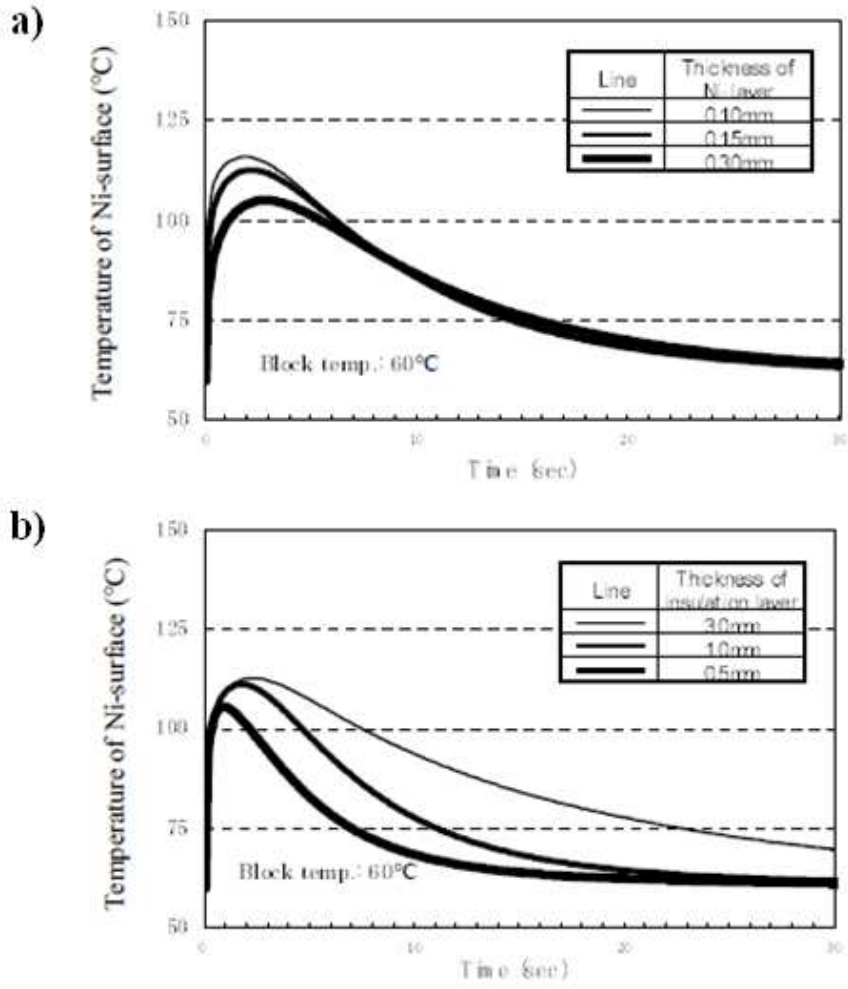

Figure 2.14 – Thermal behaviour of the metal surface layer in varying (a) its thickness and (b) the thickness of the insulation layer.

2.5.8 Convective heating

The convective medium (oil, liquid or heated gas) imposes a convective heat flux at the fluid–solid interface. The heated fluid may be circulated inside the mould or directly introduced to the mould surface from the mould cavity. The internal convective heating method is the most common method of controlling mould temperature in the traditional injection moulding industry. Some earlier efforts [65] in mould rapid heating and the earlier version of the variotherm mould heating process [66,67] were based on this method. In internal convective heating, heated oil has been the most widely used heating medium. But the reported heating response in these systems was quite slow, typically needing more than several minutes to achieve a 100 °C change of temperature. In order to overcome the limited heating temperature of oil, hot air and steam can be used. In particular, the steam heating method has recently generated some interest in the industry. An example of an RHCM system with steam heating is illustrated in Figure 2.15. It consists of a steam system, a coolant system, a valve exchange unit, a control and monitoring unit, an injection moulding machine, a steam-heating mould.

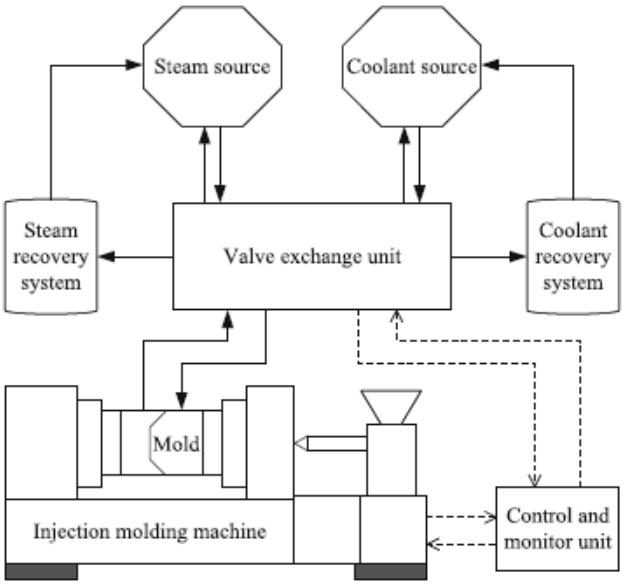

Figure 2.15 – Composition and structure of RHCM systems with steam heating.

Conventional machining like CNC drilling can be used to make straight channels. But this technology doesn't allow to produce complicated channels in three-dimension, especially close to the wall of the mould. An alternative method that provides a cooling system that 'conforms' to the shape of the part in the core, cavity or both has been proposed. This method utilises a contour-like channel, constructed as close as possible to the surface of the mould to increase the heat absorption away from the molten plastic (Figure 2.16).

Figure 2.16 – An example of RHCM mould with conformal cooling channels.

The RHCM technique with electric heating and coolant cooling is the most widely used system in the injection moulding industry. For RHCM, the heating and cooling system design of the electric-heating moulds are of great importance because they have a decisive influence on the moulding cycle and the part quality [68-73]. Figure 2.17 gives the schematic cavity structure of a typical electric-heating mould. For the cooling system, the diameter, D_c, of the cooling channel is about 6–8 mm. Considering the factors of the mould strength and the cooling efficiency, the distance, H_c, from the centre of the cooling channel to the cavity surface and the pitch, P_c, between adjacent cooling channels are, respectively, 3–4.5 times and 2.5–3.5 times of the diameter of the cooling channel. For the heating system, the diameter, D_r, of the heating rod is about 4.5–6.5 mm. The distance, H_r, from the centre of the heating rod to the cavity surface and the pitch, P_r,

between adjacent heating rods are, respectively, about 1–1.5 times and 2.5–3.5 times of the diameter of the heating rod. During the heating process, the empty cooling channels can improve the heating efficiency by retarding the heat loss. Before heating, the remaining water in the cooling channels of the mould must be drained out. In order to achieve a good heating effect, the clearance between the heating rod and the wall of the mounting hole in the cavity or core should be smaller than 0.05 mm. Xi-Ping Li et al. [74], proposed a strategy for optimizing the distances between the neighbour heating channels in order to achieve a uniform temperature distribution on the cavity surface.

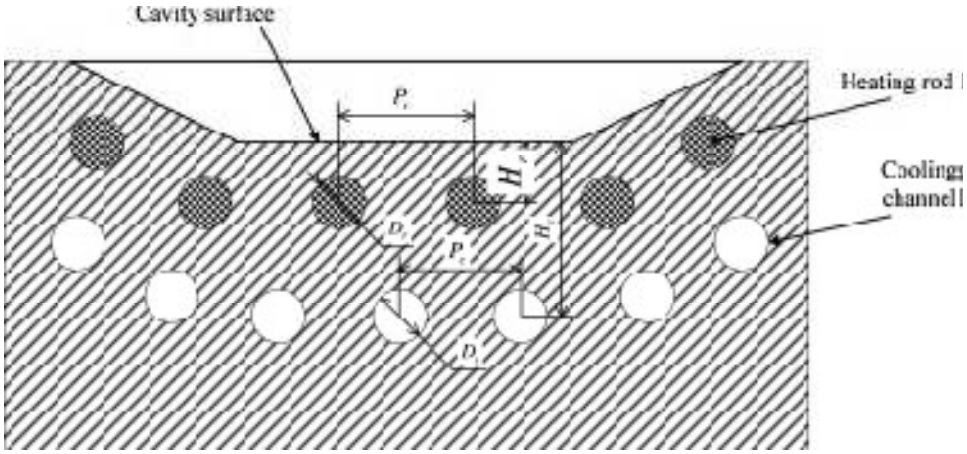

Figure 2.17 – The schematic cavity structure of a typical electric-heating mould.

However. the temperature profiles of conventional channels show local differences, which cannot be avoided. This problem has been solved with the new ball-filled (BF) mould, developed by the Kunststoff-Institut Lüdensheid, Germany. Figure 2.18 shows the schematic structure of the innovative ball-filled mould. It utilizes the entire area behind the cavity for homogeneous heating and cooling. This provides for efficient flow through the cooling area, thus affecting the cavity's surface very directly. A cooling process fitting closely around the contours with simultaneous high water flow rates can be achieved. Only those parts of the mould that are close to the cavity are heated, which ensures extremely fast and energy-efficient heating and cooling processes. BFMOLD^{TM}® can be integrated in the mould for a wide range of moulded parts, but can also be used selectively, restricted to critical parts of components.

Both conformal channels and ball filling allow rapid and uniform heating of the cavity and provide mechanical support to contrast high injection pressures. However, conformal cooling channels are expensive to produce while ball-filled slots can be realized only for parts with plane geometry.

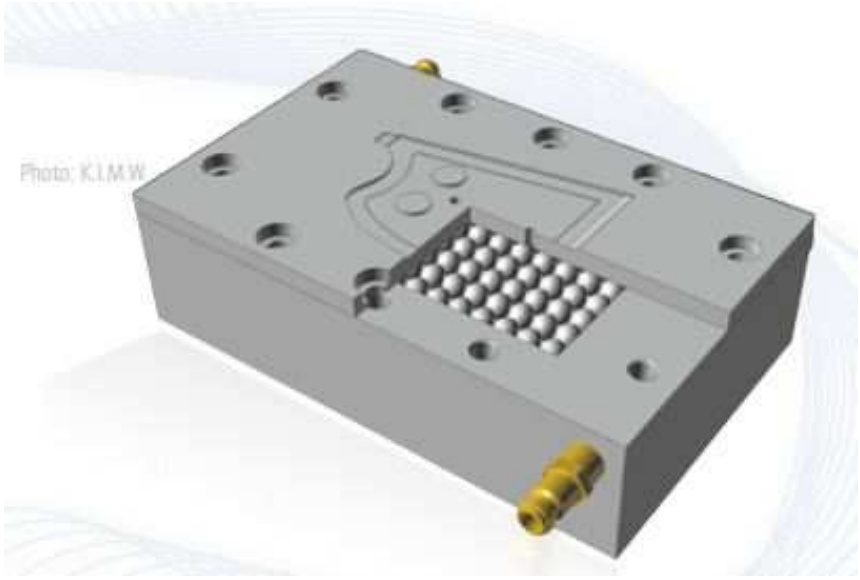

Figure 2.18 – Schematic view of the BFMOLD™® technology principle.

2.6 Applications

With a rapidly heated mould surface during the filling stage, the frozen layer is reduced, or even eliminated, if the mould surface temperature exceeds the polymer freezing or vitrification temperature. This reduction in freezing has a profound effect on the quality of the moulded part. In particular, flow induced molecular orientations are reduced, allowing a more isotropic part to be moulded. The resulting part exhibits a lower level of birefringence, reduced residual stresses, better optical properties, and improved dimensional accuracy and stability. The fluidity of the polymer is also increased, resulting in a longer flow path, better replication of surface topography and microstructures, and stronger weld lines. In addition, with active mould heating and cooling during the entire moulding cycle, the thermal history of the polymer can be controlled so as to optimize its structure and morphology. This appears to be useful for polymers, particularly for those

in which structural formation is sensitive to thermal changes within the normal time scale in injection moulding.

2.6.1 Minimizing weld lines

Weld lines are formed during the filling stage when two or more melt fronts come in contact with each other (Figure 2.19). Weld lines represent a potential source of weakness in moulded parts. Two main types of weld lines are usually to be distinguished. Cold or stagnating weld line is formed by a head-on impingement of two melt fronts without additional flow after that collision, Figure 2.20(a). Hot or flowing weld lines occur when two melt streams continue to flow after their lateral meeting, Figure 2.20(b). The low mechanical properties in weld lines are considered to be caused by several factors such as poor intermolecular entanglement across the weld line, molecular orientation induced by fountain flow, and the stress concentration effect of surface V-notch etc. This is a particular concern for parts subjected to dynamic loads. It is generally believed that the weld line strength increases as the temperature and pressure at the weld increases.

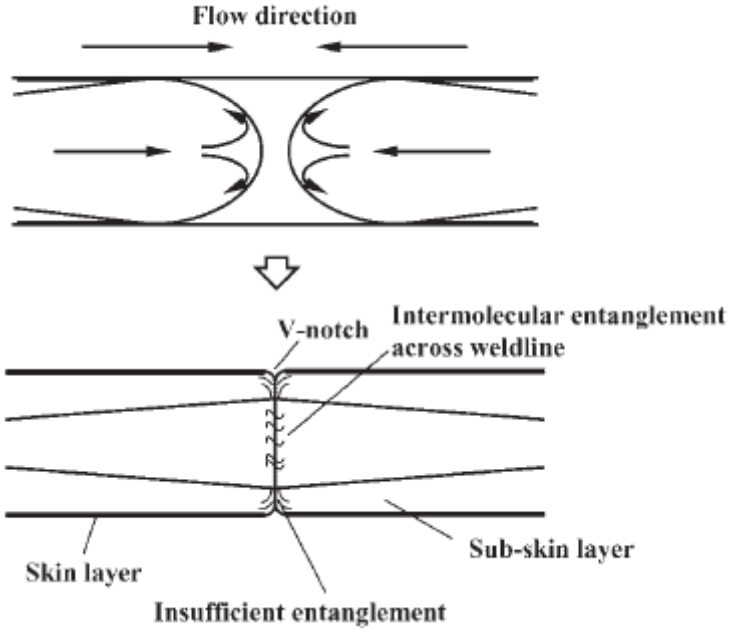

Figure 2.19 – Structure of opposite flow weld line.

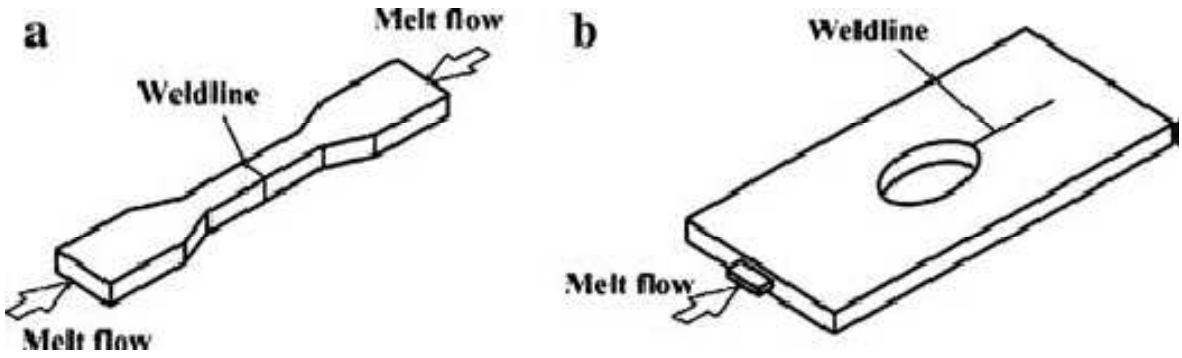

Figure 2.20 - a) Cold weld line. b) Hot weld line.

Wlodarski et al. [75] presents a quantitative examination of weld lines depth and surface finish using white light interferometry. Results are reported for ABS/PMMA mouldings made conventionally and with RHCM, in which the tool surface is pre-heated to 120°C. Rioux et al. [76] studied the weld line strength of injection moulded thermoplastic elastomers (TPEs) in terms of crack growth resistance. The specimens were moulded under identical processing conditions except the cavity surface temperature; one is 20 °C and the other is 190 °C by mould rapid heating. They found that the crack resistance in injection-moulded TPEs is increased approximately 60% by using the hot mould cavity. Ziegmann et al. [77-79] used a variotherm system for rapidly heating a double-gated micro tensile bar mould and found that the V-notch at the weld line was eliminated at an elevated mould temperature. They also found that the tensile strength of the moulded part significantly increased with the increase in the heating temperature. Moreover, the heating of the polymer by ultrasound inside the mould cavity during the injection and holding stages was found to be an effective method for strengthening weld lines.

CHAPTER 3
METAL FOAMS

The present work proposes an innovative heating and cooling system based on the use of open-cell aluminum foam to increase the efficiency of the conventional RHCM technique. Metal foams are a new class of materials with low densities and novel physical, mechanical, thermal, electrical and acoustic properties. They offer potential for lightweight structures, for energy absorption, and for thermal management.

In order to introduce this new topic, a brief overview of metal foams will be illustrated. The chapter starts with a description of the ways in which metal foams are made. Mechanical design with foams requires constitutive equations defining the shape of the yield surface, and describing response to cyclic loading and to loading at elevated temperatures. A summary of formulae for simple structural shape will be presented. The effects of micro structural metal foam properties, such as porosity, pore and fibre diameters, tortuosity, pore density, and relative density, on the heat exchanger performance will be discussed.

3.1 Introduction

Metal foam is a cellular material defined by solid material surrounded by a three dimensional network of voids. The most basic classification of aluminum foams is the degree of interconnection between adjacent cells within the microstructure of the material. If the faces are solid too, it is said to be closed-celled. If the solid of which the foam is made is contained in the cell edges only, the foam is said to be open-celled. Some foams are partly open and partly closed. The difference in cellular structure of open and closed cell foams is apparent in Figure 3.1.

As a lightweight, porous material, metal foam possesses a high strength and stiffness relative to its weight, making it an attractive option for a variety of applications. Foaming dramatically extends the range of properties available to the engineer. The properties of metal foams make them desirable materials for use in situations where high strength and stiffness to weight ratios are essential, as well as applications where energy absorption and permeability characteristics are valued. Foamed materials are also useful due to their favourable sound absorption, fire retardation and heat dissipation properties. To date, metal foams are mainly being used in aerospace, filter and impact or insulation applications.

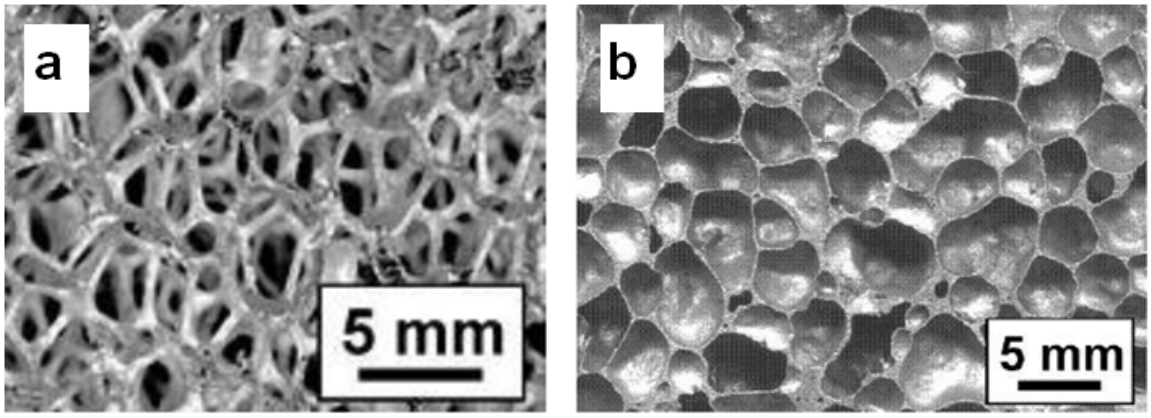

Figure 3.1 - (A) Open-cell and (B) closed-cell aluminum foam.

The low densities permit the design of light, stiff components such as sandwich panels and large portable structures, and of flotation of all sorts. In the last decades, these porous media have been largely studied because of their interesting properties that cover several different technical fields. In fact, metal foams are lightweight structures, offering high strength and rigidity, high heat transfer surface area which improve energy adsorption and heat transfer in thermal applications. Metal foams have considerable applications in multifunctional heat exchangers, cryogenics, combustion chambers, cladding on buildings, strain isolation, buffer between a stiff structure and a fluctuating temperature field, geothermal operations, petroleum reservoirs, compact heat exchangers for airborne equipment, air cooled condensers and compact heat sinks for power electronics.

3.2 Metal foam manufacturing methods

Metal foams are made by one of nine processes, listed below [80]. Metals which have been foamed by a given process (or a variant of it) are listed in square brackets.

1. Bubbling gas through molten Al–SiC or Al–Al2O3 alloys.
2. By stirring a foaming agent (typically TiH2) into a molten alloy (typically an aluminum alloy) and controlling the pressure while cooling.
3. Consolidation of a metal powder (aluminum alloys are the most common) with a particulate foaming agent (TiH2 again) followed by heating into the mushy state when the foaming agent releases hydrogen, expanding the material.

4. Manufacture of a ceramic mould from a wax or polymer-foam precursor, followed by burning-out of the precursor and pressure infiltration with a molten metal or metal powder slurry which is then sintered.
5. Vapor phase deposition or electrodeposition of metal onto a polymer foam precursor which is subsequently burned out, leaving cell edges with hollow cores.
6. The trapping of high-pressure inert gas in pores by powder hot isostatic pressing (HIPing), followed by the expansion of the gas at elevated temperature.
7. Sintering of hollow spheres, made by a modified atomization process, or from metal-oxide or hydride spheres followed by reduction or dehydridation, or by vapor-deposition of metal onto polymer spheres.
8. Co-pressing of a metal powder with a leachable powder, or pressure infiltration of a bed of leachable particles by a liquid metal, followed by leaching to leave a metal-foam skeleton.
9. Dissolution of gas (typically, hydrogen) in a liquid metal under pressure, allowing it to be released in a controlled way during subsequent solidification.

Only the first five of these are in commercial production. Each method can be used with a small subset of metals to create a porous material with a limited range of relative densities and cell sizes. Figure 3.2 summarizes the ranges of cell size, cell type and relative densities that can be manufactured with current methods.

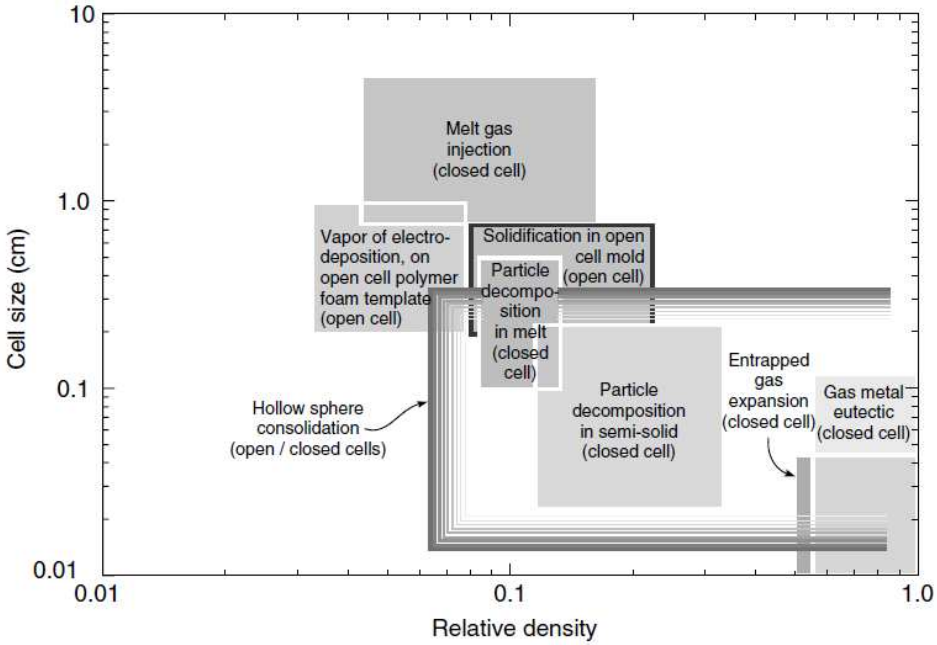

Figure 3.2 - The range of cell size and relative density for the different metal foam manufacturing methods.

3.3 Metal foam geometry representation

The structure of cells has fascinated natural philosopher for at least 200 years [81]. For over a century, it was thought that the space-filling cell which minimizes surface area per unit of volume was Kelvin's tetrakaidecahedron with slightly curved faces. Lord Kelvin stated that the optimum (minimum) surface for a formation of given volume packed in a given space was the tetrakaidecahedron, a stereometrical object consisting of six planar quadrilateral faces and eight non planar hexagons of zero net curvature.

Recently, using computer software for minimization of surface area, Weaire and Phelan [82] have identified a unit cell of even lower surface area per unit of volume. The unit cell is made up of six 14-sided cells (with 12 pentagonal and 2 hexagonal faces) and two pentagonal dodecahedra, all of equal volume. The 14-sided cells are arranged in three orthogonal axes with the 12-sided cells lying in the interstices between them, giving an overall simple cubic lattice structure. Only the hexagonal faces are planar: all of the pentagonal faces are curved. The Kelvin tetrakaidecahedron and the Weaire-Phelan unit cell are illustrated in Figure 3.3. In three dimensions a great variety of cell shapes is possible. Open cell metal foams' geometry depends upon their production process but

they retain some common characteristics such as the existence of open pore cells connected with each other. All of these unit cell packings have been suggested as idealizations for the cells in foams, together with others which, by themselves, do not pack properly unless distorted: the tetrahedron, the icosahedron and the pentagonal dodecahedron. Most foams, of course, are not regular packings of identical units, but contain cells of different sizes and shapes, with differing numbers of faces and edges.

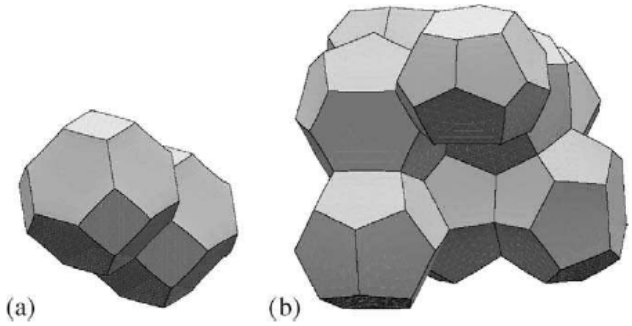

Figure 3.3 - (a) Lord Kelvin's 14-hedron assumption and (b) W-P volume constituted by 6 14-hedra and 2 pentagonal 12-hedra.

The subject is important to us here because the properties of cellular solids depend directly on the shape and structure of the cells. The most important structural characteristic of a cellular solid is its relative density (ρ^*/ρ_s) (the density, ρ^* of the foam divided by that of the solid of which it is made, ρ_s).

The fraction of pore space in the foam is its porosity and it is given by:

$$\varepsilon = 1 - \frac{\rho}{\rho_s} \tag{3.1}$$

If the foam is idealized as a packing of different polyhedra and these fill space without any distortions it is possible to calculate the relative density using the geometrical characteristic of the base polyhedron. Gibson and Ashby [81] suggest to use the tetrakaidecahedron because it gives the most consistent agreement with observed properties. The Authors derived geometric relationships for the tetrakaidecahedron unit cell. The relative density is given by:

$$\frac{\rho^*}{\rho_s} = 1.06\left(\frac{t}{l}\right)^2 \tag{3.2}$$

Thus, measuring the fibre thickness *t* and the length of the edge of the hexagonal window *l*, it is possible to estimate the relative density of the open-cell metal foam.

3.4 Mechanical properties

Significant work has been performed with the goal of attaining a confident definition of the material properties. In their comprehensive work [81], Lorna Gibson and Michael Ashby address the properties of three dimensional foam networks in great detail. Figures 3.4 shows a schematic stress–strain curve for compression. Initial loading appears to be elastic but the initial loading curve is not straight, and its slope is less than the true modulus, because some cells yield at very low loads. Open-cells foams have a long, well defined plateau stress. Here the cell edges are yielding in bending. Linear elasticity in open cell foams is governed by cell wall deformation due to axial forces and bending. The elastic modulus of the foam can be determined by the initial slope of the stress-strain curve. The long plateau is a result of the collapse of the cells by elastic buckling, plastic collapse or brittle crushing. As the collapse progresses, the cell walls touch, resulting in the rapid increase of stress.

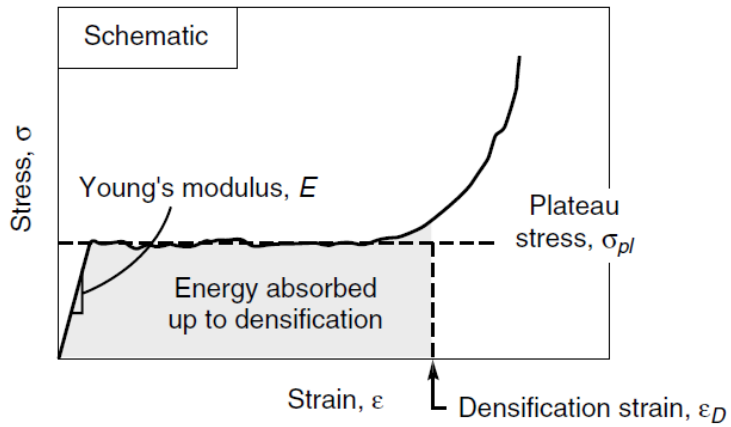

Figure 3.4 - Compressive curve for a metal foam.

Because main applications of foam result in compressive loading, Gibson and Ashby formulate expressions for the mechanical properties of foams based on the compressive behaviour. The expressions are derived using basic mechanics and simple geometry assuming a cubic unit cell with ligaments of length l and square cross section of side t, as shown in Figure 3.5.

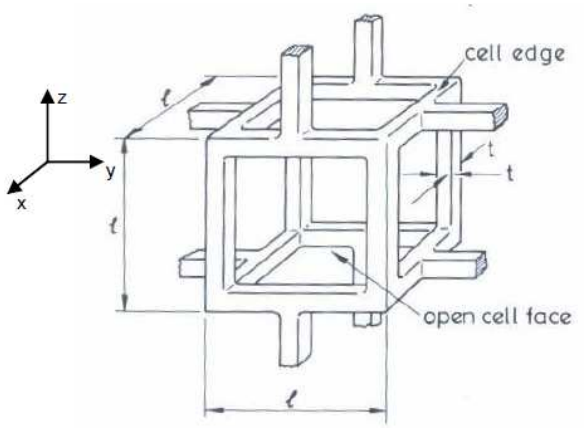

Figure 3.5 - Cubic unit cell as provided in Cellular Solids by Gibson and Ashby.

Cell structure in actual foams is more complex and typically not uniform throughout the material. While other equations could be obtained from more complicated, representative geometry, the properties can be adequately understood using this representation. Rather than properties derived explicitly, the expressions are presented as proportionalities that remain valid if the deformation mechanisms in real foam cells remain consistent with those assumed for the derivation. These proportionalities include constants that arise as the result of specific geometric cell configurations that are more representative of actual foam specimens.

Gibson and Ashby derive the expressions for elastic properties using standard beam theory and the stress and strain relationship of the entire cell. The global compressive stress is proportional to the force transmitted to the ligament, while the global strain is proportional to the displacement. These relationships are then combined using Hooke's law of elasticity to determine expression for the elastic modulus

$$E^* = \frac{\sigma}{\varepsilon} = \frac{C_1 E_s I}{l^4} \tag{3.3}$$

Using this representation of a unit cell, the relative density and second moment of area of a ligament can be related to these dimensions by $\rho^*/\rho_s \propto (t/l)^2$ and $I \propto t^4$.

$$\frac{E^*}{E_s} = C_1 \left(\frac{\rho^*}{\rho_s}\right)^2 \tag{3.4}$$

for open cell foams. The constant C_1, includes the constants of proportionality and is determined from tests data to be approximately equal to one. The shear modulus is similarly derived. Deformation under an applied shear stress is again characterized by cell wall bending. The deflection, δ, is proportional to Fl^3/E_sI, and the overall stress, η, and strain, γ, are proportional to F/l^2 and δ/ℓ, respectively. The shear modulus can be written as

$$G^* = \frac{\tau}{\gamma} = \frac{C_2 E_s I}{l^4} \tag{3.5}$$

or

$$\frac{G^*}{E_s} = C_2 \left(\frac{\rho^*}{\rho_s}\right)^2 \tag{3.6}$$

and C_2 is approximately equal to 3/8. Poisson's ratio of a foam, v^*, is defined as the negative ratio of transverse to axial strain. Poisson's ratio is a constant, independent of the relative density of the foam and a function only of the cell shape of the foam. Using Hooke's Law for isotropic material, Poisson's ratio for foam material can be determined to be

$$\nu^* = \frac{C_1}{2C_2} - 1 \approx 0.3 \tag{3.7}$$

However, this definition of Poisson's ratio is valid only for isotropic materials like the network of cubic cells idealized by Gibson and Ashby.

Figures 3.6 and 3.7 are examples of material property charts [80]. They give an overview of the main properties of metal foams.

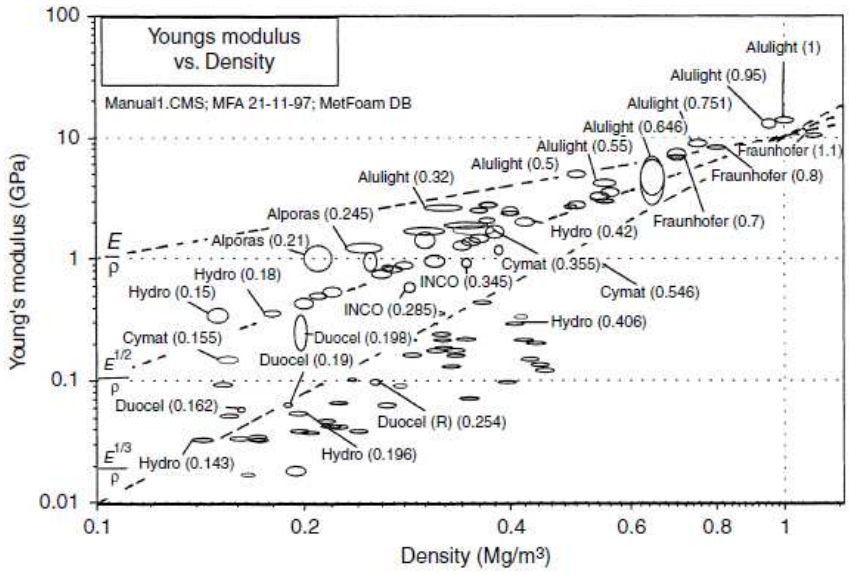

Figure 3.6 - Young's modulus plotted against density for currently available metal foams. Output from CES3.1 with the MetFoam '97 database.

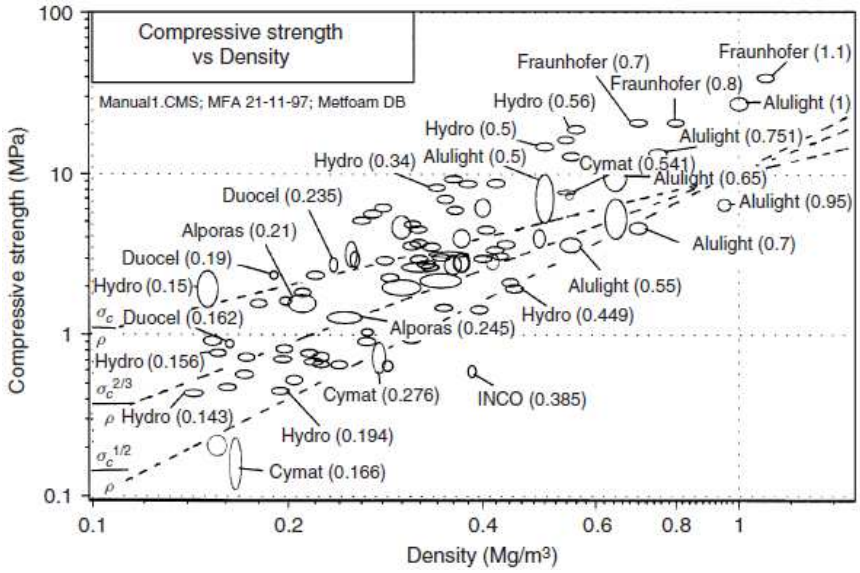

Figure 3.7 - The compressive strength plotted against density for currently available metal foams. Output from CES3.1 with the MetFoam '97 database.

3.5 Fatigue phenomena in metal foams

When a metallic foam is subjected to tension–tension loading, the foam progressively lengthens to a plastic strain of about 0.5%, due to cyclic ratcheting. A single macroscopic fatigue crack then develops at the weakest section, and progresses across the section with negligible additional plastic deformation. Shear fatigue also leads to cracking after 2% shear strain. In compression–compression fatigue the behaviour is substantially different. After an induction period, large plastic strains, of magnitude up to 0.6 (nominal strain measure) gradually develop and the material behaves in a quasi-ductile manner. The underlying mechanism is thought to be a combination of distributed cracking of cell walls and edges, and cyclic ratcheting under non-zero mean stress. Three types of deformation pattern develop:

- Type I behaviour. Uniform strain accumulates throughout the foam, with no evidence of crush band development. This fatigue response is the analogue of uniform compressive straining in monotonic loading. Type III behaviour has been observed for the Duocel foam Al-6101-T6, as shown in Figure 3.8(a). Data are displayed for various values of maximum stress of the fatigue cycle σ_{max} normalized by the plateau value of the yield strength, σ_{pl}.

- Type II behaviour. Crush bands form at random non-adjacent sites, causing strain to accumulate, as sketched in Figure 3.8(b). A crush band first forms at site (1), the weakest section of the foam. The average normal strain in the band increases to a saturated value of about 30% nominal strain, and then a new crush band forms elsewhere (sites (2) and (3)), as is sometimes observed in monotonic tests.
- Type III behaviour. A single crush band forms and broadens with increasing fatigue cycles, as sketched in Figure 3.8(a). This band broadening event is reminiscent of steady-state drawing by neck propagation in a polymer. Eventually, the crush band consumes the specimen and some additional shortening occurs in a spatially uniform manner.

A comparison of Figures 3.8(a)–(b) shows that all three types of shortening behaviour give a rather similar evolution of compressive strain with the number of load cycles. Large compressive strains are achieved in a progressive manner. In designing with metal foams, different fatigue failure criteria are appropriate for tension–tension loading and compression–compression loading. Material separation is an appropriate failure criterion for tension–tension loading, while the initiation period for progressive shortening is appropriate for compression–compression loading.

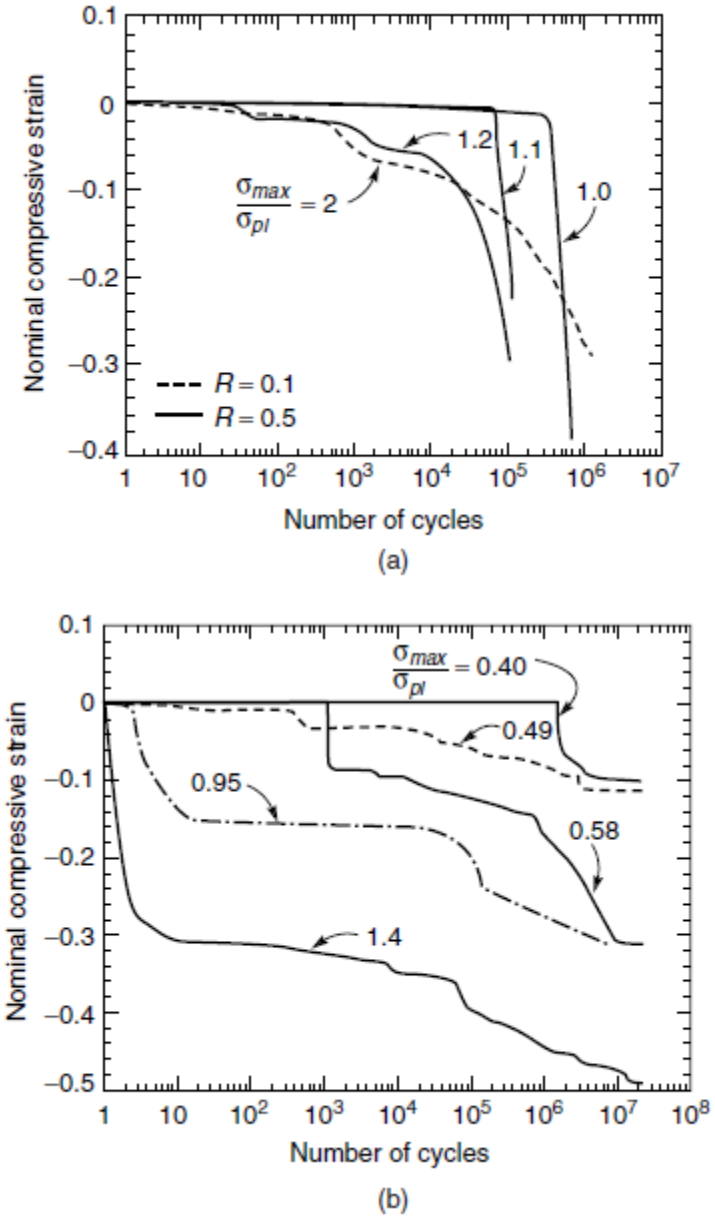

Figure 3.8 - Progressive shortening behaviour in compression–compression fatigue for a Duocel Al-6101-T6 foam of relative density 0.08. (b) Progressive shortening behaviour in compression–compression fatigue for Alcan foam (relative density 0.057; R=*0.5).*

3.5.1 S–N data for metal foams

Test results in the form of S–N curves are shown in Figure 3.9 for a Duocel Al-6101-T6 foam of relative density 0.08 [83]. Tests have been performed at constant stress range, and the number of cycles to failure relates to specimen fracture in tension–tension fatigue, and to the number of cycles, N_I, to initiate progressive shortening in compression–

compression fatigue. An endurance limit can usefully be defined at 10^7 cycles. The number of cycles to failure increases with diminishing stress level. The fatigue life correlates with the maximum stress of the fatigue cycle, σ_{max}, rather than the stress range for all the foams considered: compression-compression results for R=0.5 are in good agreement with the corresponding results for R=0.1, when σ_{max} is used as the loading parameter. There is a drop in fatigue strength for tension–tension loading compared with compression–compression fatigue. The fatigue strength is summarized in Figure 3.10 for the various aluminum foams by plotting the value of σ_{max} at a fatigue life of 10^7 cycles versus relative density [80]. The values of σ_{max} have been normalized by the plateau value of the yield strength, σ_{pl}, in uniaxial compression. The fatigue strength of fully dense aluminum alloys has also been added: for tension–tension loading, with R=0.1, the value of σ_{max} at the endurance limit is about 0.6 times the yield strength. The fatigue strength of aluminum foams is similar to that of fully dense aluminum alloys, when the fatigue strength has been normalized by the uniaxial compressive strength. There is no consistent trend in fatigue strength with relative density of the foam.

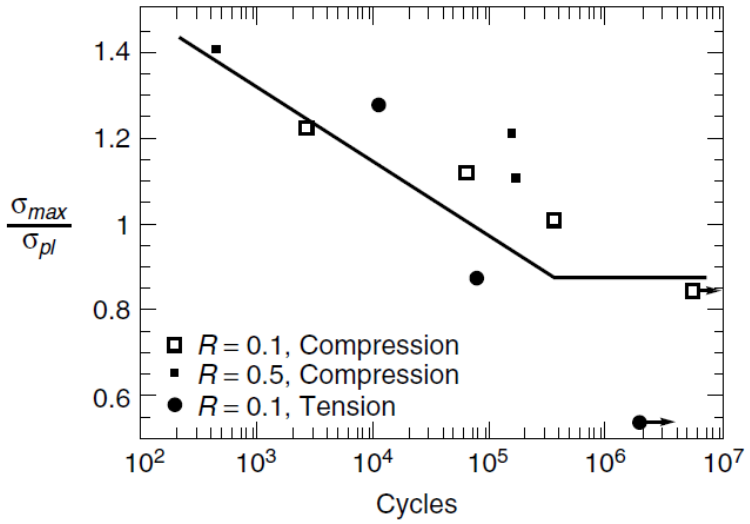

Figure 3.9 - S–N curves for compression–compression and tension–tension fatigue of Duocel Al-6101-T6 foam of relative density 0.08.

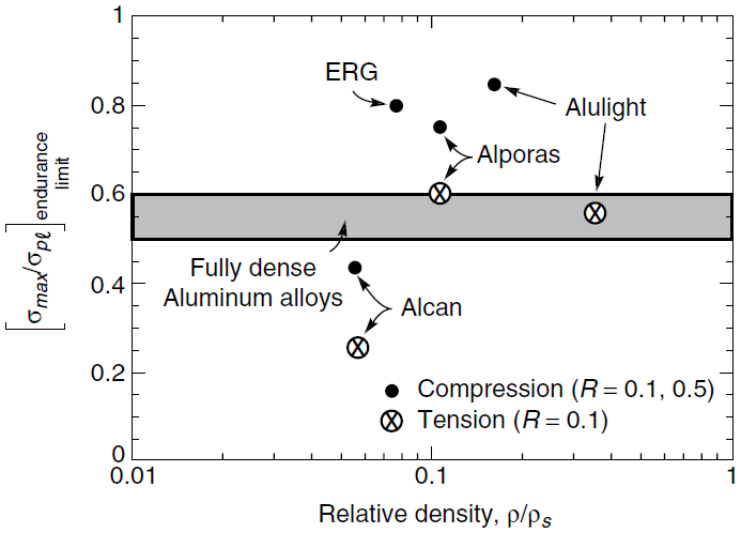

Figure 3.10 - Ratio of σ_{max} at the endurance limit to the monotonic yield strength σ_{pl} for foams, compared with that for tension–tension fatigue of fully dense aluminum alloys at R=0.1.

3.6 Thermal properties

The melting point, specific heat and expansion coefficient of metal foams are the same as those of the metal from which they are made. The thermal conductivity is given by the following equation:

$$\lambda^* \approx \lambda_s \left(\frac{\rho}{\rho_s}\right)^q \tag{3.8}$$

where q varies from 1.65 to 1.8.

3.7 Pressure drop and heat transfer correlations

Pressure drop and heat transfer coefficient are the two important factors to be considered in designing a heating and cooling system. Different models have been developed in the past 150 years to characterize the fluid flow in a porous matrix on the basis of macroscopically measurable flow quantities. The first of these models can be traced back to Darcy's publication in 1856. He established the well-known Darcy's law

which states that the pressure-drop per unit length for a flow through a porous medium is proportional to the product of the fluid velocity and the dynamic viscosity (later added by Krüger [84]), and inversely proportional to the permeability.

The porous medium's permeability is denoted with K [m^2], and it gives a measure of the ability that the material offers to a fluid to penetrate it, connecting the mean flow velocity of the fluid inside the pores, with the pressure drop in the porous medium:

$$\frac{\Delta P}{L} = \frac{\mu}{K} U + \rho \frac{C_f}{\sqrt{K}} U^2 \tag{3.9}$$

where C_f is the inertia coefficient and L is the length of the medium in the flow direction. If only the first term of the right hand side of Eq. (3.9) is retained, it becomes Darcy's law expressing the normalized pressure drop for low velocity values through porous media and is easily recognized as a linear relation between pressure drop per unit length and bulk velocity. The second term introduces the Forcheimer–Dupuit expansion, referring to higher flow velocities. Both K and C_f are strongly related to the structure of the medium.

One of the systematic evaluations of permeability and inertia coefficient of metal foams is done by Vafai and Tien [85] utilizing experimental and theoretical investigations. They reported values of 1.11×10^{-7} m^2 and 0.057 for permeability and inertia coefficient, respectively in a manner similar to those experimentally reported later [86]. As for the Reynolds number in porous media, its definition depends on the value used for its computation while the velocity used is usually the Darcian (bulk) or mean flow velocity. Use of the ligament diameter (t) gives the following definition:

$$Re = \frac{\rho U t}{\mu} \tag{2.10}$$

where U is the flow (bulk) velocity through the porous medium and μ is the dynamic viscosity of the fluid.

CHAPTER 4

DESIGN OF AN INNOVATIVE HEATING/COOLING SYSTEM BASED ON THE USE OF METAL FOAMS

The numerical investigation of the innovative rapid thermal cycling system, based on the use of open-cell aluminum foam, is the main topic of this chapter. In conventional moulding, the insert is supported by a rigid mould base. This construction ensures that the cavity keeps its strength and the dimensional accuracy under high process pressures. However, in rapid thermal cycling, the rapid change of the mould temperature, the reduced thermal mass introduces more complex design problems that require special attention to the mould strength and deformation, buckling, thermal expansion and heat loss. The advent of computer-aided engineering (CAE) technology for plastic injection moulding provides a large support to mould design. Different simulation modules allow precise determination of the effectiveness of the mould cooling system at the desired mould temperature, avoiding some mould defects.

In the present work, CAE and CFD simulations were performed for the proposed heating and cooling system based on the use of porous inserts. A mould for tensile specimens with double gates in order to obtain the weld line was designed. First an estimation of the maximum stress and deflection, the thermal expansion and fatigue of the mould will be discussed. Then the heating and cooling performance analysis of the proposed method will be presented. The CAE results illustrate the feasibility of the proposed approach in designing new rapidly heatable and coolable systems based on the use of metallic foams.

4.1 Geometrical properties

Two piece of aluminum metal foams was acquired from ERG Aerospace (Figure 4.1). The metal foam was produced from 6101 aluminum alloy, retaining 99% purity of the parent alloy.

Figure 4.1 - Open-cell aluminum metal foam sample.

The technical characteristics, provided by the material supplier, are listed in Table 4.1. The fibre diameter and the length of the fibre between two adjacent vertices were measured by analyzing different high resolution photos, as suggested by Richardson et al. [87]. Figure 4.2 shows a photo used for the measurement of fibre thickness and length of the cell edge. The measurement were carried out using the control measuring machine Werth Video Check IP-400 CNC.

Table 4.1 - Properties of the aluminum foams provided by ERG Inc..

PPI [pore/inch]	**Relative density [%]**	**Porosity, ε [-]**
5	7.9	0.921

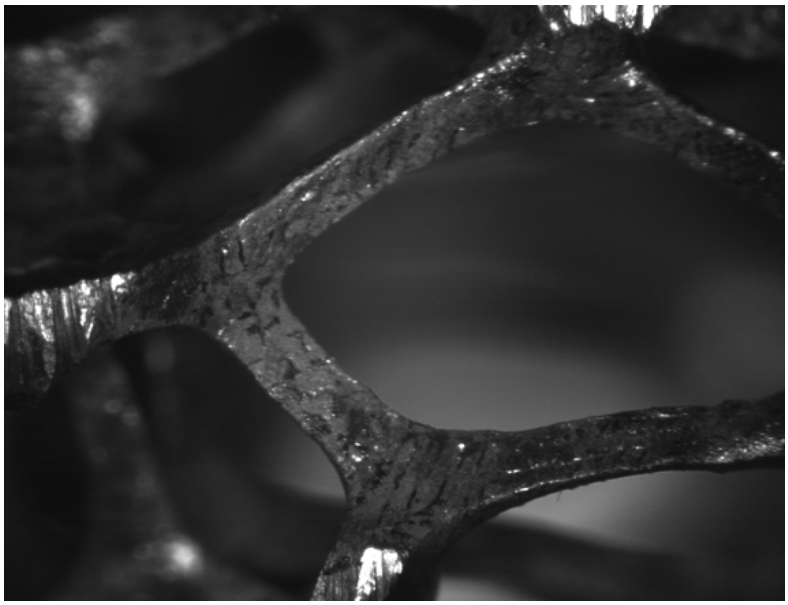

Figure 4.2 - Photo for the measurement procedure of fibre thickness and cell edges.

Starting from the measured values, it is possible to follow two different ways: the first is to calculate the porosity starting from the measured properties, while the second consists in the fibre length evaluation using the measured fibre thickness and the relative density provided by the supplier. In this work the results were obtained using the measured geometrical properties. The porosity was calculated by applying Eq. 3.1 and Eq. 3.2. It is interesting to highlight that the tetrakaidecahedron structure appears to be in good agreement with the provided porosity. Several measures for each photo were collected and then statistically analysed. The frequency of the different classes was calculated and then a normal distribution was applied. The results of the measurements are reported in Table 4.2, in terms of mean value, maximum value, minimum value and standard deviation.

Table 4.2 – Measurement of cell dimensions.

	Mean value [mm]	**Maximum value [mm]**	**Minimum value [mm]**	**Standard deviation [mm]**
Fibre thickness, t	0.54	0.685	0.389	0.050
Fibre length, l	1.96	3.569	0.910	0.499

4.2 Mould design

The heating and cooling system design are of great importance because they directly affect the heating/cooling efficiency and temperature uniformity. For an efficient temperature cycle moulding it is essential that the tool has low thermal mass. The energy input for tool heating must be minimized by appropriate tool design. Heating and cooling must be confined to a region close to the cavity surface, both to reduce energy use and to provide rapid heat transfer to and from the cavity surface. The mould temperature uniformity is crucial for the thermal stress development. In a rapid thermal cycling process the cooling uniformity is more important than the heating uniformity in the sense that the majority of the thermal stresses are due to the non-uniform and unbalanced cooling. The global cooling uniformity refers to the temperature variance of the entire mould and is ensured by minimizing the temperature drop along cooling lines. The local cooling uniformity refers to the temperature variance on the mould surface between two adjacent cooling channels. It is ensured by proper design of the location and the size of cooling channels.

In this work a new mould, based on the use of open-cell aluminum foam, was designed. Figure 4.3 gives a schematic representation of the RHCM mould. A cavity for the tensile specimens was obtained on a steel plate P20 of dimensions of 136×220×9 mm. The particular feeding system allow the specimens to be moulded generating a weld line located right in the middle of the part. The specimen dimensions are based on UNI EN ISO 527 (Type 1A) [98]. The plate was fixed with 6 screws. Figure 4.4, Figure 4.5 and Figure 4.6 show the cavity, the core and the plate for tensile specimens, respectively. The pieces of aluminum foam were connected to the rest of channels system. The block dimensions were 140×33×20 mm. The cooling channels with a diameter of 6 mm were placed at 12 mm from the mould surface. Figure 4.7 shows the CAD model of the new mould with metallic foams for the RHCM process. Instead of conventional channels, the entire space below the cavity can be used for heating and/or cooling, while the metallic foam allows an efficient through flow of water. The metallic foam provides mechanical support and simultaneously generates a cavity structure.

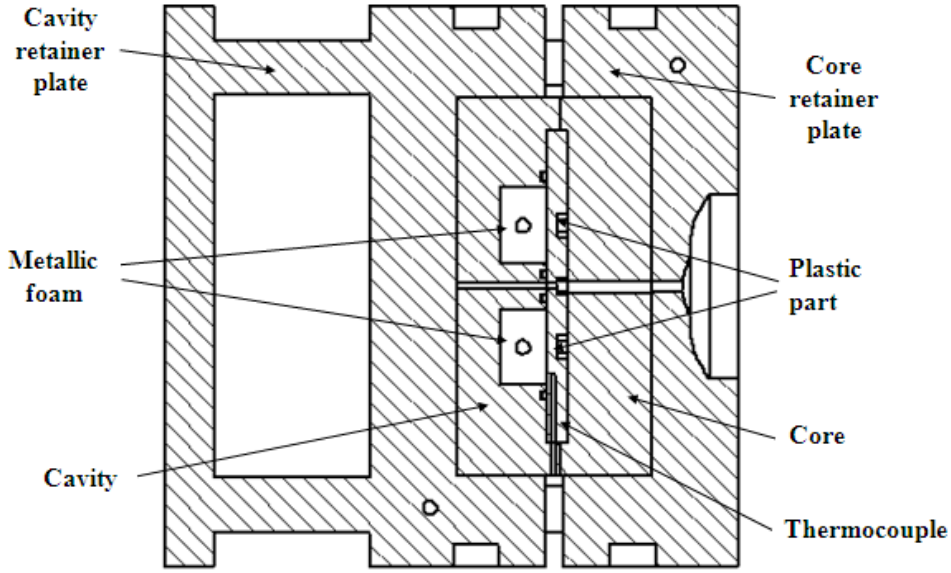

Figure 4.3 - Schematic structure of the RHCM mould with metallic foams.

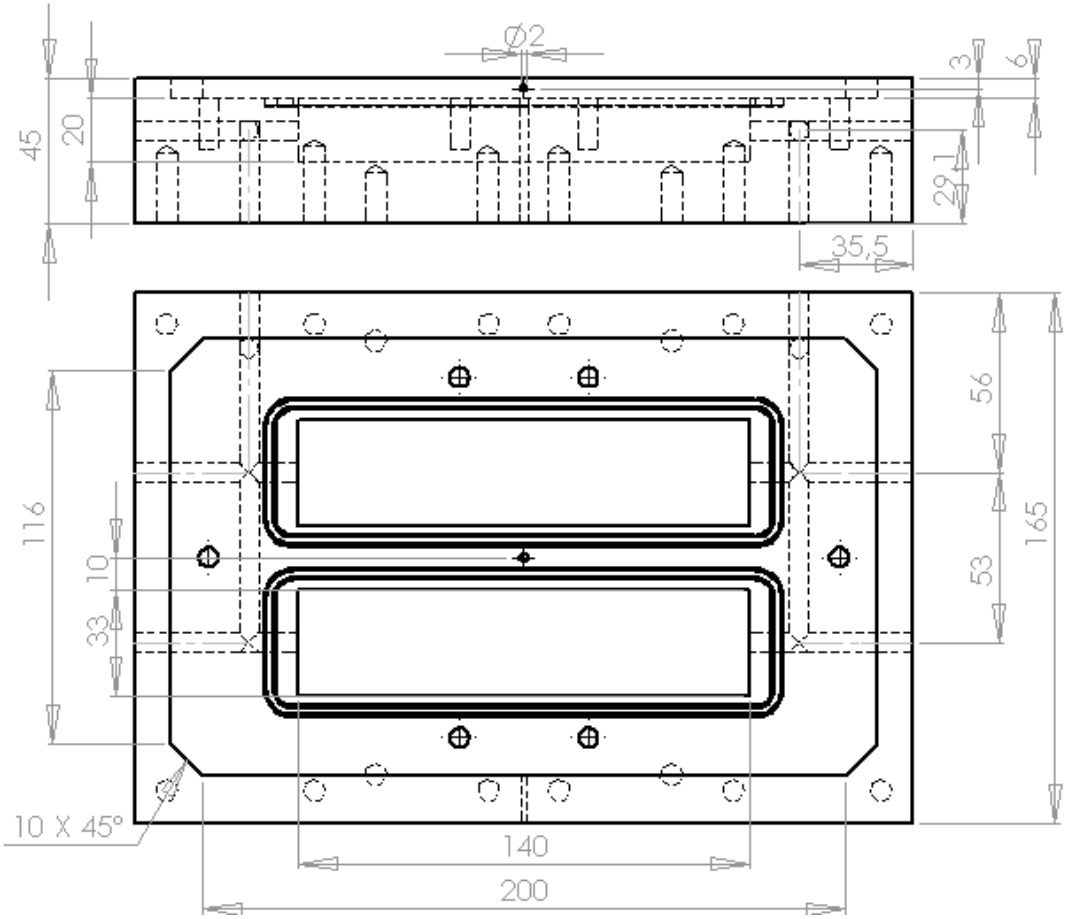

Figure 4.4 - Mobile insert drawing.

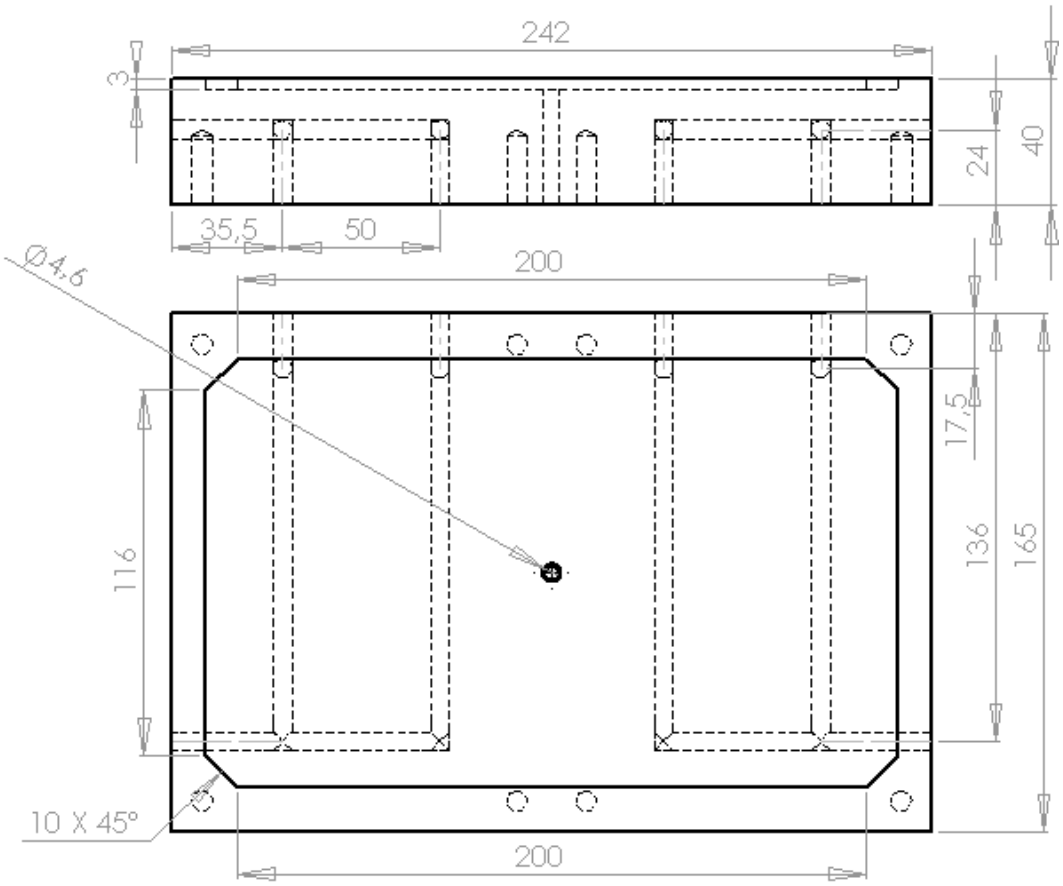

Figure 4.5 - Fixed insert drawing.

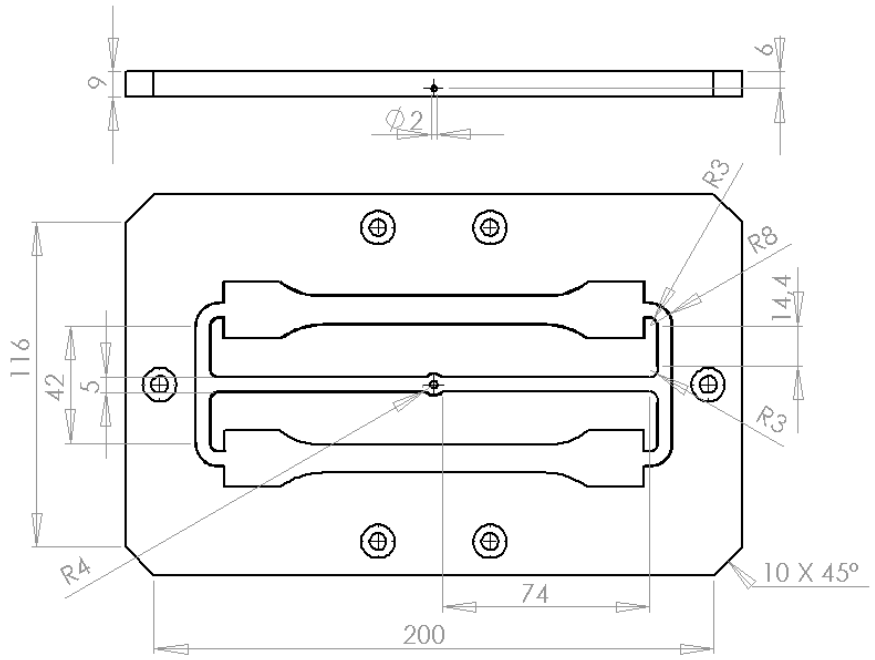

Figure 4.6 - Plate drawing.

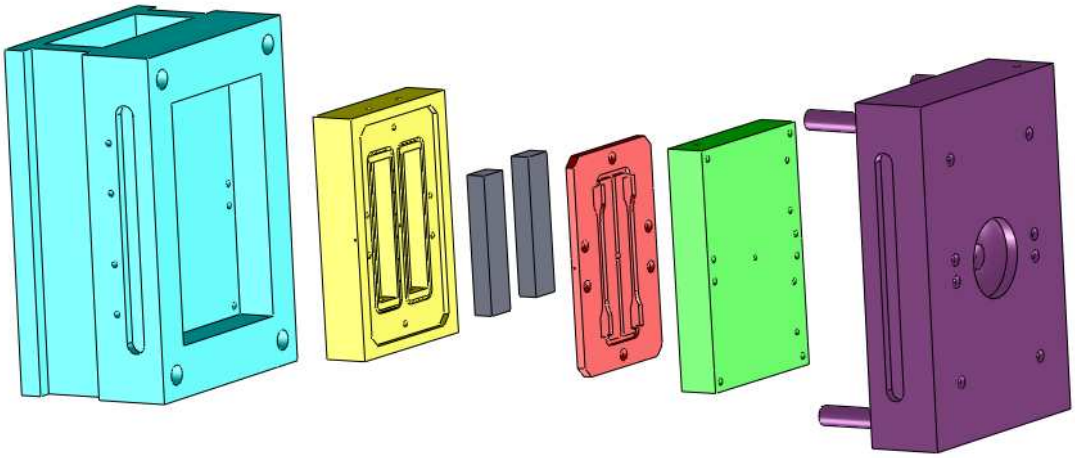

Figure 4.7 - CAD model of experimental mould.

4.3 Mechanical properties investigation

The mechanical performance of an injection mould is important as it directly affects the durability of the injection moulded part production. Minimizing mould deflection is essential when manufacturing plastic parts to tight tolerances. Therefore, understanding mould deflection during injection moulding is critical for determining the final geometry of the part. It is necessary to select a suitable mould material to prevent any deterioration during the moulding process and to withstand the mechanical impact during the locking process. During mould opening and closing in injection moulding, the mould plates are loaded by the clamping force and injection pressure. The stress could be investigated by the following equations. The maximum stress S_{max} under load W is:

$$S_{max} = -\frac{WL}{4Z} \tag{4.1}$$

where Z is the section modulus in mm^3.

$$Z = \frac{1 \times d^2}{6} \tag{4.2}$$

where the unit width is 1. S_{max} must be equal to or less than the critical fatigue stress developed by the mould plate.

The RHCM mould must be heated to a high temperature and cooled to the ejected temperature during the injection moulding process, where the peak temperature of the mould is about 110–135 °C in an injection cycle. Compared with the conventional injection mould, both the peak temperature and temperature gradient are much higher during the injection moulding process. Therefore, thermal stress of the RHCM mould caused by the temperature is much greater than the one of the conventional mould. As the porous structure of the metallic foams provides less regular support than a solid volume, the mechanical strength of the injection mould have to be high enough to withstand the force and stress from mould opening, closing and locking. A structural simulation was carried out in order to evaluate the tension field and the deformation of the foam inserts during the polymer injection phase. A linear elastic analysis was performed using ANSYS® Workbench 12.1. The cavity pressure for the mould deflection analysis was predicted using a coupled flow-thermal model. The mould cavity pressure was then used as input for the subsequent finite element mould deflection analysis.

4.3.1 Meltflow analysis

The cavity pressure for the mould deflection analysis was predicted using a coupled flow-thermal model in Autodesk Moldflow® Insight 2010. The plastic material used in this study was ABS Terluran KR 2922 supplied by Basf®. The melt density, thermal conductivity, and specific heat at about 220 ^{o}C are respectively 0.93 g/cm^3, 0.16 W/(m ^{o}C), and 2155 J/(kg ^{o}C). The material was characterized on a differential scanning calorimeter (TA Instruments Q200). The transition temperature was estimated in 95.35°C, as shown in Figure 4.8. On the other hand, the thermal conductivity and the specific heat in function of the temperature were set according to the Moldflow® database. In this software the viscosity is modelled by the Cross-WLF viscosity model equations. The model coefficients used in the numerical simulation have been set forth in Table 4.3.

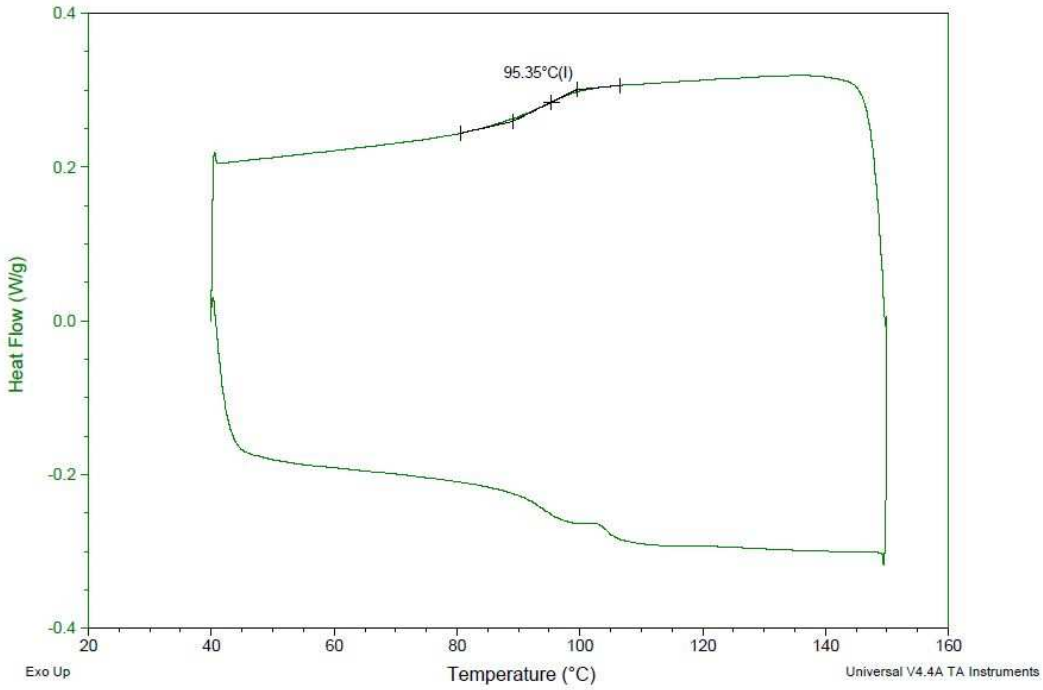

Figure 4.8 - DSC analysis result for the glass transition temperature.

Table 4.3 – Cross-WLF model coefficient for ABS Terluran KR 2922.

Cross-WLF parameters	Unit	Value
n		0.349
τ	Pa	23270
D_1	Pa·s	3.047E+016
D_2	K	343.15
D_3	K/Pa	0
A_1		38.637
A_2	K	51.6

The temperature of the cavity surface before melt injection was set at 10°C higher than the glass transition temperature. The injection speed and the melt temperature were set to the highest limits of the moulding window in order to decrease the viscosity of the polymer during the injection phase. The processing conditions are summarized in Table 4.4.

Table 4.4 – Process parameters.

Process parameters	Unit	Value
Melt temperature	°C	250
Mould temperature	°C	105
Injection speed	mm/s	50
Holding pressure	MPa	15
Holding time	s	7
Ejection temperature	°C	60
Water temperature (heating stage)	°C	130
Water temperature (cooling stage)	°C	30

The model was discretized into 31728 elements. The mesh was generated by the Moldflow® program automatically. A sensitivity analysis of software simulation to the mesh dimension was conducted. Once the model was concluded, the boundary conditions were accurately defined. The geometrical model, including feed system, is shown in Figure 4.9.

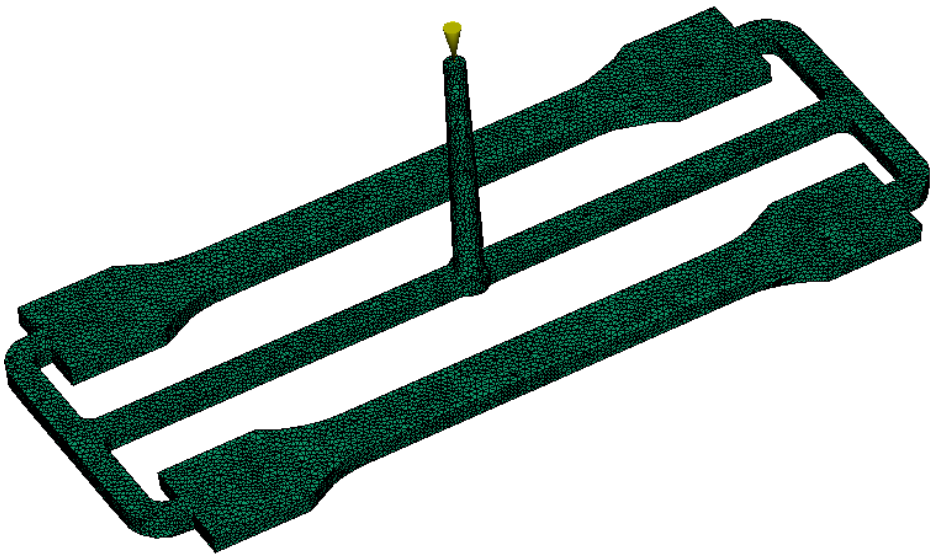

Figure 4.9 - Complete mesh model.

A significant pressure jump versus filling time can be observed in the filling simulation results. Figure 4.10 shows a maximum cavity pressure of 15.31 MPa into the sprue (Figure 4.10). The pressure in the cavity is slightly lower. In the structural simulation the cavity pressure was considered uniform and equal to the maximum value of 3.5 MPa, which was predicted near the gate, as shown in Figure 4.11.

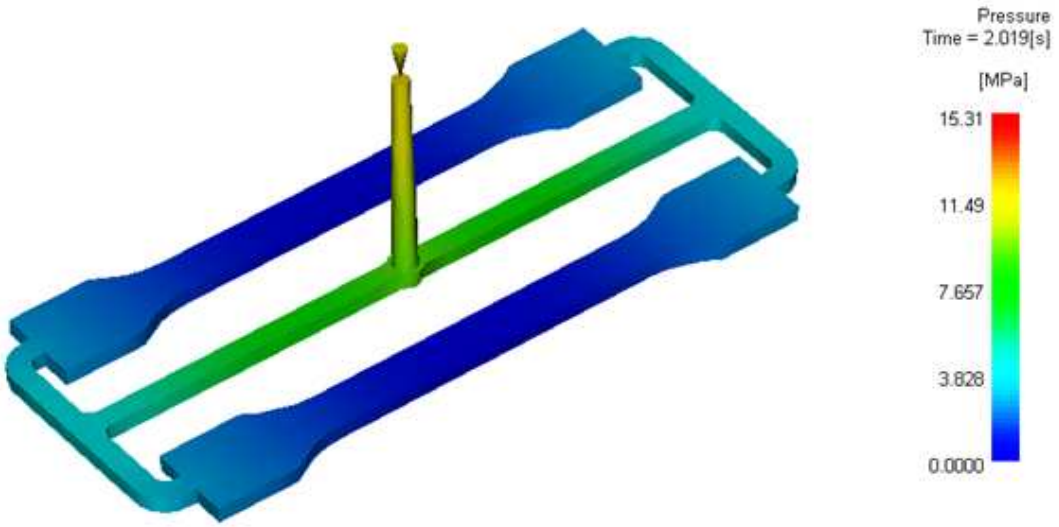

Figure 4.10 - Pressure distribution during cavity filling.

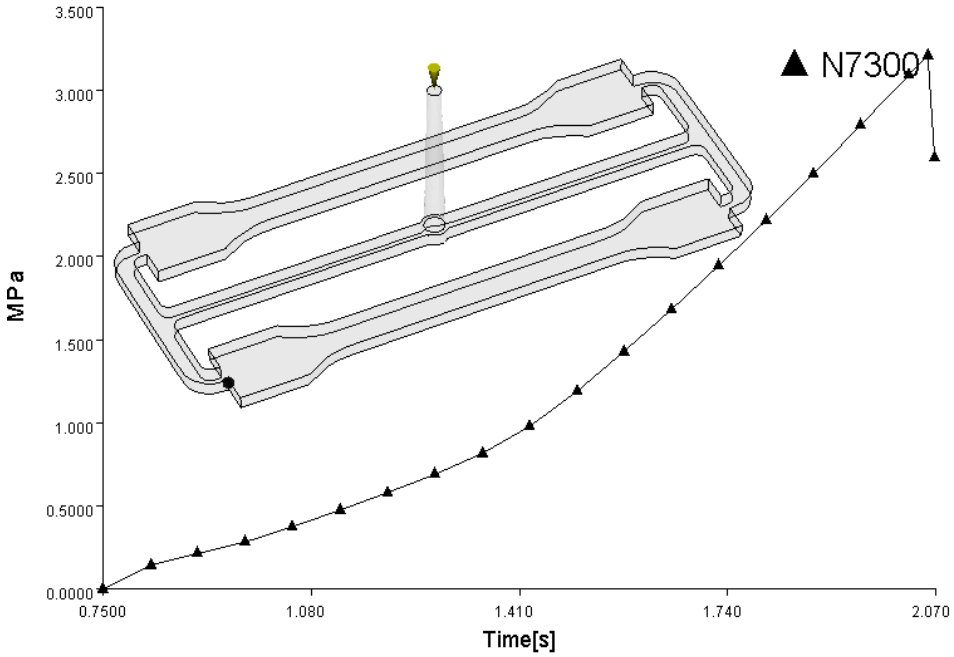

Figure 4.11 - The time evolution of cavity pressure during the filling stage.

4.3.2 Mould strength and deflection

A structural simulation was carried out in order to evaluate the tension field and the deformation of the metallic foam during the injection phase. A linear elastic analysis was performed. The metallic foam behaviour was obtained by homogenizing of microstructures for determining the properties of the entire material. The mechanical and thermal properties of the aluminum foam are shown in Table 4.5 and Table 4.6.

Table 4.5 - Mechanical properties of the aluminum foam and mould.

Name	Young's modulus (MPa)	Shear modulus (MPa)	Poisson's ratio	Compressive yield strength (MPa)
Aluminum foam	453	169.9	0.3	2.53
Mould	2×10^{5}	7.69×10^{4}	0.3	250

Table 4.6 - Thermal properties of the aluminum foam and mould.

Name	Thermal conductivity (W/m°C)	Heat capacity (J/kg°C)	Coefficient of thermal expansion 0-100°C (m/m°C)	Density (kg/m^3)
Aluminum foam	9	895	23×10^{-6}	213,3
Mould	34	460	12×10^{-6}	7850

The five components used for this model are: the movable mould half, the fixed mould half, the fixed insert, the mobile insert and the plate for tensile specimens. Clamping pressure and cavity pressure constitute the loading on the mould and the injection-moulding machine throughout the moulding process. Because of the symmetry of the components, the displacement boundary conditions, and the cavity and clamping pressures, a quarter symmetry model was utilized in the structural simulations. Contact was defined between the mould halves and between the mould halves and their inserts. In every injection cycle, the temperature and temperature gradient of the mould vary greatly.

Accordingly, the thermal load is applied to the mould insert. All the boundary conditions except the thermal load imposed on the model are shown in Figure 4.12. The finite element model of the mould is shown in Figure 4.13. When all the boundary conditions are imposed on the model, the distribution of the stress and strain of the model can be obtained through the transient heat and stress finite element analysis.

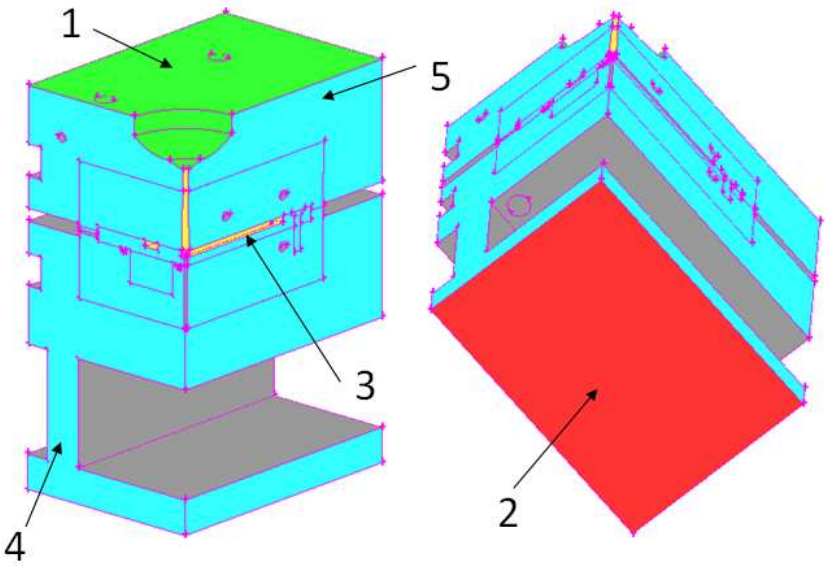

Figure 4.12 – Boundary conditions: 1 fixed constraint, 2 clamping pressure, 3 cavity pressure, 4-5 symmetrical faces.

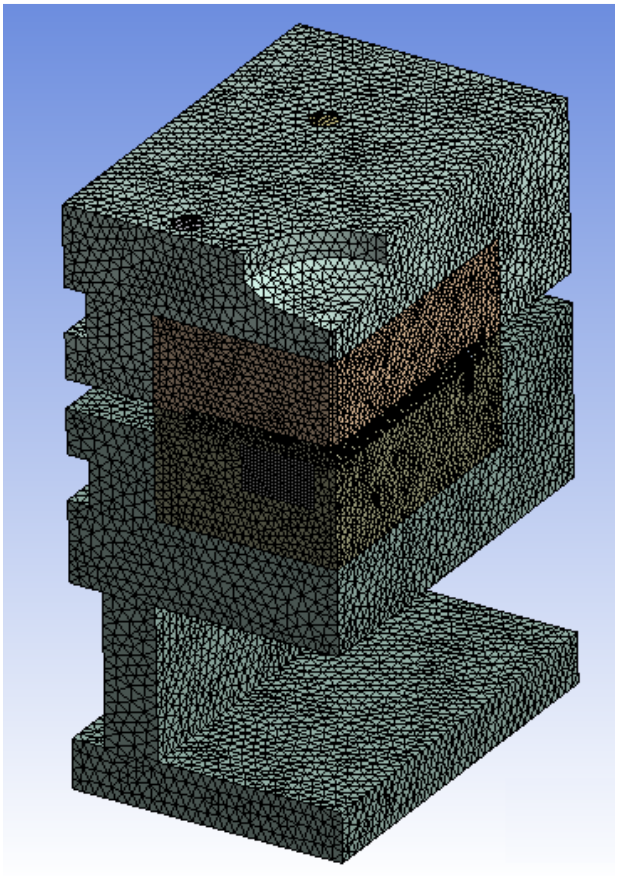

Figure 4.13 – Finite element model.

As shown in Figure 4.14, the maximum elastic deformation of the cavity surface is 0.116 mm, which confirms that the metallic-foam inserts provide the necessary structural support with low deformations. The calculated maximum stress of the aluminum foam (about 0.217 MPa) is in the elastic field, in accordance with the previous assumption (Figure 4.15). Since the thickness of the tensile specimen is 4 mm, the product thickness will be reduced by about 2.69%, if the thermal distortion in heating process is not considered in mould design and processing. It can be seen from Figure 4.16 that there is a stress concentration at the wall of the cavity and the maximum von-Mises stress is 50.41 MPa. In the following cooling stage, the concentration stress decreases gradually to 6.85 MPa. In the next moulding cycle, the cavity block is heated again and the thermal stress caused by thermal expansion increase gradually again to the maximum value. Owing to the frequent alternating concentration and release of such large stress in RHCM process, fatigue cracks may occur at the position of stress concentration and cause cavity damage.

It has been found in actual production that fatigue cracking at the position of stress concentration is the typical fatigue damage mechanism for RHCM mould.

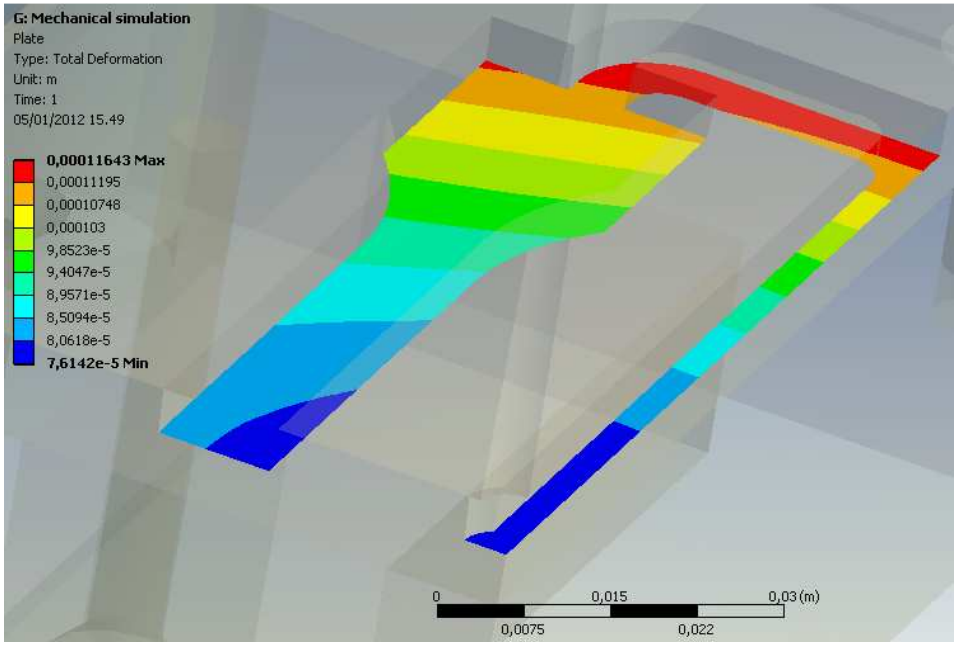

Figure 4.14 - Distribution of the cavity deformation.

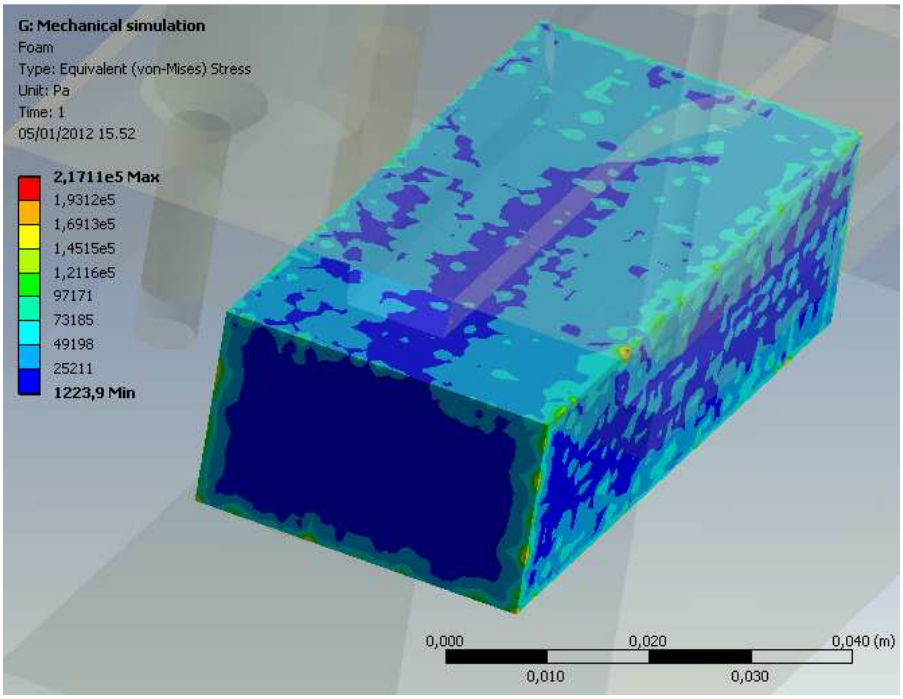

Figure 4.15 - The distribution of equivalent (von Mises) stress at 105°C resulting from the mechanical simulation.

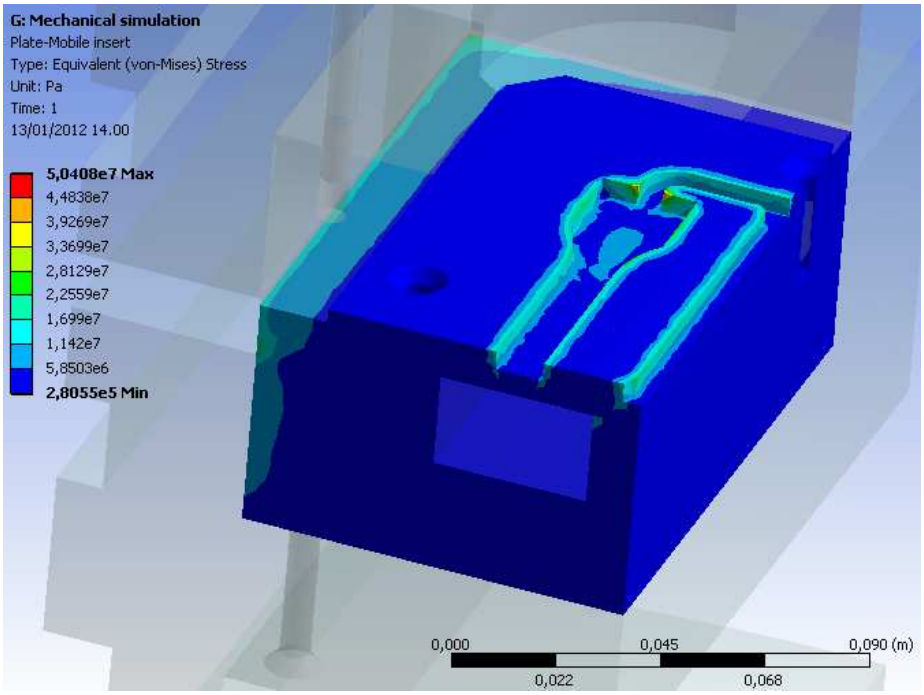

Figure 4.16 - The distribution of equivalent (von Mises) stress at 105°C resulting from the mechanical simulation.

4.4 Fatigue analysis

As the mould stands a great clamp force repeatedly in injecting and packing stages, the stress suffered by the RHCM mould is the combination of thermal and mechanical stresses, and it is cycle stress. In addition, there are many other factors that influence the mould lifetime. Therefore, fatigue cracks will appear more easily on the RHCM mould than that on the conventional mould. The local stress–strain method is used in this part of the work to estimate the local crack initiation lifetime in the mould. It is based on the strain–life curve [89]:

$$\frac{\Delta\varepsilon}{2} = \frac{\sigma_f'}{E}\left(2N_f\right)^b + \varepsilon_f'\left(2N_f\right)^c \tag{4.3}$$

where, Δε is the total strain amplitude, and $2N_f$ is the number of half cycles, reversals, to failure. σ_f' is the regression intercept called fatigue strength coefficient, and it is

considered to be a material property with the fatigue strength coefficient that is approximately equal to the monotonic fracture stress σ_f, It is the failure load divided by the true area when the specimen fractured. E is the modulus of elasticity. b denotes the regression slope called the fatigue strength exponent, and it is the slope of $lg(\Delta\varepsilon_e/2)$-$lg(2Nf)$ which shows the relationship of the elastic strain amplitude and lifetime in double logarithmic coordinates. ε_f' is the regression intercept called fatigue ductility coefficient, and it is approximately equal to the monotonic fracture strain, ε_f. $\varepsilon_f = ln(L_f/L_0)$ where, L_0 is the length of the specimen when there is no load and L_f is fractured length. c stands for the regression slope called the fatigue ductility exponent, and it is the slope of $lg(\Delta\varepsilon_p/2)$-$lg(2Nf)$ that shows the relationship of the plastic strain amplitude and lifetime in double logarithmic coordinates. The Morrow mean stress correction is used to modify the strain–life curve. The entire strain– lifetime curve becomes:

$$\frac{\Delta\varepsilon}{2} = \frac{\sigma_f' - \sigma_0}{E}\left(2N_f\right)^b + \varepsilon_f'\left(2N_f\right)^c \tag{4.4}$$

where, σ_0 is the mean stress.

Figure 4.17 gives the counter plot of the safety factor with respect to a fatigue failure at the given design life (10^6 loading cycles). The fatigue analysis results show that no fatigue failure occurs within the safety of the design. For the metal foams, the fatigue life was estimated using the S-N curves presented in the paragraph 3.5. During the injection moulding process, the metal foam is loaded by a stress, σ, which varies from -0.095 MPa tat 60°C o – 0.217 MPa and 105°C. The load ratio R is 0.44 and the ratio between the maximum stress and the yield strength is 0.09. For compression-compression loading, with R=0.5, the value of σ_{max} at the endurance limit is about 0.8 times the yield strength. So no fatigue failure occurs within the safety of the design. However, there are many other factors that influence the mould lifetime, as the quality of the tool steel, the surface condition of the mould, the handing maintenance, ect. . These factors could generate fatigue cracks on the RHCM mould, shortening its lifetime.

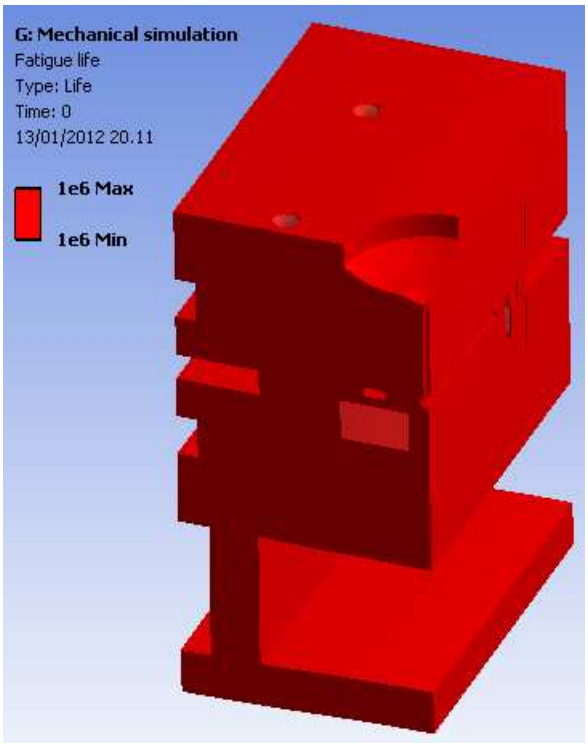

Figure 4.17 – The fatigue life resulting from the mechanical simulation.

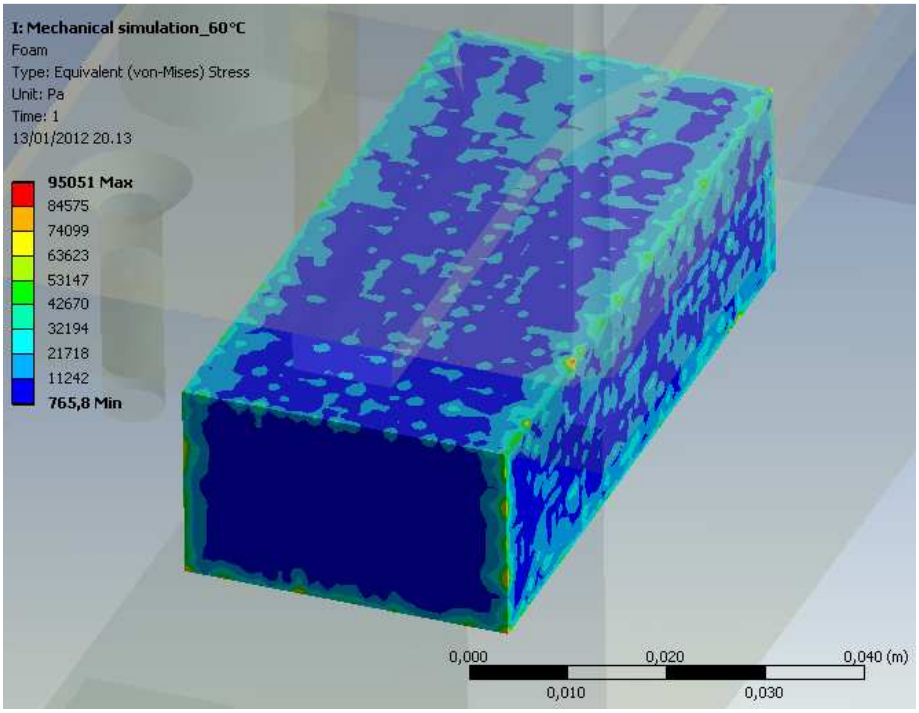

Figure 4.18 - The distribution of equivalent (von Mises) stress at 60°C resulting from the mechanical simulation.

4.5 Cooling performance investigation

The aim of this part of the work was to experimentally investigate the heat transfer during water flow through high porosity open-cell metal foams. A 3D thermal analysis was run simulating a cycle of rapid heating and cooling. Heat transfer during the injection-moulding cycle includes heat exchange originated from polymeric melt to the mould material by conduction. The heat is then conducted from the mould material to the coolant, which flows from the inlet with high fluid pressure and run into the porous structure passageway in the cavity mould half. The coolant brings the heat from the polymer and flows away via the outlet. As the porous structure follows the shape of the mould cavity surface, it increases the contact area of heat transfer from the polymeric melt and a near uniform cooling performance can be achieved.

4.5.1 Simulation methodology

Metal foams present random microstructures consisting of open cells randomly oriented and mostly homogeneous in size and shape. An accurate pore scale model of the flow and heat transfer in the open cell metal foam was developed. The assembly of elementary unit cells forms the conformal conditioning surface which generates a multiple orientation passageway. The limited computational resource didn't allow to apply the accurate pore scale model of the flow and heat transfer in the open cell metal foam to the entire domain. The final computational domain was part of a wider volume of metal foam. The block dimensions, shown in Figure 4.19, were 33×22×10 mm. After the topology of the computational domain was constructed, it was spatially discretized with an unstructured grid of tetrahedral volume elements resulting in a base case mesh of 3.4×10^6 elements. The mesh was generated using Gambit® 2.3.16. Figure 4.20 shows a detail of surface grid on ligament's pore. The geometry constructed was properly mirrored in space, taking advantage of symmetries. Boundary conditions included fixed pressure drop in order to represent fully developed flow, far from inlet–outlet boundaries. The foam pieces were in aluminum with density, of 2700 kg/m^3. In simulation, the heat transfer mode around all external surfaces of plate was set at a free convection to the air; air temperature is 15 °C and heat transfer coefficient is 10 W/(m^2 °C). A cycle of rapid heating and cooling a were done based on this model. The initial mould temperature was

set at 60 °C. Then the mould was heated with water circulating at a temperature of 130 °C until the temperature in correspondence of the thermocouple position reached the temperature of 95 °C. Eventually, the mould was cooled with water at 30 °C. At the beginning, the mould was setup at 60 °C. Figure 4.21 shows the final computational domain used for the thermal analysis. The temperature history in correspondence of the point A was collected (Figure 4.22). The point B was chosen in correspondence of the thermocouple position. In order to evaluate the system efficiency, an heating and cooling system with 6 conventional tempering channels (10 mm diameter with the centre 15 mm beneath the surface) for the same mould was designed and analyzed by means of numerical simulations.

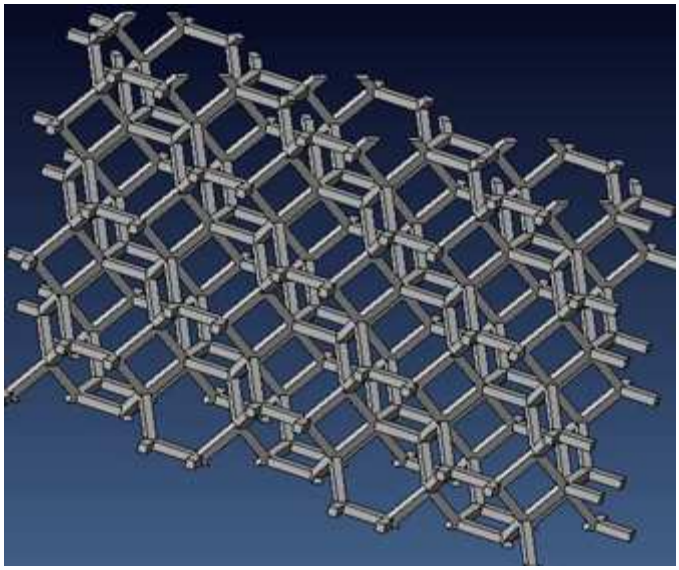

Figure 4.19 - Computational domain constructed after repetition of the metal foam volume.

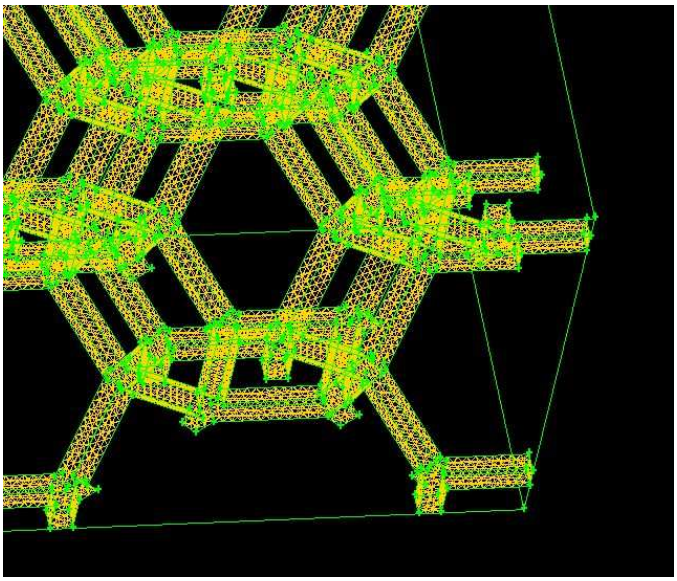

Figure 4.20 – Detail of surface grid on ligament's pore.

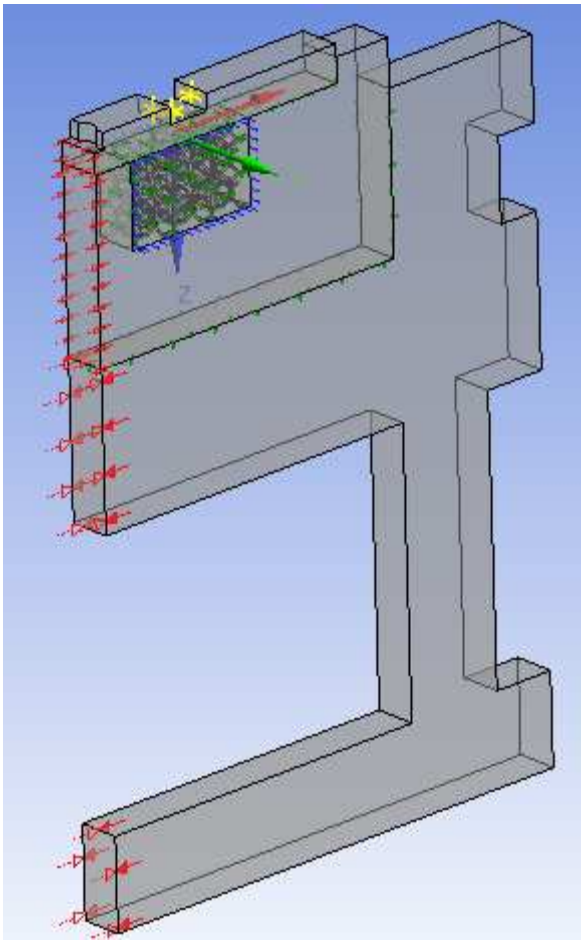

Figure 4.21 – Final computational domain..

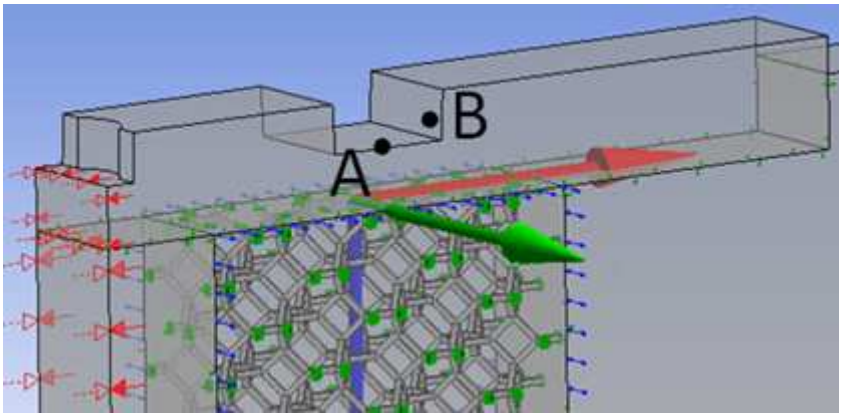

Figure 4.22 – Control points for the evaluation of the temperature history.

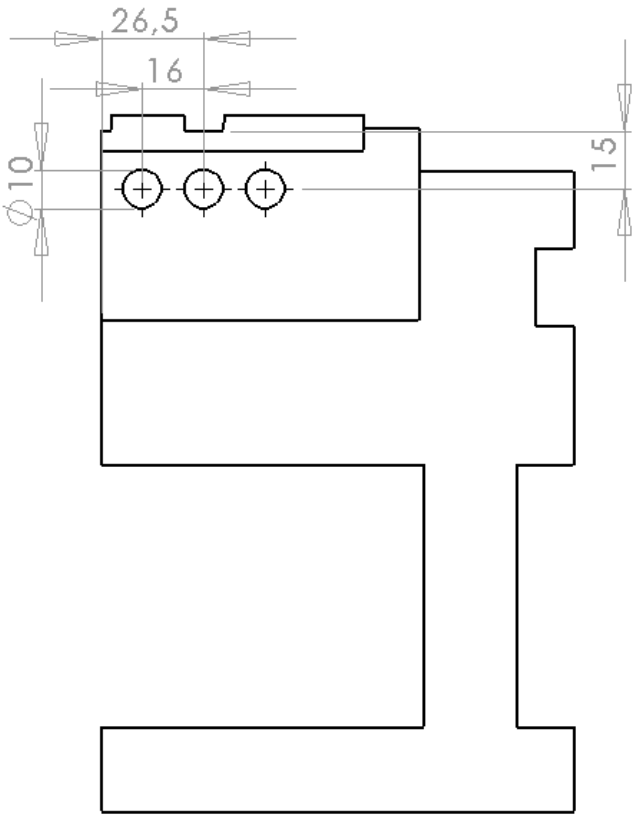

Figure 4.23 – Mould with conventional channels.

4.5.2 Numerical results

Figure 4.24 shows the temperature history in correspondence of the middle of the cavity surface (point A) and the thermocouple position (point B). In this case, the

different temperature between point A and B at the end of the filling stage is about 10 °C. In the heating process and in the previous time of cooling, the temperature at point A is higher than point B; however, at the end of the cooling, the temperature at point B is higher than point A. The cooling and heating time in correspondence of the point B are 18.1 °C/s and 15.9 °C/s, respectively. The temperature at point A is 107 °C (more than 10 °C upper than T_g) at the end of the heating phase. When the heating stage is completed, the temperature distributions and uniformity along the cavity surfaces are all shown in Figure 4.25. It can be seen that the cavity surfaces of the two mould structures have a relatively uniform temperature distribution over a large portion of mould plate, especially in the middle area of the cavity surface. The reason is that the cooling configuration closely matches the shape of the part being moulded. Heat can transfer more evenly from the mould surface. Figure 4.26 shows the temperature distribution at the end of the heating stage for RHCM with conventional channels.

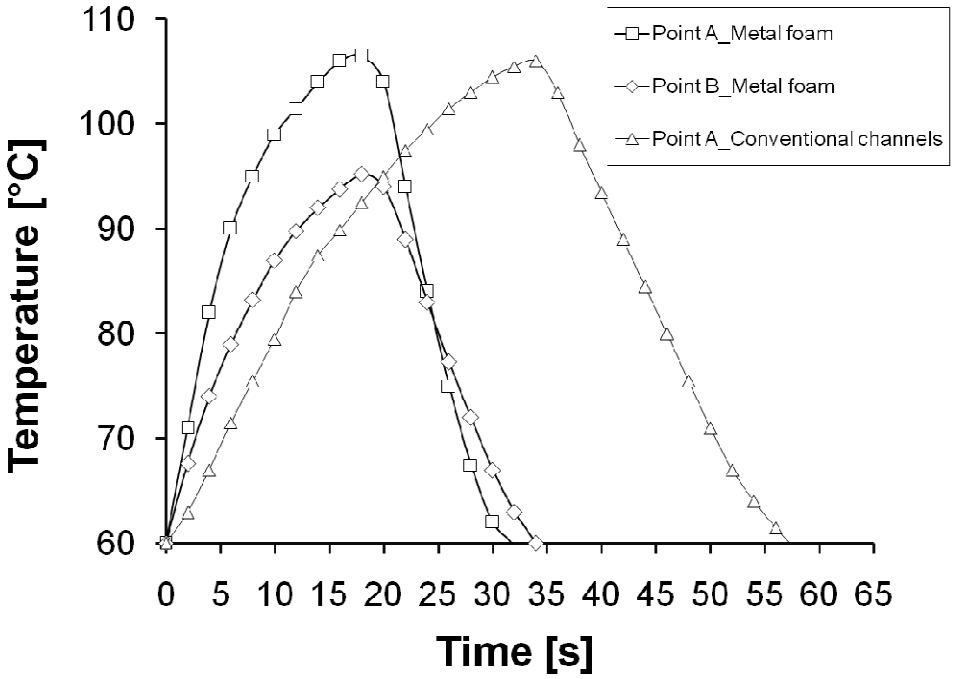

Figure 4.24 – Temperature history in correspondence of the thermocouple position and point A.

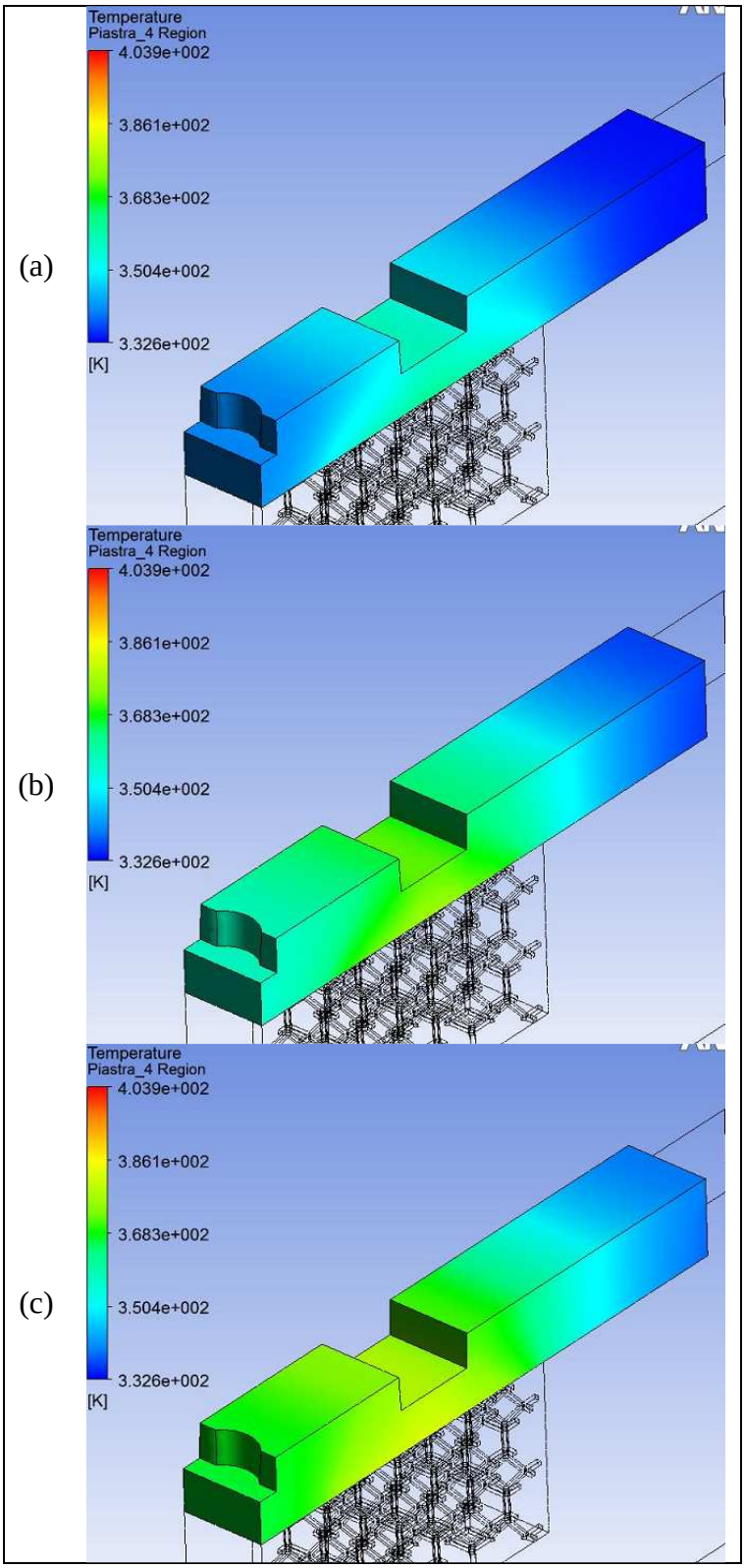

Figure 4.25 – Temperature distribution during the heating stage at time (a) 5s, (b)10s (c)19s.

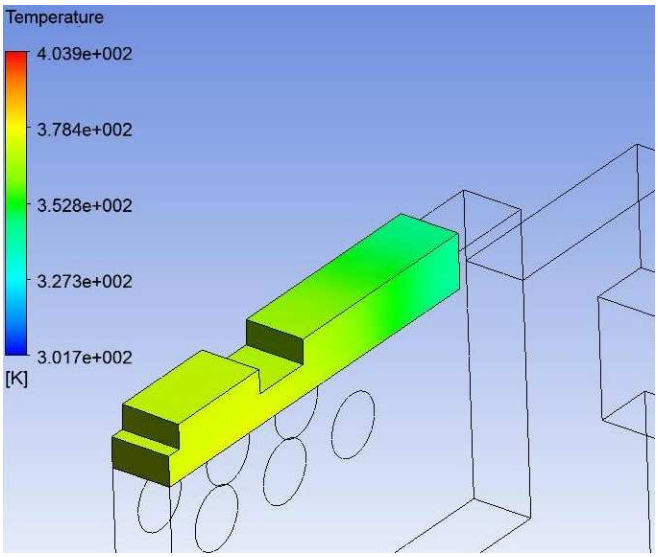

Figure 4.26 - Temperature distribution with conventional channels.

CHAPTER 5
EXPERIMENTAL INVESTIGATION ON RHCM PROCESS

The experimental investigation of the innovative rapid thermal cycling system, based on the use of open-cell aluminum foam, is the main topic of this chapter. In order to perform these tasks and determine the capabilities of the new RCHM process, a series of experiments was conducted at the Te.Si. Laboratory of DIMEG. In this chapter a description of the apparatus used for accomplishment of the RHCM process will be presented. To test the efficiency of the new RHCM system the new double-cavity mould for tensile specimens was manufactured and a test production was carried out. The numerical results were compared with experimental data and their accuracy was verified.

5.1 Experimental equipment

The experimental investigation of the RHCM process was carried out at the Te.Si. Laboratory of DIMEG. A set of RHCM tooling was built and installed into the ENGELTM injection machine located at that laboratory. The experimental equipment consists of four main components: injection moulding machine, mould, heating/cooling unit and monitor control system.

5.1.1 Injection Machine

The injection machine is an all-electric 1000 kN ENGELTM injection moulding machine with a screw diameter of 40 mm (Figure 5.1). Connected to the machine are the drying unit of the row plastic material (Figure 5.2).

Figure 5.1 - The injection moulding machine at the Te.Si. Laboratory of DIMEG.

Figure 5.2 - Drying unit.

5.1.2 Heating/cooling unit

The high-performance heating/cooling device equipped with both a hot-water and a cold-water circuit is the Tempro plus C160 Vario, provided by Wittmann Battenfeld. The heating/cooling system is equipped with a radial pump for high flow at different pressure range. The powerful pump (pressure up to 6 bar) guarantees a high flow of process water and thus a short preheating time and because of its direct cooling design, a high cooling capacity. In pressurized operation, two gauges ensure that the internal pressure is always approximately 1 bar over the steam pressure curve. Figure 5.3 compares the pump characteristics of different heating/cooling devices. The mould temperature controller allows a precise temperature control up to 140 °C. A control and monitoring unit based on self-optimizing microprocessor controller (+/-1 °C) was used to coordinate the actions of the components as the valve exchange unit and to ensure a continuous production process.

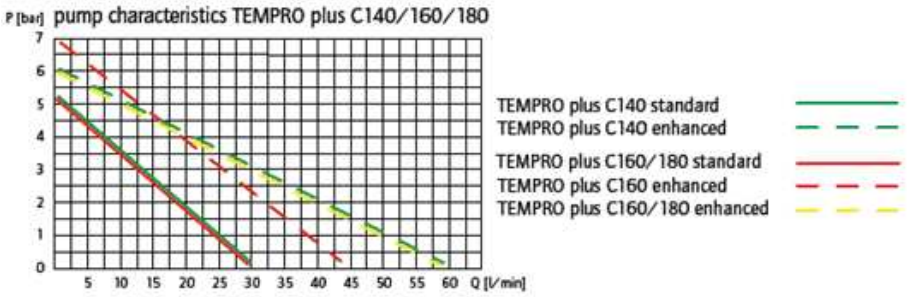

(a) (b)

Figure 5.3 - The high-performance heating/cooling system (a) and the pump characteristics tempro plus C140/160/180 (b).

5.1.3 Mould with metallic foams

The RHCM mould with metallic foam for tensile specimens was manufactured (Figure 5.4). Two pieces of open-cell aluminum foam with a reticulated structure were placed just under the cavity surface and connected to the rest of channels system. A K-type thermocouple was placed in the cavity plate near the weld line location, at 1 mm from the cavity surface, to measure the mould temperature profile during the moulding cycle. The thermal transducer is connected directly with the injection moulding machine control system, which makes temperature control and display operate easily. Figure 5.5 shows the RHCM mould for the test production.

Figure 5.4 - Cavity with aluminum foam.

Figure 5.5 - The mould for tensile specimens with the new insert.

5.1.4 Monitor control system

The control and monitor system was used to control all units. It is used to integrate the valve exchange system, the injection mould and the moulding machine and coordinate their actions for a stable process.

The monitor control system and human–machine interface (HMI) is the core of the whole mould temperature control system. The operator can observe the mould temperature changes in the

moulding process. In-line monitoring of the injection moulding operations requires continuous measurements of different parameters while the machine is running. In RHCM production process, the mould temperatures measured by the thermocouples are transmitted to the monitor control system. For this reason a thermocouple is equipped close to the cavity surface of the mould for an efficient mould temperature control. Signals to be acquired are read by means of a National Instruments 6036 E data acquisition card that also provides A/D conversion and multiplexing (8 differential input channels, 2 analogue output channels, 16 bit resolution with a maximum sampling rate of 200 kS/s (input/output)). A National Instruments SCB-100 shielded board is also employed to isolate the transducer signal from the data acquisition system. An Intel Pentium 2.4 GHz based personal computer running LabVIEW for Windows (National Instruments) is used. In order to acquire signals from the injection machine located at the Te.Si. Laboratory an electrical connection between the SCB-100 shielded board and the I/O signal board of the ENGEL machine was made. The “start filling” digital signal from the injection machine is used as a switch in order to provide the computer with a signal corresponding to the start of a new injection cycle. Figure 5.6 shows the components of the developed data acquisition system for process monitoring. The monitoring program was created using a combination of LabVIEW (National Instruments) and .NET (Microsoft) programming software. All required settings, such as number of channels to read, acquisition rate, channels names, are configurable using the main window of the program, as illustrated in Figure 5.7. The monitoring software can display acquired data both in-line, during the process, and off-line, from data saved to PC disk.

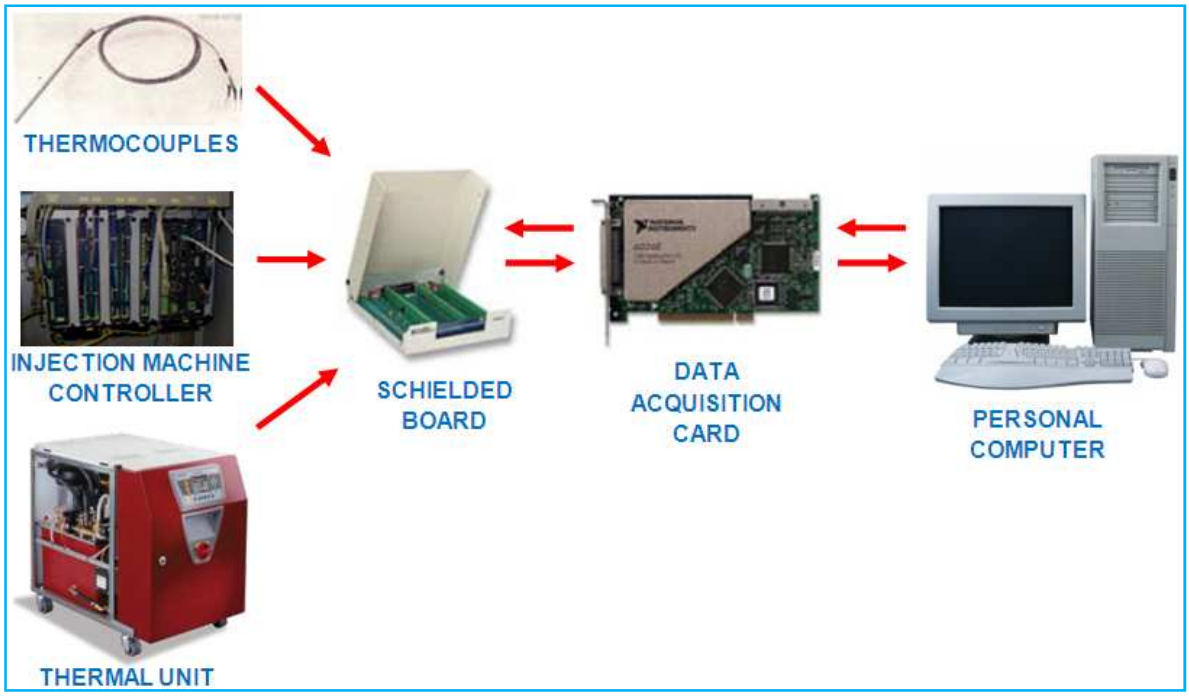

Figure 5.6 - Components of monitor control system.

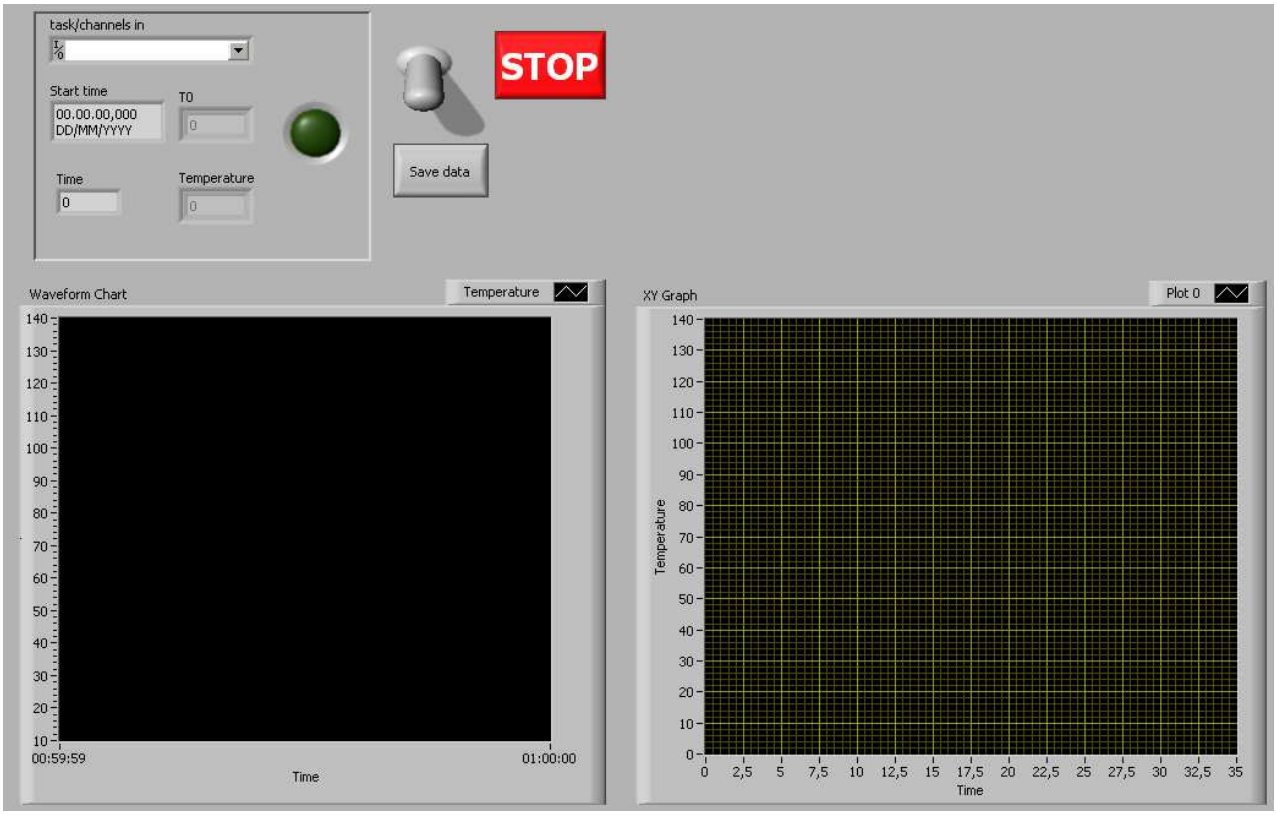

Figure 5.7 - Main window of the monitoring software.

5.2 Process principle

The hot and cool water are alternatively circulated in the heating and cooling channels of the mould. Figure 5.8 gives the schematic structure of the whole RHCM system based on the use of metallic foam. The real lines between different devices represent the pipe connections and the dashed lines represent the signal connection. At the outset of the moulding cycle, the hot medium from the heater is circulated in the mould channels by opening valve 1 and 4 to heat the mould. When the cavity surface temperature rises to the required high value, usually higher than the glass transition temperature of the resin, the valve 1 and 4 will be closed. At the same time, the resin melt is injected into the mould cavity for filling. After filling and packing operations, the valve 3 and 5 are opened to let the cool water circulate in the mould channels to cool the mould. The pump is equipped in the cooling and/or heating loop lines to enhance the turbulence of the fluid and increase the heat transfer efficiency. Once the mould is cooled down to the required low temperature, when the polymer melt solidifies and is strong enough to be ejected, the valve 3 and 5 will be closed to stop cooling. Just after that, the mould is opened to eject out the par which will be then taken out by the operator or the manipulator. Then the remaining coolant in the pipelines will be drained out and the mould will be heated again by opening valve 1 and 4 for the next moulding cycle.

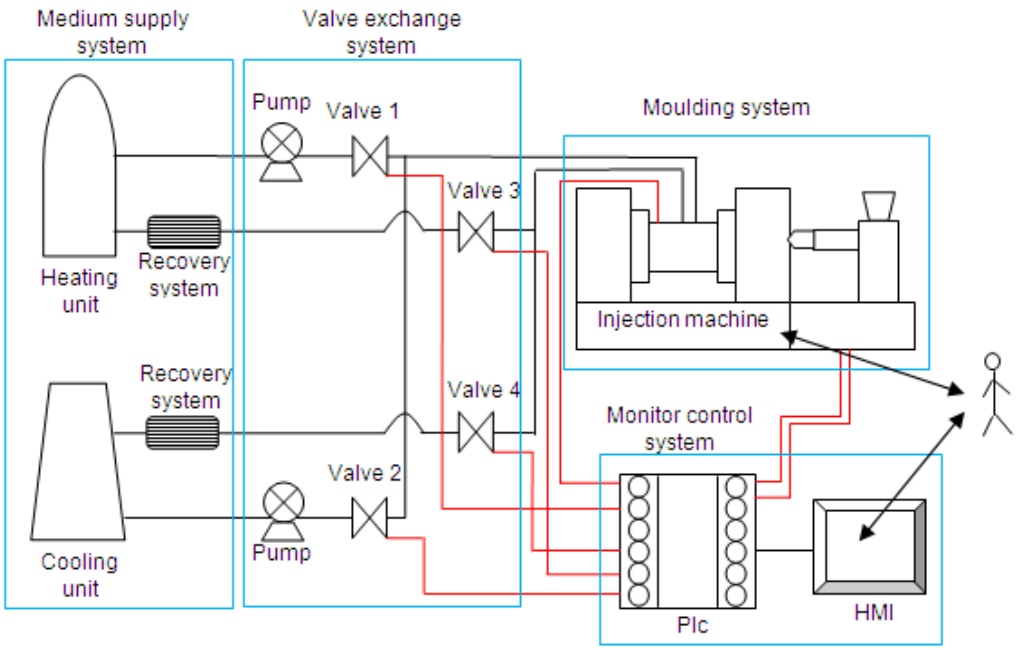

Figure 5.8 - The schematic structure of the RHCM system.

5.3 Test production

Before the test production, the mould was preheated at a temperature of 60 °C. Then the cavity surface is heated right after the mould opening signal with water circulating at a temperature of 130 °C until the temperature in correspondence of the thermocouple position reached the temperature of 95 °C. After the polymer is injected the valve exchange device is switched over to cooling and the mould was cooled with water at 30 °C. The process was cycled according to the previous sequence. During the moulding tests, 30 cycles where carried out to stabilize the process. Subsequently, 10 parts obtained from the following 30 cycles have been randomly collected and analyzed. Heating and cooling time values were calculated using the temperature profile measured by the thermocouple. The same procedure was followed to mould reference specimens keeping the mould temperature at a constant value of 60 °C. Figure 5.9 represents the tensile specimens moulded with the RHCM process. Figure 5.10 shows the comparison of the tensile specimens produced with RHCM process and conventional injection moulding process, CIM, respectively. While the parts moulded by the conventional process present a clearly visible weld mark, the specimens produced using the RHCM system are weld-line free and their surface gloss has clearly improved. This is mainly because that the high cavity surface temperature can prevent the melt freezing prematurely in the filling and packing stage and improve the entanglement of polymer molecule chains, resulting in superior aesthetics and higher weld strength.

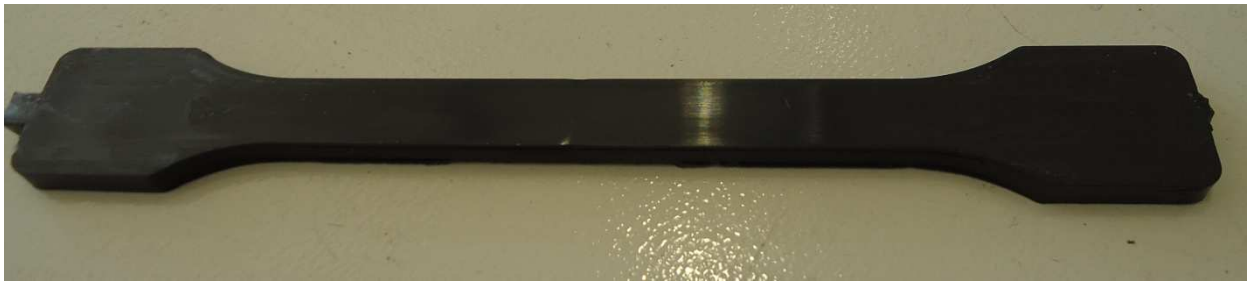

Figure 5.9 - Tensile specimen moulded by RHCM process.

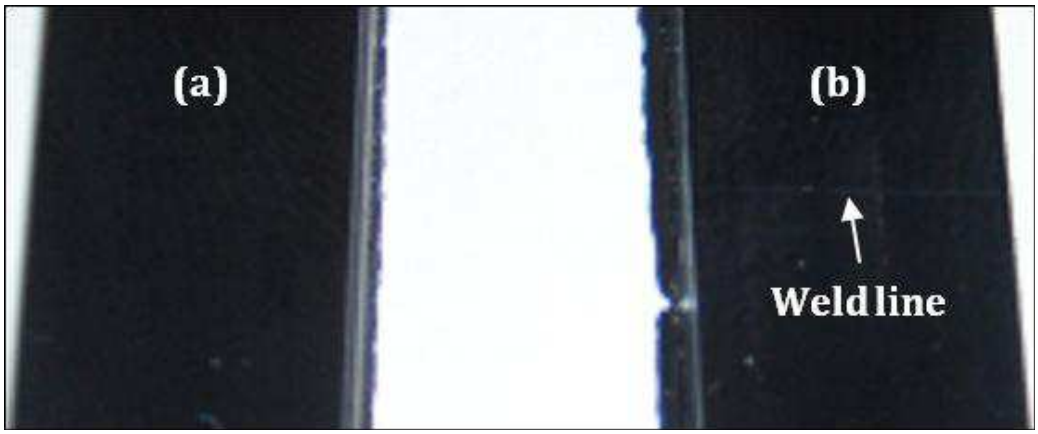

Figure 5.10 - Comparison of the specimen produced with CIM and RHCM.

Experiment result was used to verify the simulation prediction. A K-type thermal couple was placed close to the cavity surface to detect the temperature history. The temperature profiles in correspondence of both the thermocouple position was collected and compared to the experimental data (Point B). As shown in Figure 5.11, the temperature increase from 60 °C to over 95 °C in 18.9 s, and cool down to 60 °C in 15.9 s. The overall cycle time is 75 s. Figure 5.11 shows how the numerical results are in good agreement with the experimental data.

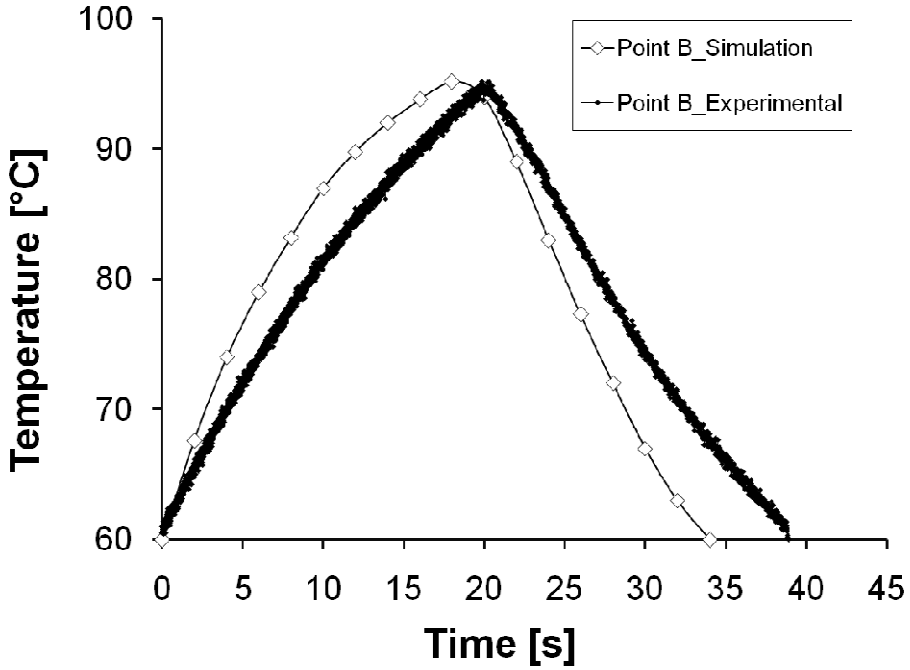

Figure 5.11 - Comparison of temperature history between experimental data and simulation results.

CHAPTER 6
ANALYSIS OF MICROSTRUCTURED SURFACES REPLICATION

In this chapter an experimental investigation in variothermal injection moulding of micro structured surfaces has been performed. The innovative technology for rapid heating and cooling of injection moulds has been used to analyze the effect of fast variations of the mould temperature on the improvement of micro features replication. The manufacturing of micro features on the cavity surface and the precise characterization of the microscopic structures will be accurately described.

6.1 Flow hesitation at surface microstructures

Increased difficulties are encountered when mould surfaces with well-defined microstructure surfaces are involved in replication. In recent years, polymer components with surface microstructures have been in rising demand for applications such as lab-on-a-chip and optical components. This replication, however, is not perfect, and the replication quality depends on the plastic material properties, the topography itself, and the process conditions. Because of the vast difference in melt flow thickness between the surface structure and the substrate, there exists a race tracking problem and the polymer hesitates at the entrance of the microstructures, as shown in Figure 6.1. Because of this time lag, the filling difficulty in surface structures is increased as compared with that in strip-type cavities. To achieve the required accuracy and prevent premature material freezing when producing high-aspect-ratio micro features, high injection pressures and mould temperatures are required. For replication of the polished mould surface, the mould temperature must be above the solidification temperature of the polymer during the filling stage and part of the holding stage. However, the final properties of the moulded part are limited by the physical capabilities of the actual equipment.

The surface quality that results when replicating micro features is one of the most important process characteristics in micro injection moulding and it constitutes a manufacturing constraint in applying this technology to a wider range of micro engineering applications. The surface topography of injection-moulded plastic parts can be important for aesthetical and technical reasons. The aesthetical implications of surface topography relate to visual and tactile perception issues such as gloss and colour perception. These parameters have a high priority in many electronic consumer products like mobile phones and audio-visual equipment.

To achieve good replication of surface micro/nanostructures, particularly with high aspect ratios, it is necessary to heat the mould to temperatures close to or even above the polymer solidification temperature. In order to attain such high temperatures in the mould and to guarantee demoulding

without damage at the same time, the process of variothermal temperature control has been proposed.

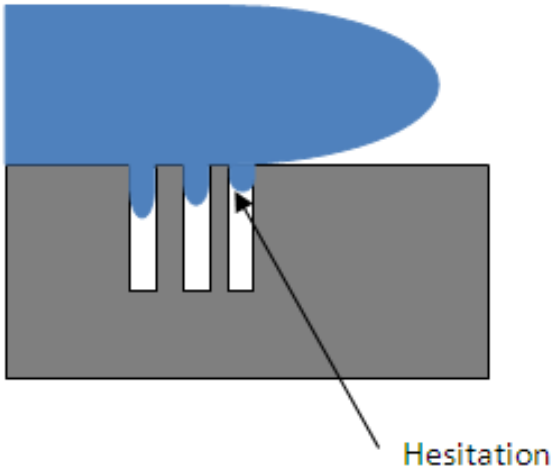

Figure 6.1 – Example of flow hesitation at surface microstructures.

6.2 Micro structures design

To study the influence of rapid mould temperature variation on surface topography replication, a series of radial micro channels was designed and located on the surface of the specimen. The main objective of the design of the micro structures was to create a geometry that could work as an effective test bench to put in evidence the effect of RHCM process in comparison to the conventional injection moulding process, in terms of the degree of micro structures replication. Furthermore, geometry and dimensions were selected according to existing industrial devices, such as encoders and blood separators.

According to the above mentioned requirements, a series of radial micro channels was designed and located on the surface of macro component, as shown in Figure 6.2 and Figure 6.3. The geometry is divided into four equal sectors. Each sector is composed by six straight micro channels whose dimensions are reported in Table 6.1. This particular configuration was designed in order to analyze the influence of the feature orientation (in relation to the flow direction) on the degree of replication. For this reason the circle was located in a position where the filling flow front is unidirectional.

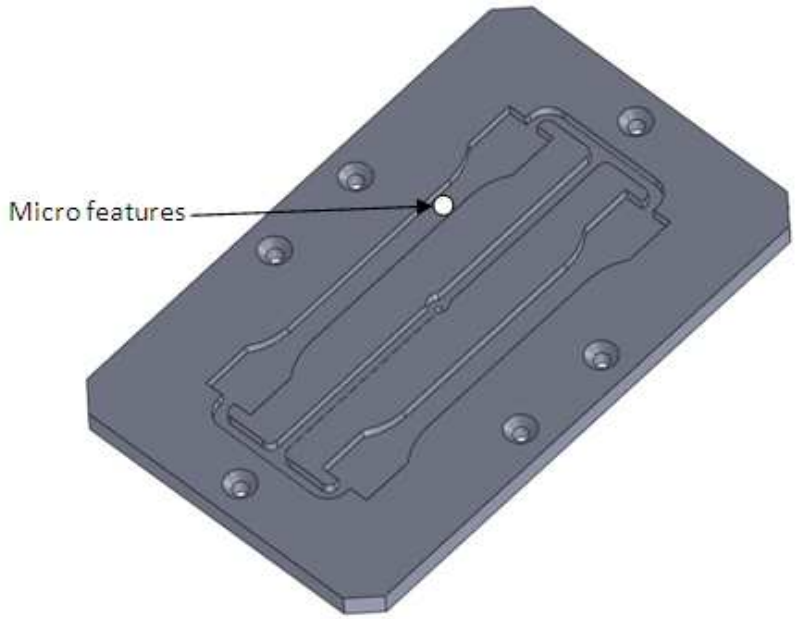

Figure 6.2 – The surface micro structures located on the surface of the cavity plate.

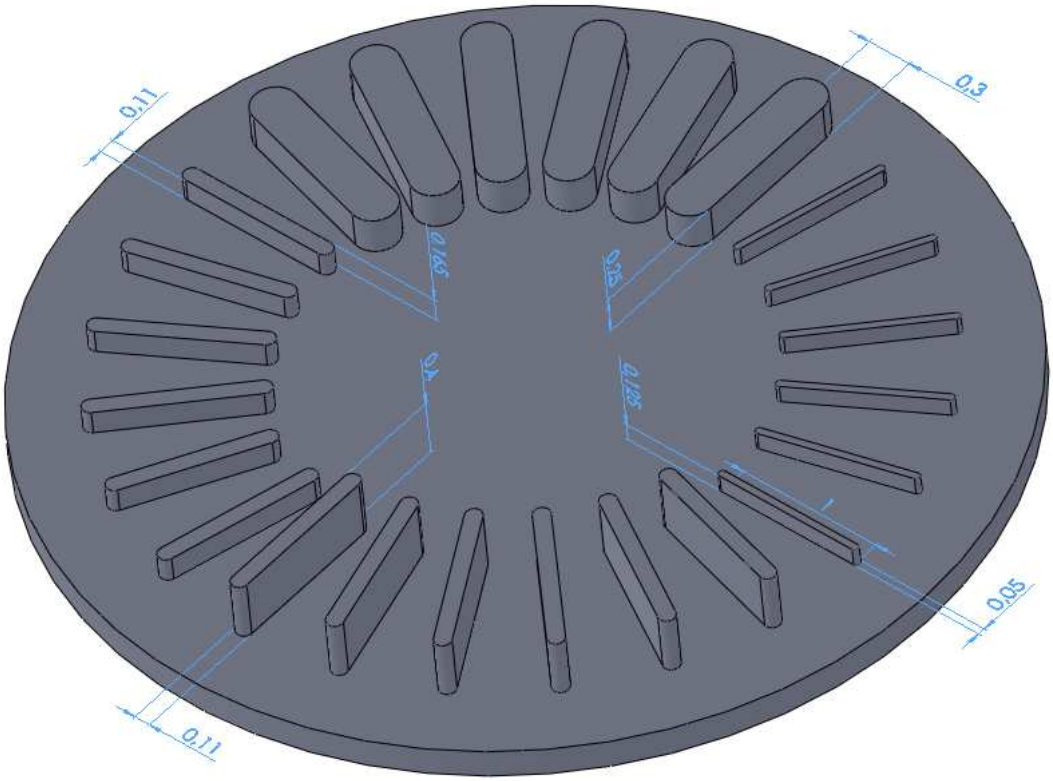

Figure 6.3 – The designed surface micro structures.

Table 6.1 - Dimensions of the micro channels.

Sector	Length [mm]	Width [mm]	Depth [mm]	Number of slots	Aspect ratio
1	1	0.30	0.250	6	0.833
2	1	0.11	0.165	6	1.500
3	1	0.11	0.400	6	3.636
4	1	0.05	0.125	6	2.500

6.3 Cavity manufacturing

Due to the dimensions and high tolerances required for the features of the final part, the micro channels were manufacture by micro electro discharge machining. Electrical discharge machining (EDM) is a thermo-electric process which erodes material from the work-piece by a series of discrete sparks between the work-piece and the tool electrode, both submerged in a dielectric fluid. The sparks, occurring at high frequency, continuously and effectively remove the work-piece material by melting and evaporation. The dielectric acts as a deionising medium between two electrodes, and its flow evacuates the resolidified material debris from the gap. Generally, EDM allows the shaping of complex structures with high machining accuracy in the order of several micrometres and achievable surface roughness Rz=0.4 μm. The process is well suited to machining hard materials to single figure micron tolerances. Good surface finishes were achieved by using a minimal discharge and reducing the gap between the electrode and component to sub-micron tolerances. The μEDM process allowed the machining of accurate features in the micro dimensional range.

The micro channels were manufacture by micro electro discharge machining (Sarix SX-200). Tungsten carbide (WC) electrodes with standard diameters of 314 μm, 150 μm and 110 μm were used as tool electrode. Their characteristics are tabulated in Table 6.3. Stiffness and rigidity of tungsten carbide is very high when comparing to tool steel. This is because tungsten carbide electrode size can be reduced to very small size and prevents bending or swinging during machining. Wear resistance of tungsten carbide is also better than that of tool steel. This provides advantages for micro-hole drilling since less deterioration occur in the shape of target holes. Dielectric liquid used for flushing was a hydrocarbon oil (Hdma 111).

Table 6.2 – Tungsten Carbide (WC) properties.

Properties	Value
Density	15.8 g/cm^3
Melting point	2870°C
Boiling point	6000°C
Thermal conductivity	84.02 W/(m·K)
Mohs hardness	9

Machining conditions for the different types of electrode are given in Table 6.3. A CAD/CAM system is used to generate tool paths of 3D micro channels. Esprit CAM with EDM module is used to generate G-code for milling operation. The result of the milling process simulation is represented in Figure 6.4. By using SX-MMI panel, electrical and technological parameters are set then drilling operation is performed. The micro electric discharge machining of the plate with micro channels is represented in Figure 6.5. Good surface finishes have been achieved using a minimal discharge and reducing the gap between electrode and component to sub-micron tolerances. Figure 6.6 shows the effective depth of the micro channels recorded by the control system of the micro electro discharge machining.

Table 6.3 - Machining conditions for different electrodes.

	Electrode		
	uEl110-400	**El314-250**	**uEl50-125**
Diameter [μm]	110	314	150
Length [μm]	700	1250	500
Frequency [kHz]	160	160	180
Current [A]	100	100	80
Open voltage [V]	100	100	77
Gap voltage [V]	72	72	74
Impulse duration [s]	4	4	2

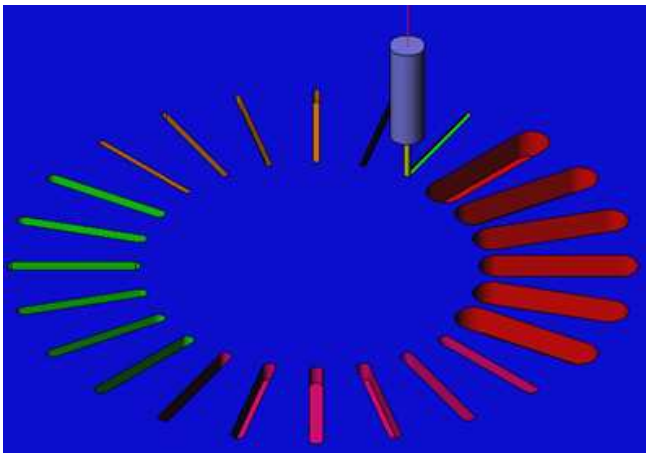

Figure 6.4 – Milling process simulation.

Figure 6.5 - Micro electric discharge machining of the plate with micro channels.

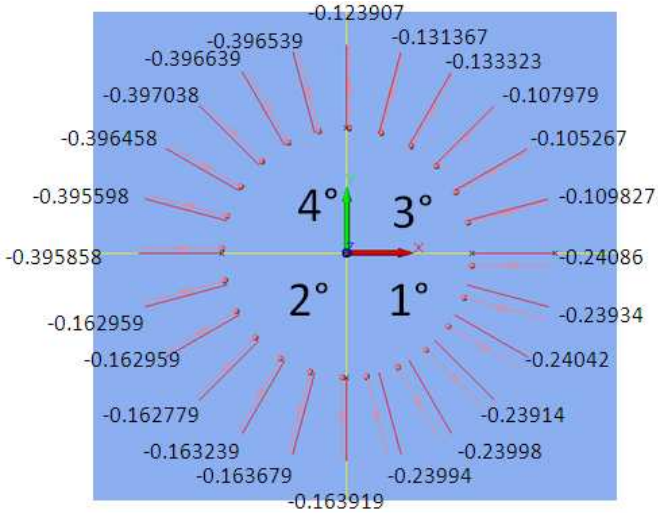

Figure 6.6 – Effective depth (mm) of the micro channels.

6.4 Characterization of the moulded parts

The experimental campaign was carried out on the injection moulding machine Engel Emotion 440/100 described in the paragraph 5.1.1. The acrylonitrile-butadiene-styrene copolymer, ABS (Terluran KR 2922), was the material used in this study. In order to evaluate the effect of the fast variations of the mould temperature, tensile specimens was produced by CIM and RCHM. The injection speed and the melt temperature were set to the highest limits of the moulding window in order to decrease the viscosity of the polymer during the injection phase. For the conventional injection moulding process, the mould temperature was set at 50°C. Figure 6.7 shows the micro features of the specimens produced by the conventional process and employing the RHCM system.

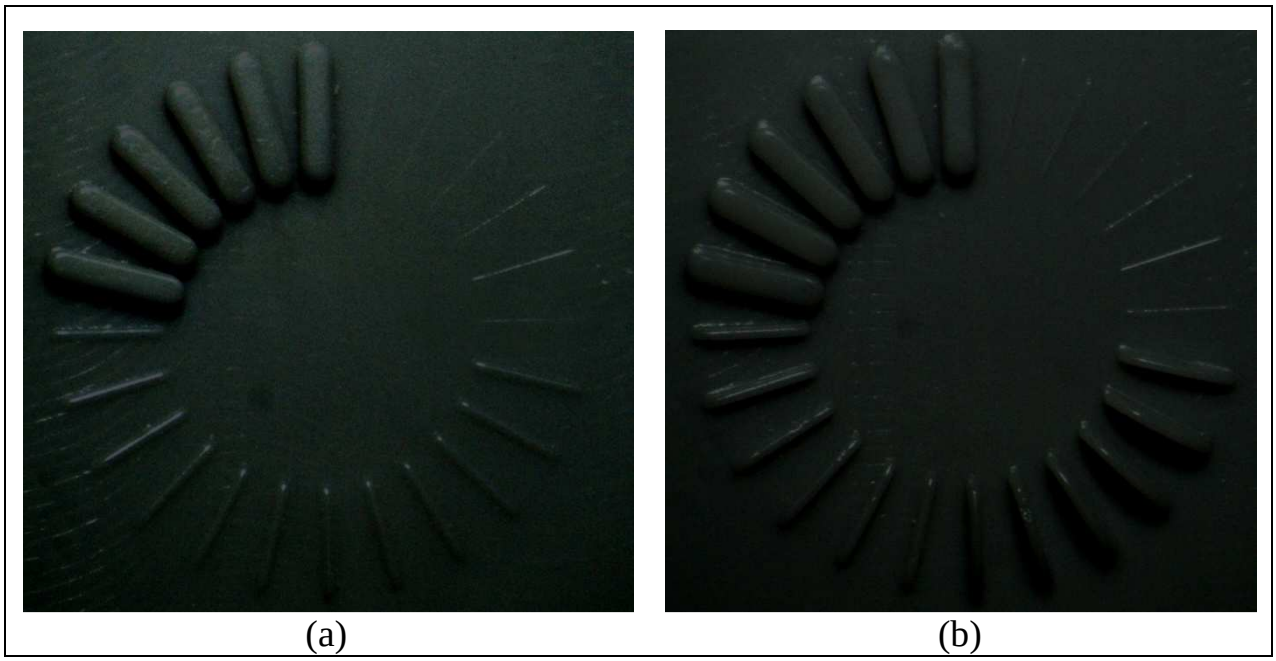

Figure 6.7 – Micro features produced (a) by the conventional process and (b) employing the RHCM system.

To measure the obtained degree of replication, a white light interferometer (GBS SmartWLI) was used to characterize the surface topography of the tensile specimens. The instrument consists of an optical microscope in connection with a beam splitter. One beam is sent through the objective lens of the microscope and reflected from the sample. The other beam is reflected by a reference mirror. Before being registered at a CCD camera, the two beams are recombined. If the optical paths travelled by the two beams differ by an integer number of wavelengths, there will be constructive interference. If the path difference is an odd integer of half wavelengths, destructive

interference will be observed. If the surface of the sample is in focus, the two beams will recombine to create bright and dark bands called fringes, representing the topography of the sample. This instrument can detect height information with a height resolution of 0.1 nm and profile heights ranging up to 400 µm. Each micro structure was measured and its maximum height value was eventually estimated. In Figure 6.8 an example of measurement is reported for the same features replicated with and without employing the RHCM system. The obtained micro features were quite regular, showing an even filling pattern except for the extremities, which are clearly affected by the resistance of the side walls. Micro features height values are reported in Figure 6.9 and correlated to the flow direction. From the comparison of the replication results it can be clearly observed that the degree of replication is strongly increased by employing the proposed RHCM system. In particular, it is interesting to notice that the use of the proposed solution especially enables the replication of the most critical features, characterized by the smallest values of thickness and aspect ratio. The still incomplete filling of the features belonging to the 2nd and 3rd sectors is probably due to the presence of entrapped air. Eventually, the feature orientation effect on the degree of replication shows no interaction with the mould temperature variation.

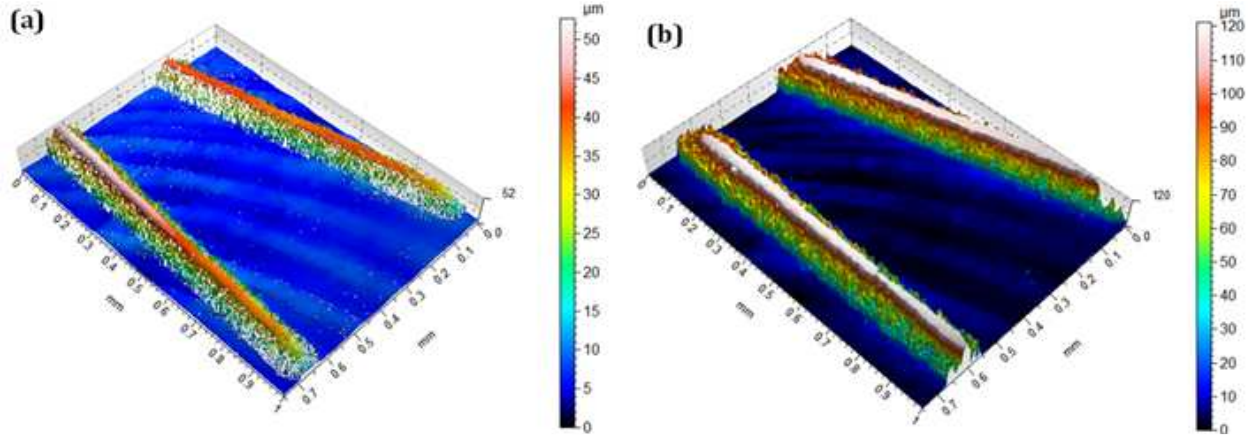

Figure 6.8 - Example of micro features 7 and 8 replicated (a) by conventional injection molding and (b) employing the RHCM system.

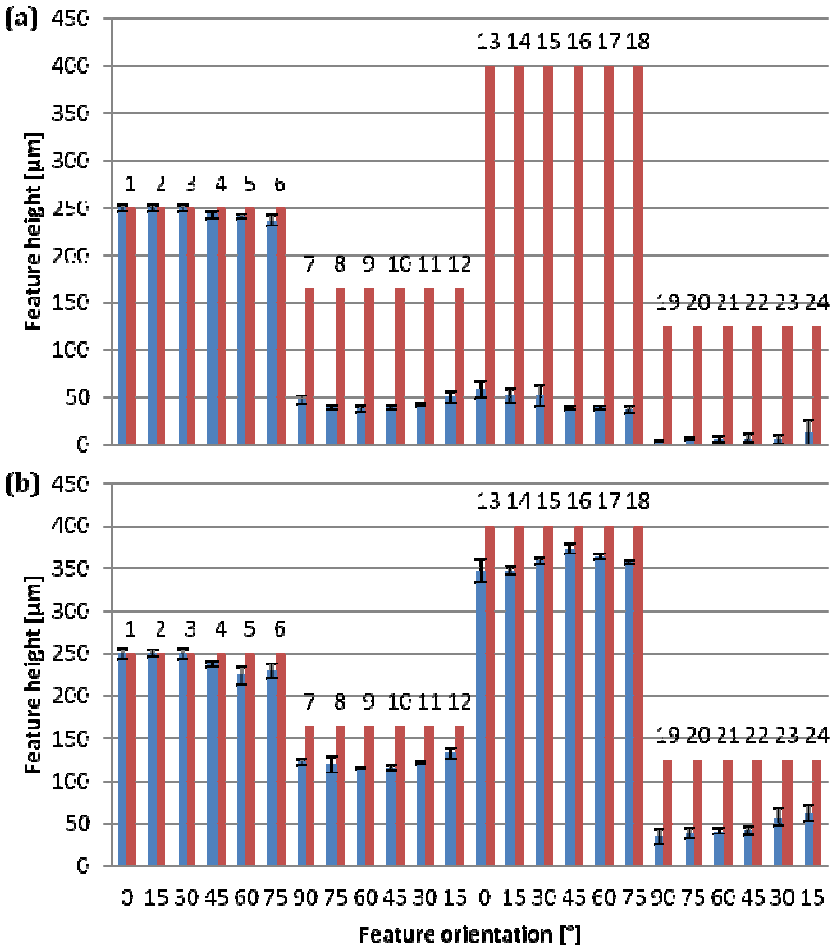

Figure 6.9 - Micro features height average values for specimens produced (a) by the conventional process and (b) employing the RHCM system.

CHAPTER 7
MECHANICAL CHARACTERIZATION

Temperature cycle moulding in its various implementations has been widely reported to eliminate visible weld lines. Despite the large body of literature available, no results have been available to evaluate the effect of RHCM on mechanical properties in this region. In this study, the effect of fast variation of the mould temperature on the weld line strength of three different thermoplastic materials has been investigated. Tensile tests were carried out on specimens produced by conventional injection moulding and employing the RHCM system. The relation between V notch size and ultimate tensile stress was studied.

7.1 Introduction

Weld lines form when plastic melt splits and then recombines at some downstream location in the mould cavity during the injection phase. This is inevitable in the moulding of complex parts that have core inserts or runner branching for multigated parts. The mechanical properties of the injection moulded part is negatively affected by the weld line formation. The weak strength of weld line can be attributed to a number of possible factors, including:

- V-notches at the weld surfaces;
- incomplete molecular entanglement or diffusion;
- presence of contamination or micro voids at the weld interface.

The weld quality depends on the way in which the flow fronts meet and bond to each other. If the processing conditions are adequate, the macromolecular chains diffuse through the original interface and give the weld a strength close to that of the bulk. If the conditions are not adequate, the diffusion is not sufficient for good healing of the interface, and this leads to a dramatic reduction in the mechanical properties. Moreover the surface defects act as an initiation site for the damage. Debondue et al. [90] demonstrated how the elimination of the V-notch brings a significant improvement in the tensile strength in conventional injection moulding (Figure 7.1).

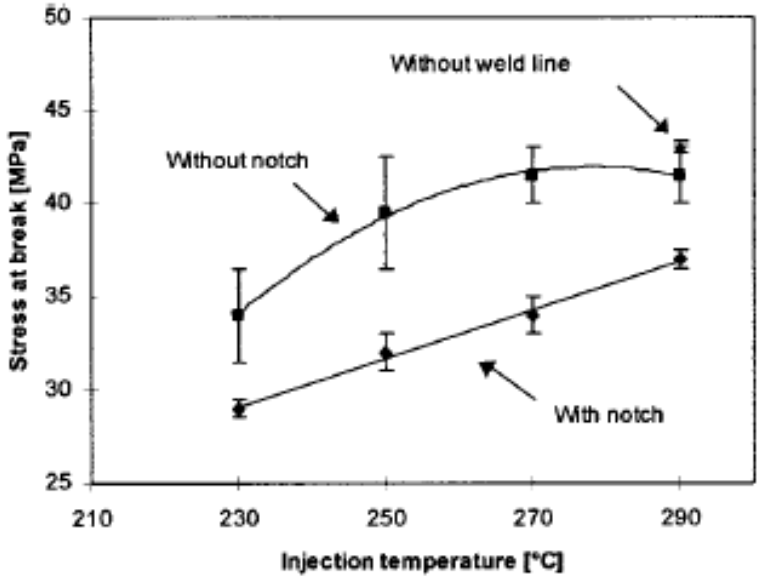

Figure 7.1 - Evolution of the tensile strength when the weld line notch is eliminated (PS).

Processing parameters generally have a limited influence on the mechanical properties of the weld line, except for the mould temperature and, to a lesser extent, the melt temperature and injection speed. In conventional injection moulding the mould temperature can be varied in a limited range. RHCM allows to increase the mould temperature of more than 50 °C and to produce plastic parts without the characteristic V-notch at the weld surface. In this study, tensile tests for different thermoplastic materials were carried to quantitatively evaluate the effect of RHCM on the mechanical strength in the weld line zone.

7.2 Moulding

Three engineering polymers often used in automotive applications were chosen:

1. ABS (Terluran KR 2922) from Basf®;
2. PA66 with 50% glass fibres (LNP-VERTON RV00AES) from Sabic®;
3. PP with 30% glass fibres (Celstran PP-30GF-02) from Ticona®.

Moulding of tensile specimens was executed at the process conditions shown in Table 7.1. Under each set of process conditions, 10 shots were made to ensure that the process was stable before the samples were collected. If no significant variation was observed during these first 10 runs, the moulded parts from the next 10 runs were collected as the samples for mechanical characterization.

Table 7.1 - Process parameters setting.

	ABS		PA66		PP	
	CIM	**RHCM**	**CIM**	**RHCM**	**CIM**	**RHCM**
Mould temperature (°C)	60	110	60	130	60	120
Melt temperature (°C)	250	250	280	280	240	240
Ejection temperature (°C)	60	60	60	60	60	60
Injection speed (mm/s)	50	30	50	30	50	30
Holding pressure [MPa]	20	20	20	20	20	20
Holding time [s]	6	6	6	6	6	6

7.3 Tensile test

An MTS 322 servo-hydraulic testing machine was used to perform displacement controlled tests on the tensile specimens (Figure 7.2). Tests were controlled with strain measured by the extensometer while in the elastic region and by the vertical crosshead displacement of the machine as the specimen passed yield point. Tests were conducted at room temperature, namely at 20±1°C. Test speed was set to 2 mm/s, according to standard UNI ISO 527-2 [98]. A range of preliminary experiments were performed using samples manufactured during the stabilisation stage between experiments. These experiments allowed the testing technique to be refined to minimise the occurrence of testing errors, such as specimens slipping in the jaws. The data was processed using National Instruments' Labiew software to generate engineering stress/strain curves. A photograph of the test setup showing the extensometer attached to the specimens is provided in Figure 7.3.

Figure 7.2 - MTS testing machine.

Figure 7.3 – Test setup.

7.3.1 Results

Values reported was determined for each moulding, averaging results from 10 measurements to ensure statistically significant results. Outputs of the tensile tests were modulus, yield strength, ultimate tensile strength (UTS) and elongation at break. UTS was calculated as ratio between the maximum force recorded during the test divided by the cross section area of the specimen prior the test. Cross sections areas were calculated on three specimens for each experimental setting and the average value of 40±0.010 mm^2 was used to calculate UTS. Strain at break was calculated as the ratio between the elongation until specimen breakage ΔL divided by the length L=50 mm according to [98].

Table 7.2 summarizes the averaged results of the experimental tensile tests. PP-GF30 and PA-GF50 exhibit a brittle mode of failure. Instead, ABS shows a more ductile response. Examples of each behaviour can be seen in Figure 7.4. ABS, PA-GF50 and PP-GF30 all show an increase in the mechanical properties between the conventional process and RHCM. Young's modulus increases of 5.71% for ABS and 15.47% for PA-GF50 with the fast variation of the mould temperature. The elastic modulus does not vary significantly for PP-GF30. The variotherm system allows to improve the UTS by about 2 % for ABS and PA-GF50 and by 11.55% for PP-GF30. The specimens moulded with the RHCM process exhibit consistent improvements in elongation at break. In particular PP-GF30 shows an increase by approximately 58% between the conventional process and RHCM with the mould at a temperature of 120°C. The polymer reinforced with long glass fibres deforms quite extensively in the region around the weld line. This failure would suggest a significantly improved knitting of the material at the flow front has been achieved. The variotherm system can therefore be used to improve the mechanical properties in the weld line zone.

Table 7.2 - Mechanical properties for conventionally moulded and RHCM parts. Standard deviations of the means are shown in parentheses.

	ABS			PA			PP		
	CIM	**RHCM**	**Impr.**	**CIM**	**RHCM**	**Impr.**	**CIM**	**RHCM**	**Impr.**
Young modulus (MPa)	1204.8 (50.82)	1277.8 (92.13)	5.71%	6076.4 (142.81)	7188.6 (180.25)	15.47%	3723.67 (112.12)	3752.83 (121.43)	0.8%
Yield strength (MPa)	35.8 (1.92)	37.8 (2.32)	5.59%	67.4 (3.21)	67.79 (2.72)	0.58%	38.87 (1.32)	42.13 (1.24)	8.37%
Ultimate tensile strength (MPa)	43.1 (1.73)	44.08 (2.28)	2.28%	68.38 (3.82)	70.21 (2.67)	2.67%	40.57 (0.96)	45.25 (1.2)	11.55%
Elongation at break	9.44 (0.33)	9.51 (0.68)	6.85%	4.38 (0.29)	4.84 (0.15)	10.54%	3.40 (0.76)	5.37 (0.25)	58.11%

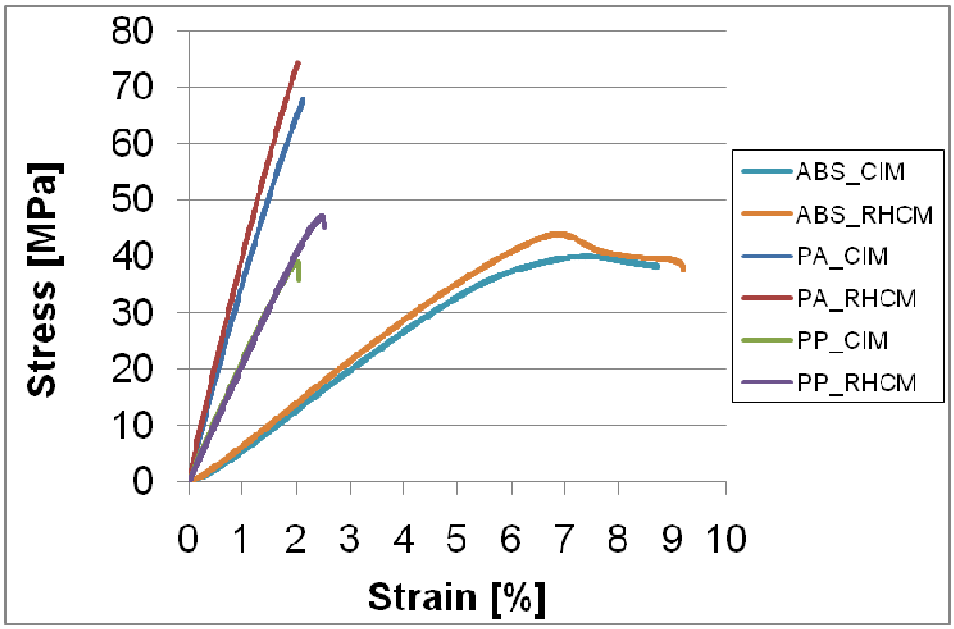

Figure 7.4 – Stress-strain curves.

7.4 Weld line appearance and roughness measurement

Based on the tensile test theory, it is confidential that the v notch in edge of specimen contributes more influence for decreasing the ultimate tensile test results. So the V notch profile in the edge of samples was measured. The characterization of the weld lines was carried out by means

of a profilometer. Surface roughness was determined for each moulding, averaging results from 3 scan profiles of 5 mm length. The profile test of a V notch in the weld line's different area was executed and the comparisons were made among different weld line specimens. The scanning test was separately performed in the middle of weld lines.

To provide a basis for comparison, weld lines formed in conventional processing were first examined. A plot of the surface height data provided by the profilometer for the conventional processing is given in Figure 7.6 (a). The scan through the weld line shows the characteristic sharp V-shaped groove. The graph in Figure 7.6 (a) is to be compared with Figure 7.6 (b) and shows how the visible weld line is reduced using RHCM. The weld line depth is the same order of magnitude as roughness.

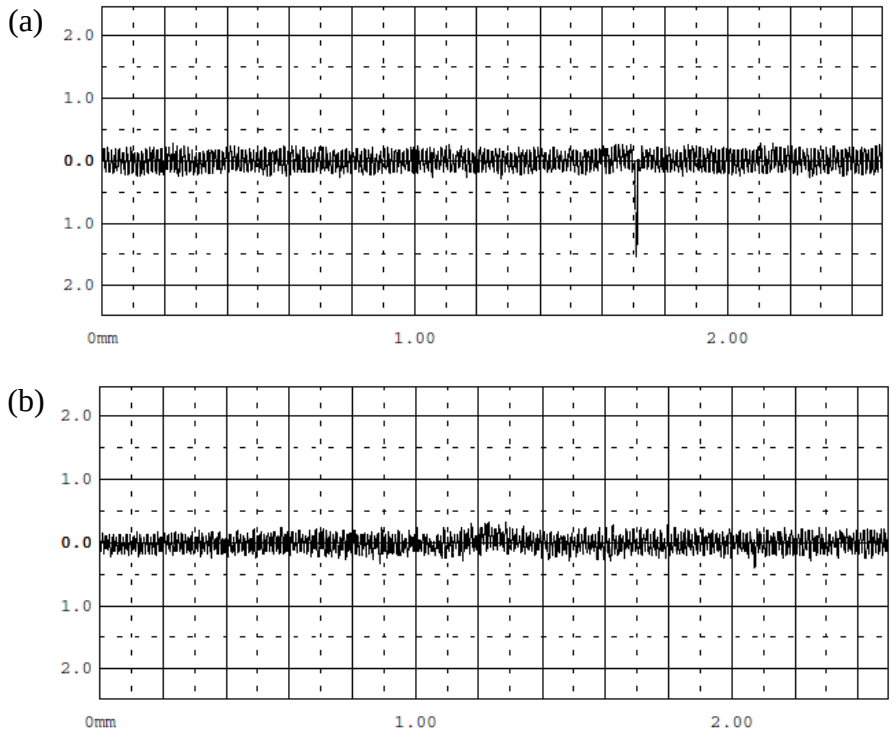

Figure 7.5 – Profiles of sections scanned by the profilometer with CIM (a) and RHCM (b).

Table 7.3 summarizes the averaged results. ABS, PA-GF50 and PP-GF30 all show a significant reduction in the weld line depth - by approximately 30% for ABS and PA-GF50, 40% for PP-GF30 - between the convectional process and temperature cycle injection moulding. By comparing the test results of experiment, it can be concluded that a smaller V notch area relates to a higher

ultimate tensile stress of the weld line. PP-GF30 showed the most significant improvements in the weld line depth and ultimate tensile strength.

Table 7.3 - Comparison of surface roughness for conventionally moulded and RHCM parts. Standard deviations of the means are shown in parentheses.

	Weld line depth [μm]		
	ABS	**PA**	**PP**
Conventional	1.02 (0.3)	1.74 (0.41)	1.41 (0.35)
RHCM	0.69 (0.21)	1.2 (0.22)	0.82 (0.31)
Reduction	32.35%	31.03%	41.84%

CHAPTER 8
RAPID HEAT CYCLE MOULDING FOR AESTHETICAL APPLICATIONS

In recent years, the rapid growth of the 3C (computer, communication, and consumer electronics) industry has driven demand for producing plastic parts with high-quality finish. The surface gloss of thermoplastic parts is an important characteristic as it affects the optical behaviour and the aesthetics. Studies were published showing that the processing parameters, in particular the mould temperature, affect the gloss of injection moulded parts.

In this chapter, the influence of RHCM on the surface quality of plastic parts will be investigated. At the beginning, a literature review of the knowledge about the influence of processing parameters on the gloss of injection moulded parts will be presented. Then the design phase of a new mould for the production of high gloss cover plates will be described. Two different heating/cooling systems, the ball filling and the system based on the use of metal foams, were tested. Obtained results regarding the effect of the fast variation of the mould temperature on the surface gloss are then reported.

8.1 Introduction to surface quality

Gloss varies with the refractive index of the polymer, the angle of incidence, and the topography of the surface. Previous studies on polymer injection mouldings have shown that the gloss increases with increasing mould temperature [92–93] for some rubber-modified thermoplastics. The effect of the mould temperature was typically much higher than that of the melt temperature, the effect of the latter being negligible for acrylonitrile-butadiene-styrene (ABS). An increasing holding time levelled off the gloss for ABS after an initial increase, whereas an increasing holding/packing pressure typically increased the gloss for the same rubber-modified thermoplastics discussed so far. All the studies examined point to that the cooling time has a negligible effect on the gloss. Oliveira at al. [94] studied the modifications of the surface morphology and micro topography of injection moulded ABS parts caused by the processing conditions and to relate them with gloss. This work showed that the surface finish and appearance of injection moulded parts is highly dependent on the process parameters, in particular the mould temperature (Figure 8.1).

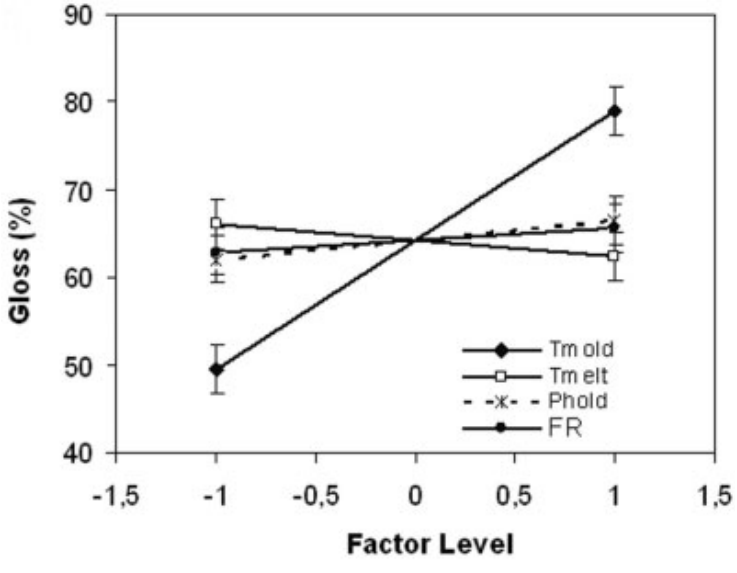

Figure 8.1 - Effect of the processing parameters on the gloss f a plastic part (Tmold: mould temperature, Tmelt: melt temperature, Phold: holding pressure, FR: flow rate) [19].

Surface gloss is a subjective impression created by the light flux reflected by a part. In industrial practice, specular gloss is often expressed in relation to the reflection from an ideal polished black surface in the specular direction (cf. ASTM D2457 or ASTM D523). The gloss is measured with a glossmeter and the results are expressed in gloss units (GU), which are calculated as the reflectometer reading for the surface concerned calibrated with respect to that of a standardized black glass plate with a known refractive index. Spectrophotometers operating in the reflection mode and diffractive optical sensors have also been used to study the gloss differences of injection moulded plastics products.

In this study the effect of fast variation of the mould temperature on surface gloss was analyzed using a spectrophotometer.

8.2 Mould design

To investigate the influence of mould temperature in RHCM, an existing tool, that produces a 64×24×2 mm cover plate, was modified. A cover plate must possess high-quality appearance. The conventional injection moulding process does not satisfy the requirement because of obvious defects on the product's surface. As the additional post-processing, such as spraying process is needed, the whole production flow is prolonged; the cost is increased and the environment is

polluted, too. The RHCM technology can be applied to improve the surface quality of plastic parts. In this work a cover plate was chosen as test case to study the efficiency of the new system based on the use of metal foams in improving the gloss of plastic parts. Figure 8.2 and Figure 8.3 show the cover plate and the corresponding mould structure for RHCM process, respectively. The layout of the heating/cooling system in the cavity block is shown in Figure 8.4.

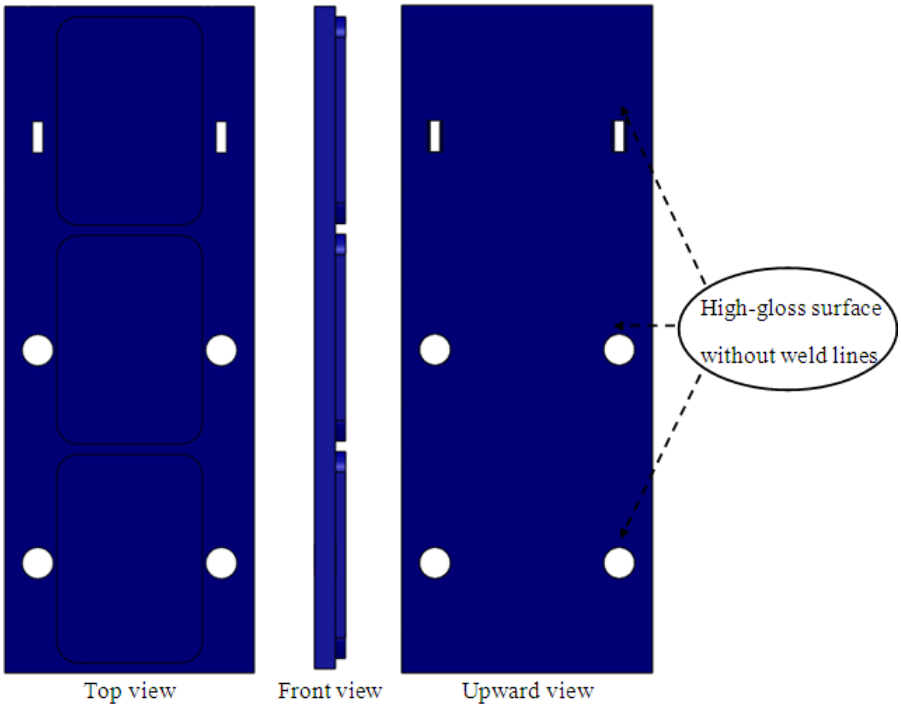

Figure 8.2 – Cover plate.

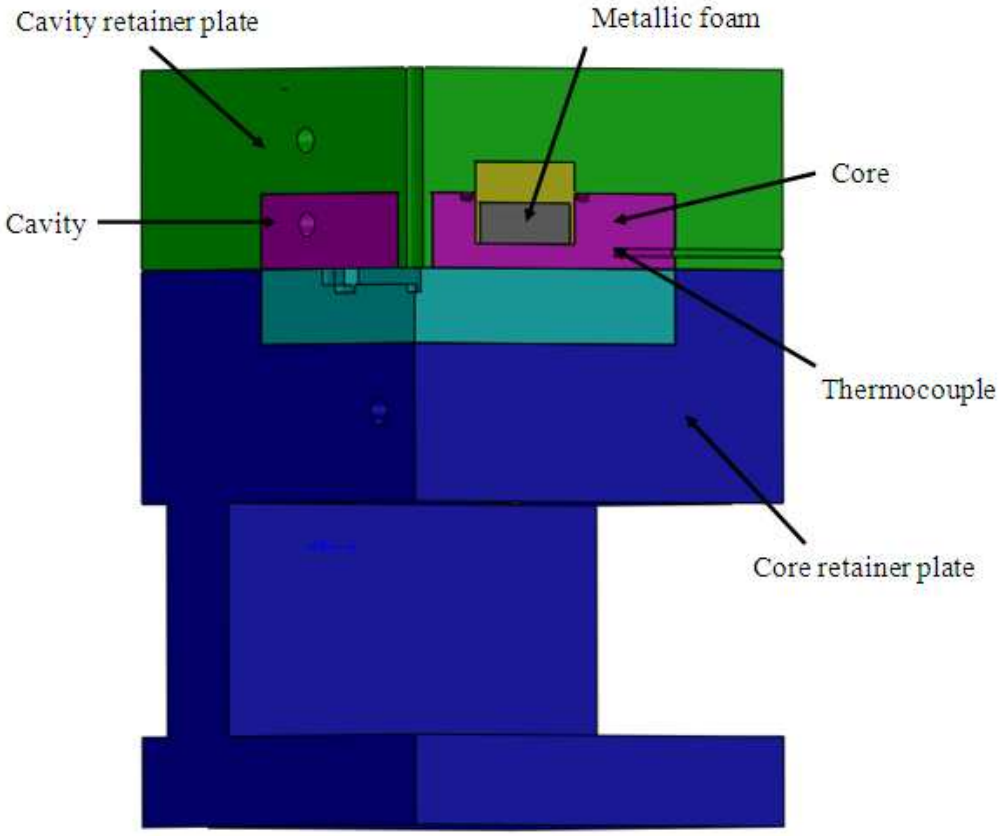

Figure 8.3 – RHCM mould structure of the cover plate.

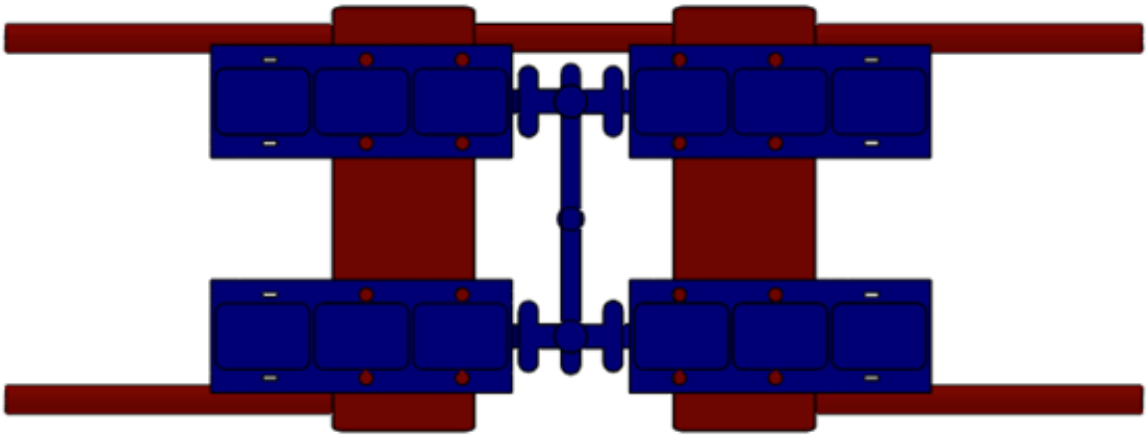

Figure 8.4 – Layout of the heating/cooling systems in the cavity block.

Two slots were realized at a distance of 6 mm from the cavity surface and were filled with three different inserts (Figure 8.5). In the first case, a 90×33×20 block of open cell aluminum foam of mm was used. The metal foam, supplied by ERG Materials and Aerospace Corporation, has 5

pores/cm. In the second arrangement, a 90×30×10 mm block of aluminium foam was used. As comparison, the cover plate was produced replacing the aluminium foam with a ball filling. The balls have a diameter of 10 mm (Figure 8.6).

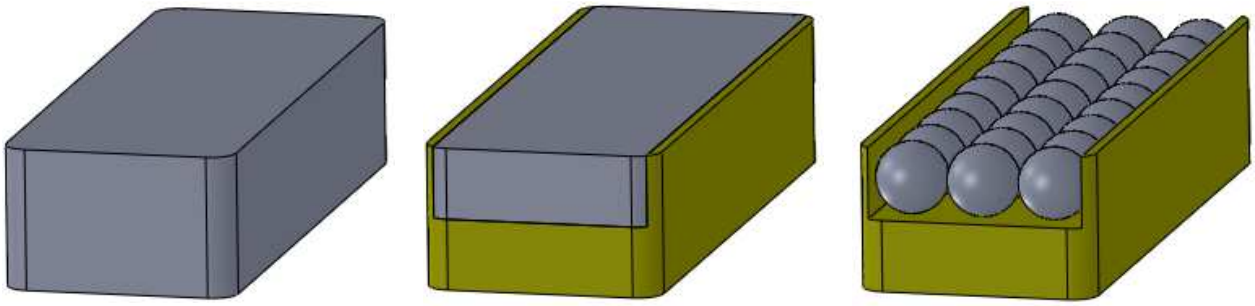

Aluminum foam (90×33×20 mm) | Aluminum foam (90×30×10 mm) | Ball filling (90×30×10 mm)

Figure 8.5 – Layout of the different heating/cooling systems.

Figure 8.6 – Fixed insert with ball filling.

Only the cavity side has heating/cooling channels close to the cavity surface. This is mainly because that only the outer surface of the flat television frame is required to have excellent appearance and the inner surfaces of the frame will be hidden inside of the final flat television after assembly. Consequently, only the cavity block needs to be thermally cycled by rapid heating and

cooling while a conventional continuous cooling method used in CIM is sufficient for the core side. As discussed in the previous sections, the layout of heating/cooling channels in the cavity block is one of the most crucial factors for the successful application of RHCM process. A reasonable design of the heating/cooling channels should achieve rapid heating/cooling of the mould and at the same time ensure sufficient mould strength and service life. The new RHCM mould for the production of high gloss cover plates is shown in Figure 8.7.

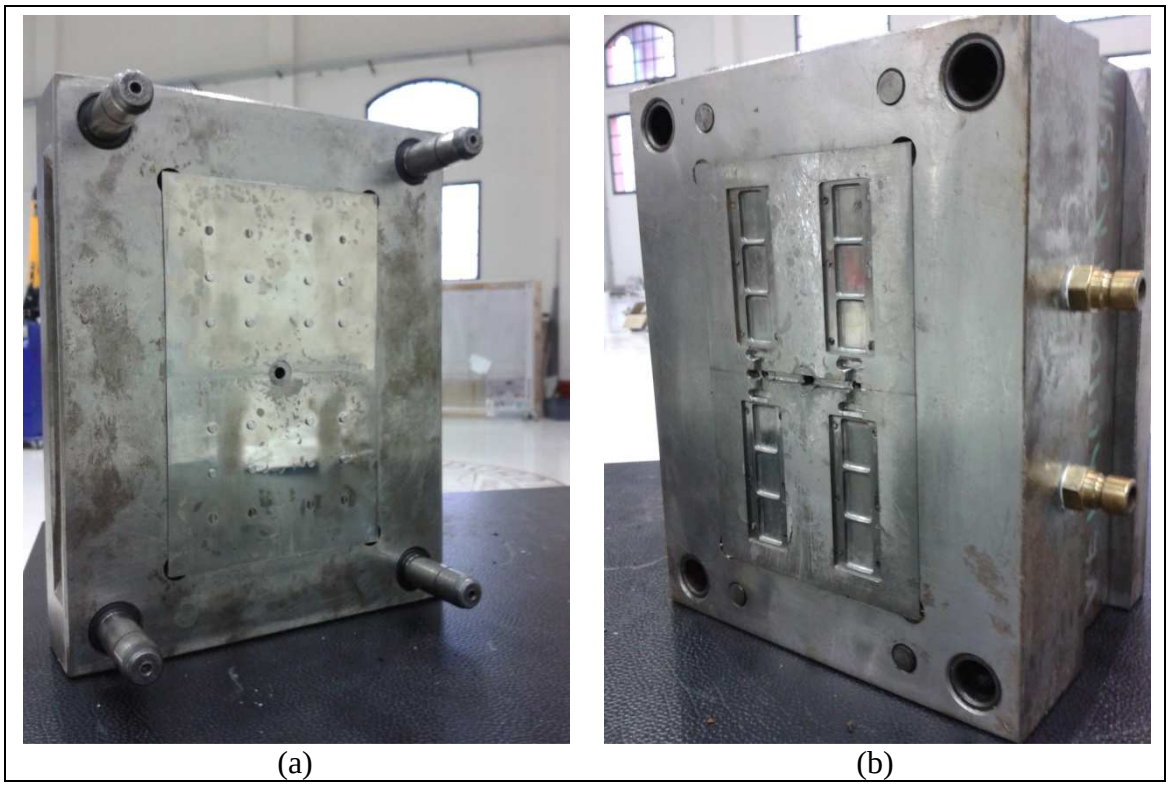

(a) (b)

Figure 8.7 – The new RHCM mould for cover plate. a) The fixed part b) The rotating part.

8.3 Temperature measurement

The polymer used in this study was a commercial acrylonitrile-butadiene-styrene copolymer (ABS Terluran KR 2922). ABS is commonly used in applications where the surface appearance is important. The injection speed and the melt temperature were set to the highest limits of the moulding window in order to decrease the viscosity of the polymer during the injection phase. The initial mould temperature was set at 60 °C. Then the mould was heated with water circulating at a temperature of 140 °C until the temperature in correspondence of the thermocouple position reached the temperature of 100 °C. Then, the mould was cooled with water at 30 °C. A Tempro plus

C160 Vario, provided by Wittmann Battenfeld, was used as heating/cooling unit. A K-type thermocouple was placed in correspondence of the point T on the cavity surface to measure the mould temperature profile during the moulding cycle (Figure 8.8).

As shown in Figure 8.9, the first technology based on the use of metal foams allows to drastically reduce the heating and cooling times to about 10 s and 15 s, respectively. The temperature histories for the other heating/cooling systems are quite similar. However, the comparison between the ball filling technology and the RHCM system with metal foams shows how the new system developed in this work allows to reduce the entire cycle time of about 4 s.

For RHCM, the required heating and cooling time of the mould mostly depends on the mass of the cavity/core to be heated and cooled. A mould with a low thermal mass exhibits a low thermal inertia and can be rapidly heated and cooled. Increasing the thickness of the blocks of metal foam, the volume of the material being heated is reduced with a consistent improvement in cycle time.

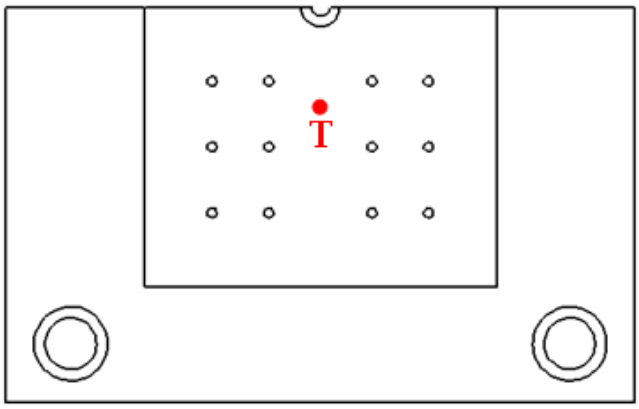

Figure 8.8 – Control point for the evaluation of the temperature history.

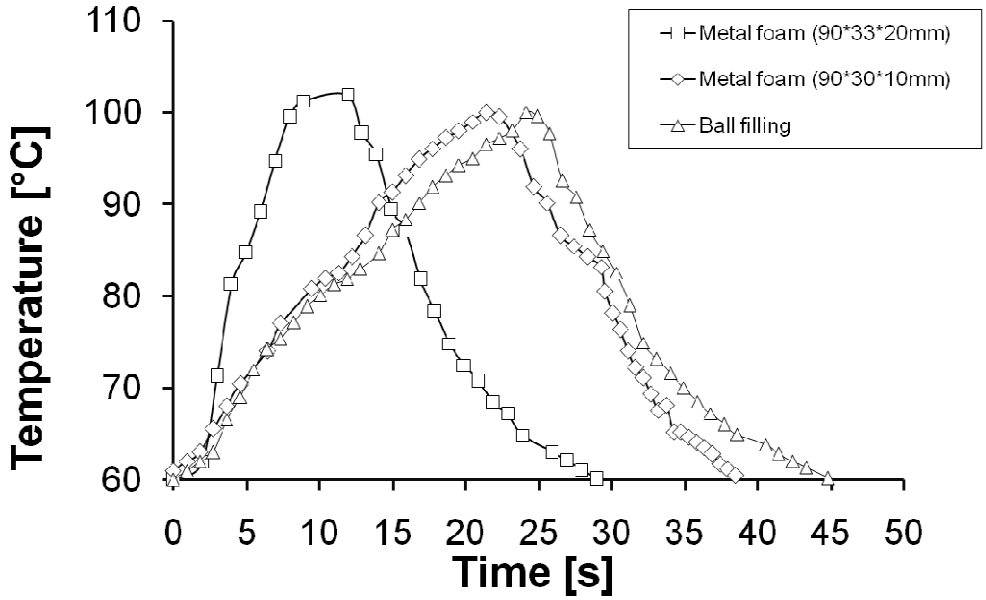

Figure 8.9 – Comparison of temperature history between the different heating/cooling systems.

8.4 Effect of RHCM on the product quality

All heating/cooling systems allow to produce high gloss parts without weld lines. The cover plate moulded using the new RHCM system based on the use of metal foams is shown in Figure 8.10. The surface gloss was measured by using a FTIR Spectrum One-Perkin Elmer spectrophotometer operating in reflection mode (Figure 8.11). The measurements by spectrophotometer were carried measuring the total reflectance at point A (Figure 8.12). The angle of incidence of the spectrophotometer is fixed equal to 8°. The diameter of the probe beam of the spectrophotometer was adjusted to 3 mm. The diffuse reflectance was measured by trapping the specular component away. The specular reflectance was calculated by subtracting the diffuse reflectance from the total reflectance. The process variables that were analyzed in the moulding program were the mould temperature and the ejection temperature.

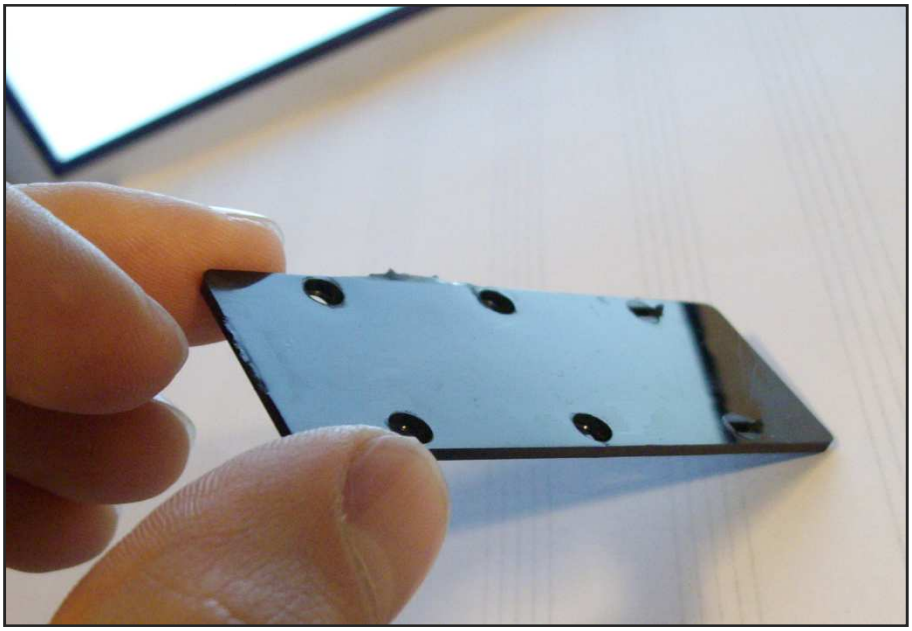

Figure 8.10 – Cover plate.

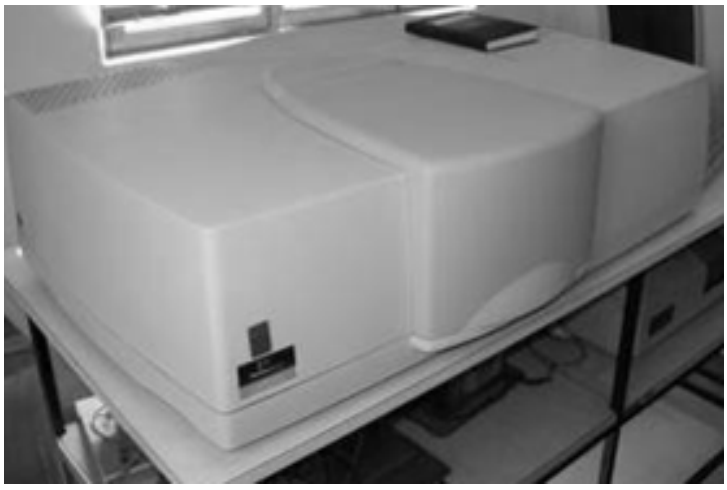

Figure 8.11 - FTIR Spectrum One- Perkin Elmer spectrophotometer.

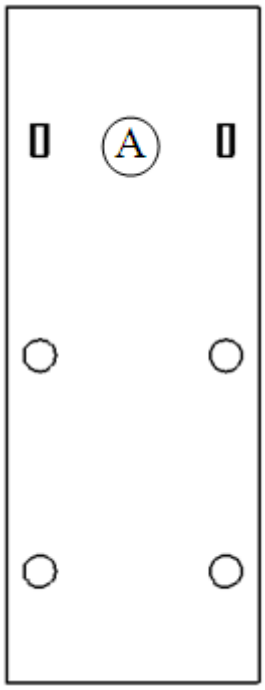

Figure 8.12 - Test location of the injection mould plastic product.

Figure 8.13 shows the comparison of gloss when water heating was used with the target temperature of 100°C, 80°C and 60°C. It was found that with the higher target temperatures, the gloss was clearly improved. The results show a significant reduction in the surface gloss between the convectional process and temperature cycle injection moulding with mould temperature higher than T_g. When the mould temperature was increased at 80°C, a slight improvement of the specular reflectance was observed. Such high-glossy surface can be explained considering the high cavity surface temperature that prevent the solidification of the resin melt in filling and packing stages. The resin melt in RHCM process can accurately duplicate the morphology of the cavity surfaces.

When the ejection temperature was varied from 60°C to 70°C, a slight improvement of the specular reflectance was recorded. This can be explained considering the combined effect of high cavity surface temperature, that prevent the premature melt freezing, and the fast cooling of the moulded part, which contrasts the stress relaxation of the polymer molecular chains after the detachment from the mould surface.

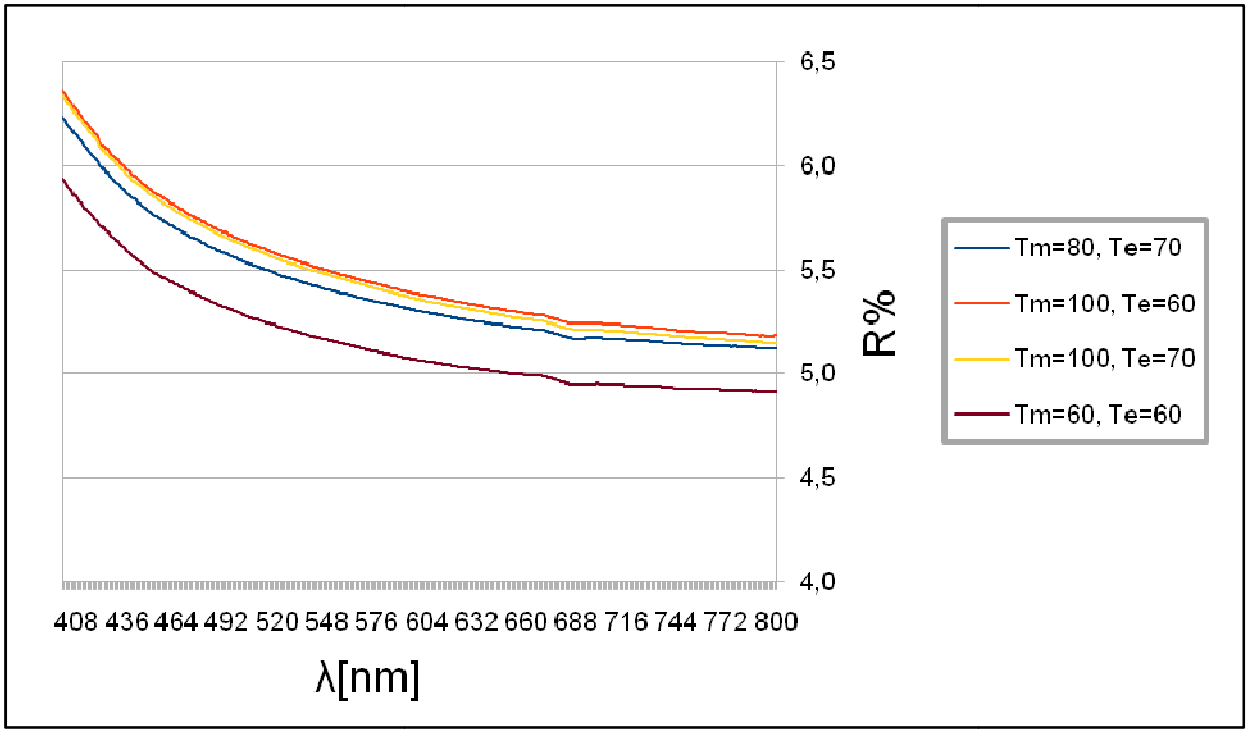

Figure 8.13 - Specular reflectance from the test location (Tm: mould temperature, Te: ejection temperature).

CHAPTER 9

INFLUENCE OF PROCESS PARAMETERS ON SURFACE FINISH AND WELD LINE STRENGTH IN MICRO INJECTION MOULDING

Micro injection moulding is a new advanced technology which can realize the manufacture of fine and precision parts with microstructures in one step with high efficiency at low cost. This novel manufacturing technology has become a hot research topic all over the world. The mechanical properties and the appearance of micro injection moulded parts are highly affected by weld line formation. Weld lines often result in poor optical surface appearance of injection moulded parts. Furthermore, the typical weld line's V shape gives rise to a stress concentration. Weld lines are mainly influenced by material composition, mould design and process conditions. Despite the wealth of literature available on micro injection moulding, the development theory of the moulding problems in RHCM, like reduced strength weld line, voids, no uniform shrinkage, etc., is incomplete.

The objectives of the present research is to identify the improvements of surface finish and weld line strength by a detailed quantitative examination using RHCM. In order to observe the development of a micro scale weld line, a visual mould with a variotherm system was used. A detailed description of the apparatus used for the experimental campaign will be presented This study focuses on the process analysis, in particular:

- Characterization of weld lines on micro injection moulded parts.
- Influence of the micro injection moulding process parameters on the geometrical properties of the weld lines in the RHCM.
- Influence of the micro injection moulding process parameters on the mechanical properties of the weld lines in the RHCM.
- Comparison between the conventional injection moulding process and RHCM for a material filled with carbon nanotubes and different cavity configurations.

9.1 Experimental equipment

The experimental investigation was carried out at the Centre for Polymer Micro and Nano Technology of University of Bradford (UK). The experimental equipment consists as follows.

9.1.1 Cavity design

Using exchangeable inserts in the tool, two different cavity configurations were used in this mould in order to investigate the effects of the shape of micro parts on surface finishing and weld line's mechanical properties. A micro moulding scale tensile test bar cavity was designed, based on

ISO 527 tensile test standard, but at 1/15 scale. The micro tensile part was prepared by the double gate injection mould. Design details can be seen in Figure 9.1. A flat cavity of thickness 0.25 mm, width 3.5 mm and length 7.5 mm as shown in Figure 9.2 was used. Injection occurs on the top face of the large flat disc region at the left and the cavity is shown on the right side with a 1 mm hole in its centre.

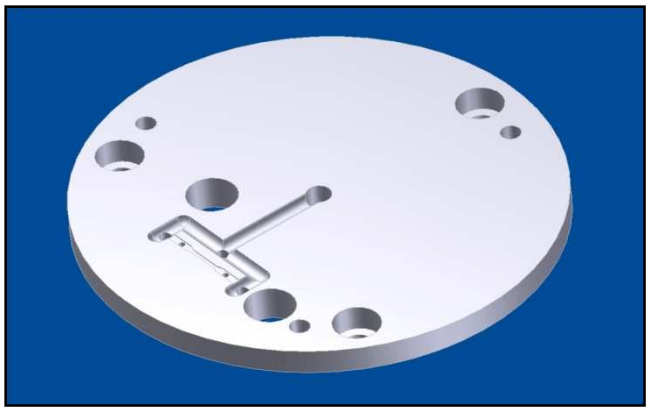

Figure 9.1 - Double gated cavity plate design.

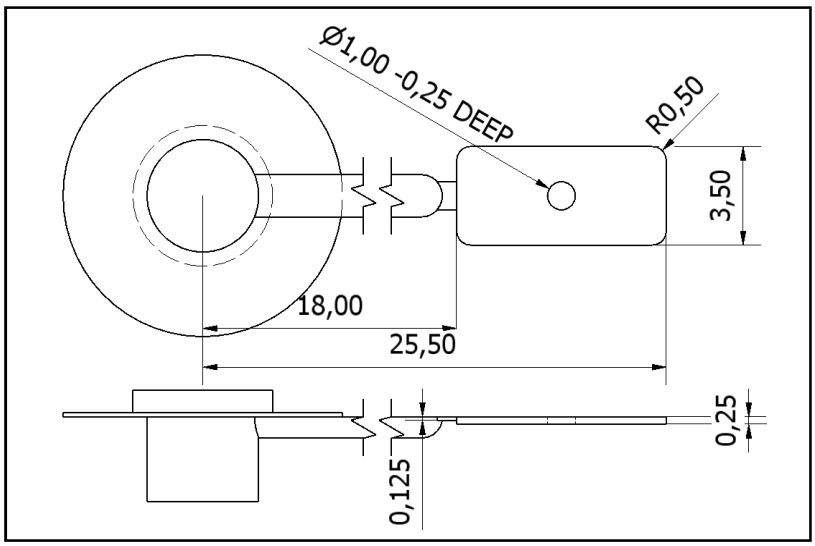

Figure 9.2 - Flat cavity with circular hole.

9.1.2 Variotherm mould design

The variotherm unit was applied on both sides of the tool and it was composed of electrical heating, water and air cooling, shown in Figure 9.3. After closing the mould, through two heating

pipes the mould temperature is heated up to a temperature higher than the glass transition temperature of PC. In the second step water and air cooling are started following the end of the packing phase. The temperature of the rotating part is rapidly reduced via two cooling channels using water as cooling medium. A transparent sapphire window forms the fixed surface of the mould cavity. The thickness of the sapphire window is 4 mm. The temperature of the fixed part is cooled via air flowing in order to have approssimately the same cooling speed. When the mould temperature reaches the desired demoulding temperature, specimen are ejected. The electrical heaters and thermal transducers are connected directly with the injection moulding machine control system. Four thermocouple in different zones of the mould are used to monitor the process. The temperature graph of the heating/cooling system against time is shown in Figure 9.4. The mould was heating from 110 to 155 °C, within 25 s. It took 40 s for cooling the mould from 155 to 110 °C.

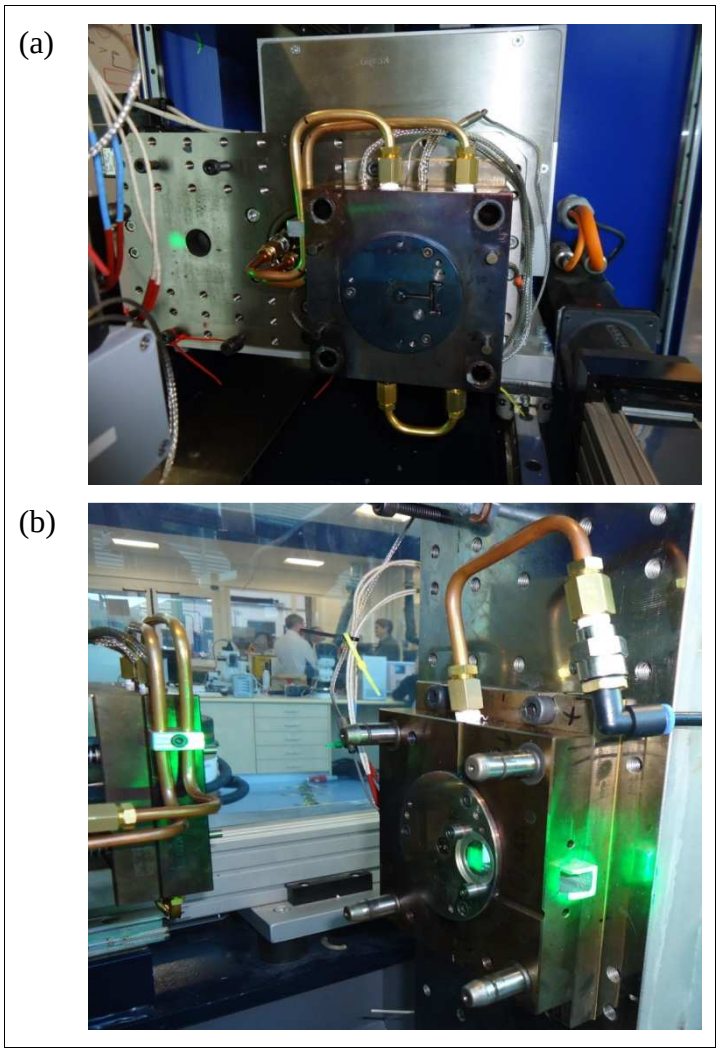

Figure 9.3 - The new RHCM mould. a) The rotating part b) The fixed part.

(a) (b)

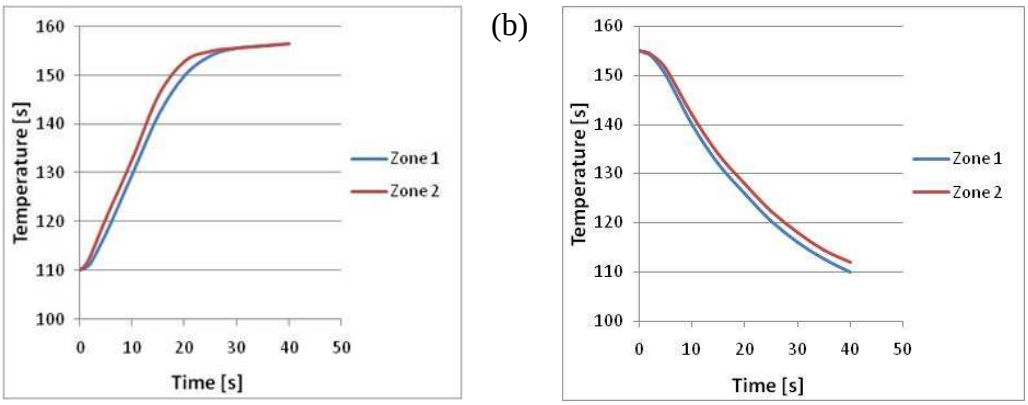

Figure 9.4 - Temperature changing graph. (a) Temperature changing during heating process. (b) Temperature changing during cooling process.

9.1.3 Flow visualization

A visual mechanism was integrated to be used in combination with the variotherm system to observe and record the weld line developing process. Cavity filling was imaged directly using a high speed flow visualization system. The visual and variotherm mould is shown in Figure 9.5. The transparent sapphire window forms the fixed surface of the mould cavity and a 45° first surface mirror is mounted in the bolster plate to enable the cavity to be viewed. A Mikrotron MC1310 high speed camera is connected to the acquisition PC using a National Instruments PCIe-1429 capture card and images are acquired using National Instruments Labview software. The system was able to image the cavity at a rate of 4997 frames per second with an exposure time of less than 1/30000 s which proved adequate for high resolution capture of the flow fronts during an injection. These images can be used to provide a range of information regarding the filling behaviour of the PC material as the two flow fronts approach and impinge on each other.

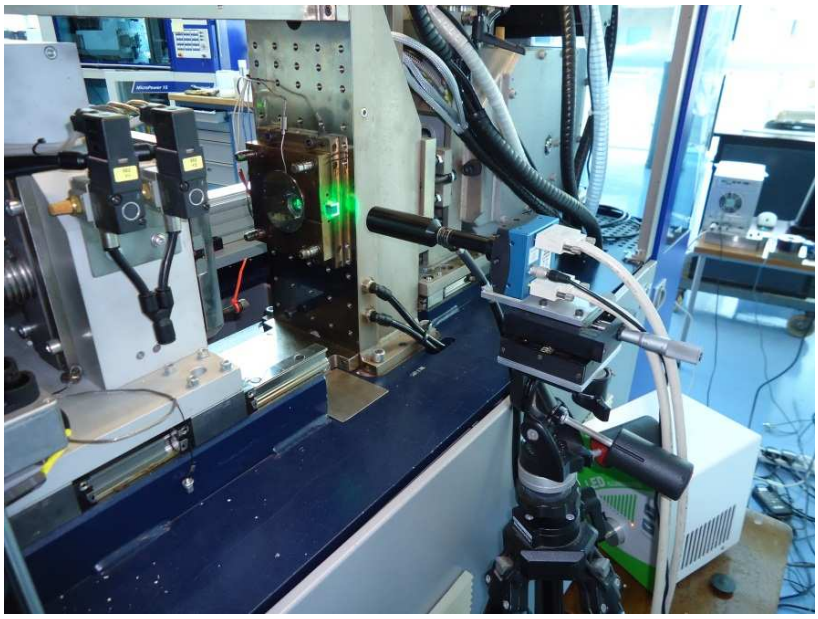

Figure 9.5 - Flow visualization apparatus.

The flow front appears as two distinct lines, one where the material comes into contact with the sapphire window at the wall and a second where the apex of the flow front lies, in the centre of the cavity (Figure 9.6).

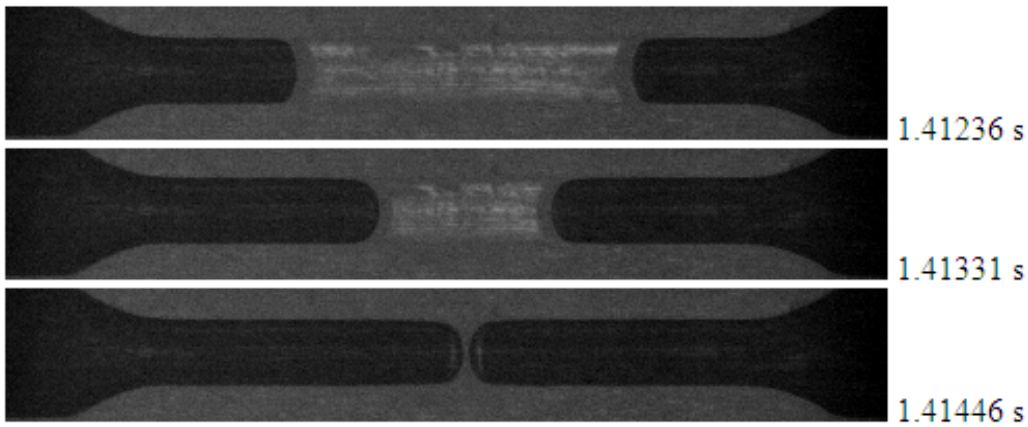

Figure 9.6 - Images showing cavity filling phenomena.

The distance between these two points can be used to provide information about the parabolic shape of the flow front. The second measurement which has been recorded for each experiment is the velocity at which the flow fronts collide during the process, and it is referred to as the

impingement velocity. In order to accurately calculate these terms, a code was written using National Instruments Labview 2009 software which contains four distinct operations.

1) *Image selection*. The images are read from the file and those which show the cavity filling are selected for processing.
2) *Flow front detection*. The flow front position calculation performs an edge detection for all four flow front line for each image in the sequence. A 3rd order polynomial curve fitting is then performed.
3) *Velocity calculation*. The feature of the software calculates the first order derivatives of the polynomial curve fitting to provide velocity data for each flow front. The velocities of each of the flow front apex points are calculated just prior to the point where they collide and are combined to provide an impingement velocity.

9.2 Micro injection moulding

The experiments were carried out on a Battenfeld Microsystem 50 machine. This machine offers a maximal clamping force of 50 KN. The screw diameter is 14 mm. Polycarbonate (PC Makrolon LED2045) was employed as polymer material. Polycarbonate is relevant in micro injection moulding for its transparency and strength at high temperature. The melt flow rate of PC is 16.5g/10min. The glass transition temperature of PC is 145 °C. PC with 1% of CNT-nanocyl was used in order to evaluate improvements on the weld line shape and strength for a reinforced material. The materials used in this experiments are produced by Bayern Materials Science AG.

To investigate the influence of process parameters on the weld lines formation in a micro cavity equipped with RHCM, a campaign of statistically designed experiments was carried out. Three different process parameters were varied:

- Mould temperature (T mould);
- Melt temperature (T melt);
- Injection speed (Inj vel);

A full factorial design was carried out performing 2^3=8 moulding experiments (each parameter being varied between two levels) with 5 replications. In this way the main effects as well as interactions were evaluated. Factors levels were established with the aim of keeping a realistic industrial perspective (Table 9.1). For melt temperature, the two levels were chosen according to the maximum and minimum temperatures recommended by the material supplier. The maximum

level of the mould temperature was set taking into account an acceptable time cycle. On the other hand, the minimum level was set at the glass transition temperature in order to guarantee a better heating of the cavity surface compared to the conventional injection moulding process. The minimum level of injection speed was set to assure the complete filling of the cavity. Mould temperature was controlled using temperature sensors placed in the mould and set according to specifications given by the material supplier. Melt temperature was implemented as barrel temperature and levels were based on recommended values published by the material supplier. To perform the statistical analysis of the measured results, a definition of different outputs describing the weld lines is needed. The analysis was performed considering the following outputs related to the surface finish and mechanical properties:

- surface roughness,
- ultimate tensile strength (UTS),
- elongation at break (EAB).

Statistical analysis results are shown using the Pareto plot of the main effects. The significance level was chosen to be 0.05.

Table 9.1 - Process parameters setting.

Process parameters	Low	High
Mould temperature	145 °C	155 °C
Melt temperature	270 °C	290 °C
Injection speed	120 mm/s	200 mm/s

In order to evaluate the influence of the cooling time on the aesthetic quality of the part, other experimental tests were carried out, varying the ejection temperature on 4 levels: 125 °C, 120 °C, 115 °C and 110 °C. The maximum level was set to avoid the part's deformation or warpage due to ejection forces. On the other hand, the minimum level was set taking into account an acceptable time cycle. The other process parameters were kept constant. The roughness was measured for both front and lateral weld lines (Figure 9.7).

Figure 9.7 - Components chosen for the weld line study.

9.3 Surface analysis

An atomic force microscope (AFM) was applied to analyze the surface finishing and the weld line V notch profile (Figure 9.8). Weld lines at topographical level are free form in the micro/sub-micro dimensional level. Therefore a high resolution and high accuracy instrument with real three dimensional capabilities such as the atomic surface microscope is suitable to be used. Purposes of such measurement are scanning and measuring the depth of a micro weld line. The highly finished surface allowed for a clear location of the weld line (Figure 9.9). The images were processed to produce surface profiles along selected lines and to provide a number of statistical surface roughness measures.

Figure 9.8 - Atomic force microscope.

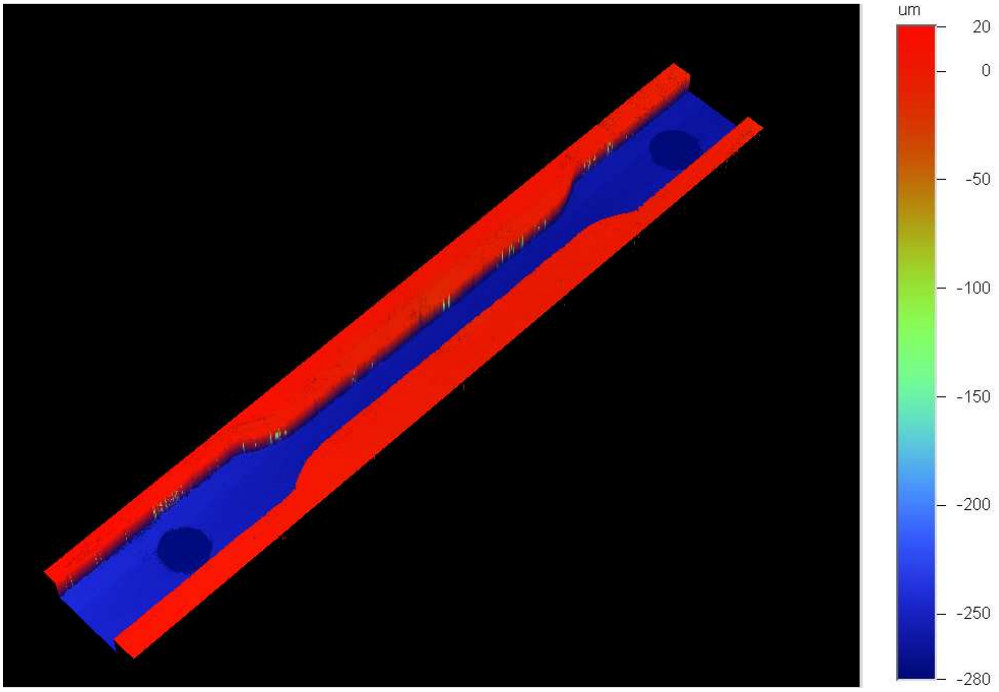

Figure 9.9 - Scanning of a cavity surface with white light interferometer.

9.4 Mechanical characterization

Weld line strength of micro tensile samples was tested on the micro tensile test machine (Bose Electroforce 3200) with small scale titanium tensile jaws, shown in Figure 9.10. A range of preliminary experiments were performed using samples manufactured during the stabilization stage between experiment. The experiments allowed the testing technique to be refined to minimize the occurrence of testing errors, such as specimens slipping in the jaws. Testing was performed at a rate of 0.01 mm/s and 0.006 mm/s. The data were processed to generate engineering stress/strain curve. In order to minimize the experimental error, five specimens were used to determine tensile strength, and mean values and standard deviations were calculated. Each performed tensile test was also recorded using the high speed camera apparatus described in Section 9.1.3.

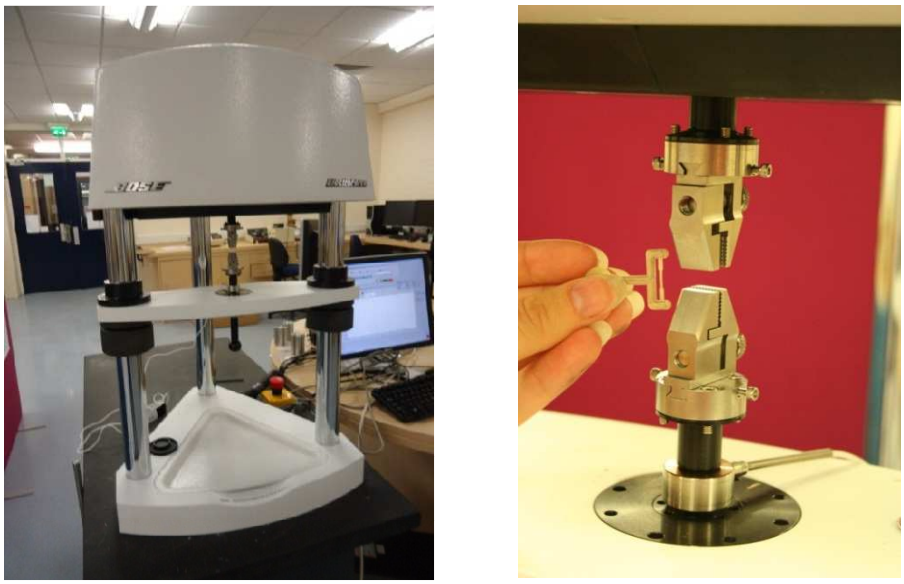

Figure 9.10 - Bose Electroforce 3200 test instrument (left), with tensile jaws and a moulded specimen (right).

9.5 Results

9.5.1 Surface characterization

Gloss on a surface is produced when a substantial part of the reflection is specular. That is when the angles of incidence and reflection are equal, as measured relatively to a plane fitted through the surface. The surface needs to be substantially flat over areas a few times larger than the wave length of visible light (390 – 750 nm). The *Ra* and *Rq* values, measured using the AFM, were consistent with this. Figure 9.11 shows the AFM scanning of a weld line's surface . Surface roughness was determined for each moulding, averaging results from 5 scan areas of 30x30 μm each.

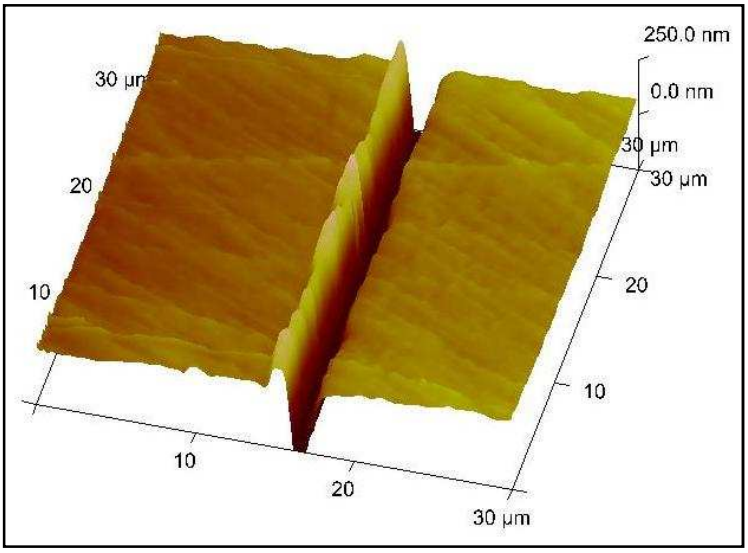

Figure 9.11 - Scanning of a weld line's surface with AFM.

Statistical analysis results are shown using the Pareto plot of the main effects for the three mentioned outputs. As reported in Figure 9.12 and Figure 9.13, the main factor affecting *Ra* and *Rv* is the mould temperature. The same conclusions can be drawn by considering the main effects plot (Figure 9.14 and Figure 9.15). The process parameters and the interactions between factors are not statistically significant on *Rq*.

Elimination of the frozen skin formation during injection has several important potential benefits, as the improvement of surface finish. Experimental results show how it is necessary to increase the temperature to 10 °C higher than T_g to obtain a glossy surface without weld lines. Furthermore, it is important to observe that the interaction between the mould temperature and injection speed affects the *Rv*. A higher fill rate results in a more rapid heat transfer, increasing mould temperature and preventing the formation of surface solid layer. An increase of injection speed leads to a decrease of the melt viscosity and, consequently, of the *Rv*. Higher injection speed determines also a reduction of injection time, avoiding premature melt freezing (i.e. incomplete filling).

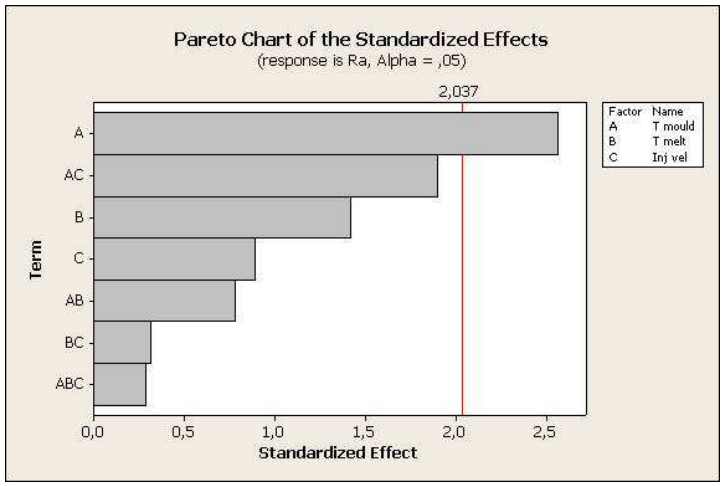

Figure 9.12 - Pareto chart of the standardized effects for Ra.

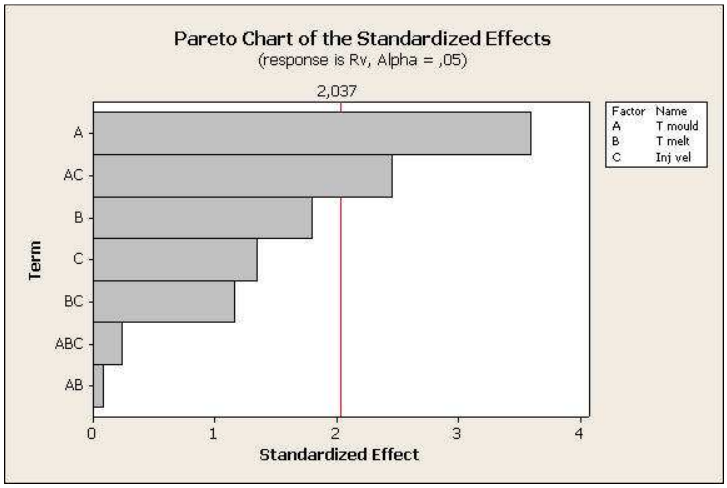

Figure 9.13 - Pareto chart of the standardized effects for Rv.

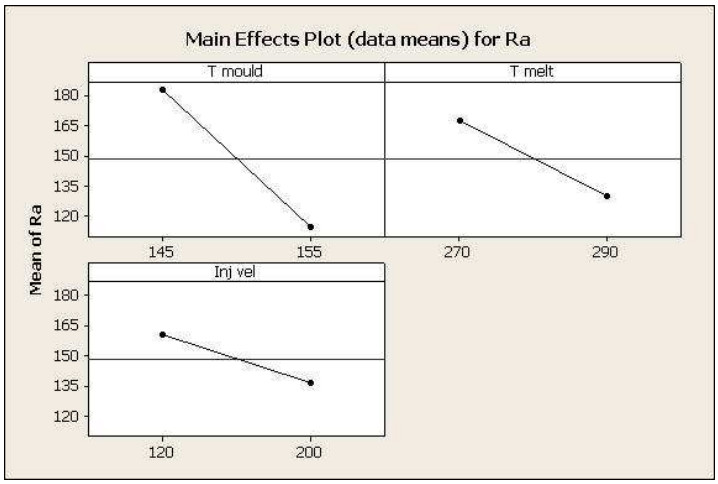

Figure 9.14 - Main effect plot for Ra.

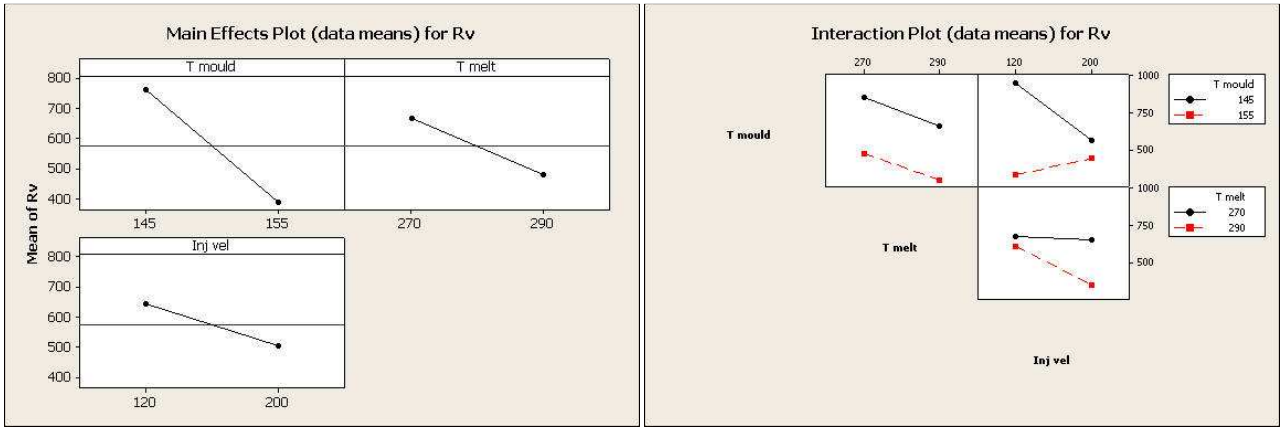

Figure 9.15 - Main effect and interaction plots for Rv.

9.5.2 Tensile properties

The specimens were tested using the apparatus discussed in the Section 9.4. The high speed camera system was used to provide high speed, high resolution images of sample failure. Process conditions and response parameters of elongation at break and ultimate tensile strength were statistically analyzed in order to evaluate the factors with the most significant effect on weld line strength. As it is evident from the Pareto analysis reported in Figure 9.16 and 9.17, the main factors affecting UTS and EAB are the mould temperature, the injection speed and their interaction.

Figure 9.18 shows the main effects of the process parameters on UTS. A higher mould and melt temperature provide a higher strength, presumably due to the better knitting of the flow fronts at the weld line. Strength is shown to be inversely proportional to injection speed. This result would suggest that a higher impingement velocity is actually detrimental to weld line strength, perhaps due to the air entrainment at the weld line. The main effects plot for elongation is shown in Figure 9.19. The melt temperature does not contribute significantly to weld line strength. Mould temperature is shown to be proportional to elongation which is due to improved knitting of the weld line geometry. Strain is inversely proportional to injection speed. This result reinforce the idea that high impingement velocities are not ideal for optimal weld line formation.

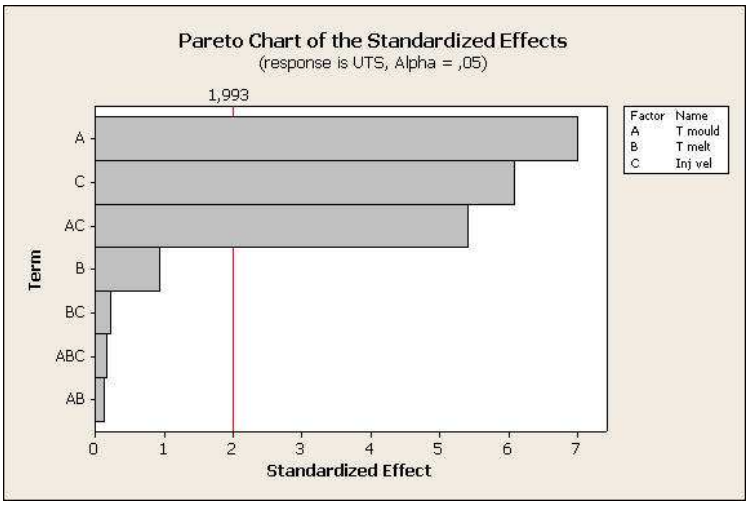

Figure 9.16 - Pareto chart of the standardized effects for ultimate tensile strength.

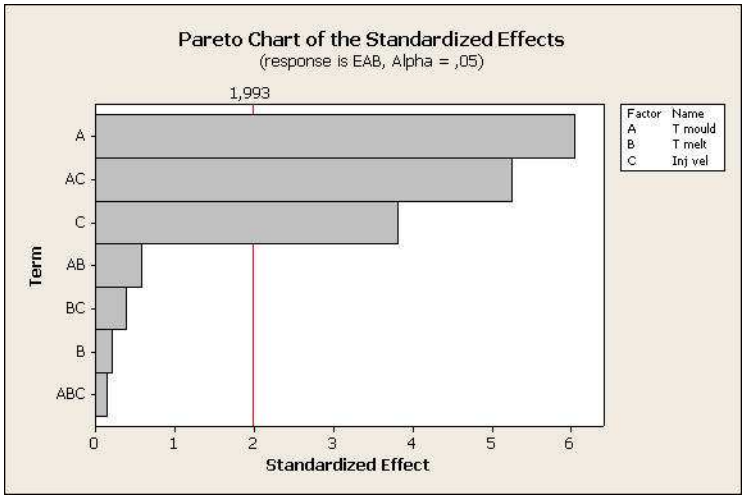

Figure 9.17 - Pareto chart of the standardized effects for elongation at break.

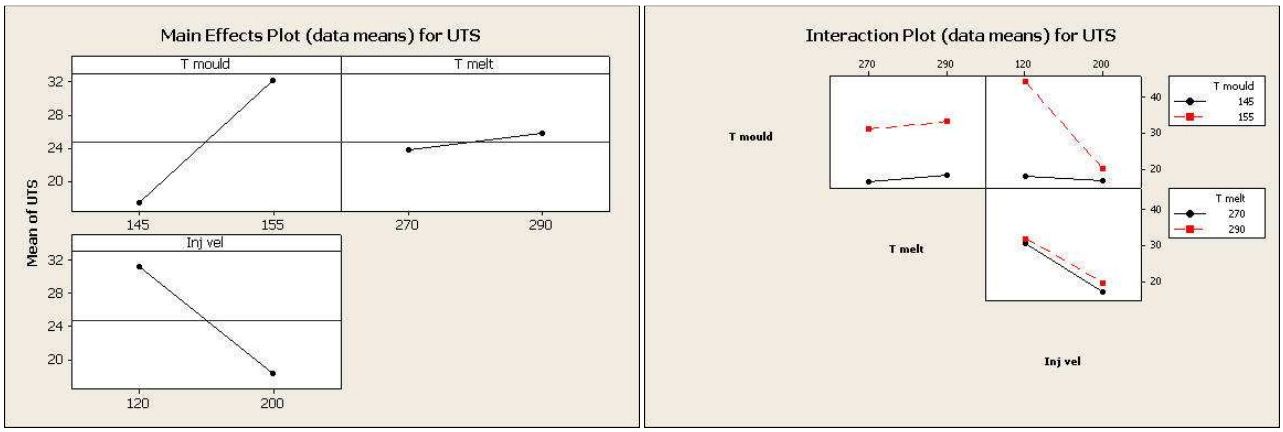

Figure 9.18 - Main effect and interaction plots for ultimate tensile strength.

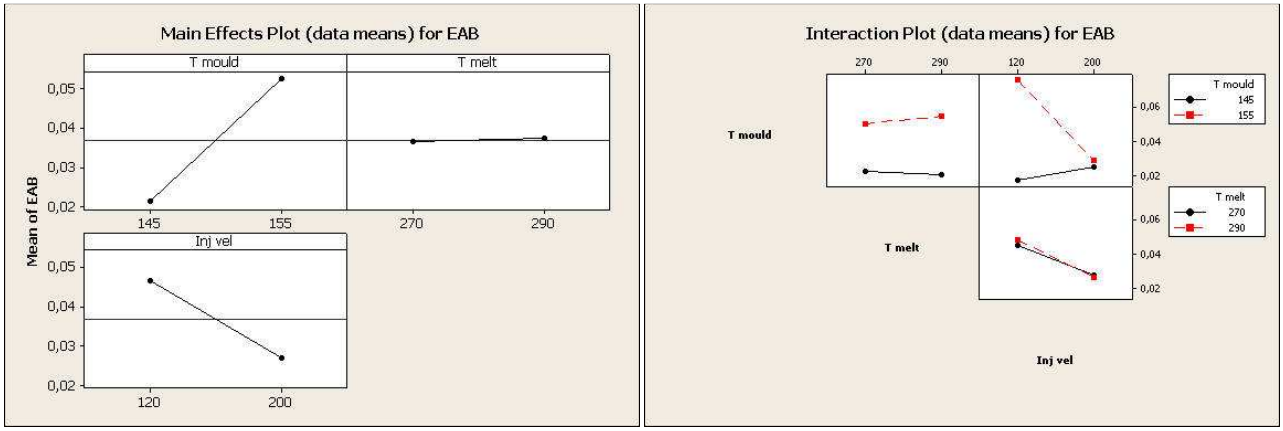

Figure 9.19 - Main effect plot for elongation at break..

Tensile tests exhibited two distinct modes of failure at different values of the injection velocity, one which appeared to be a brittle failure, and a second which showed a more ductile response. Examples of each behaviour can be seen in Figure 9.20.

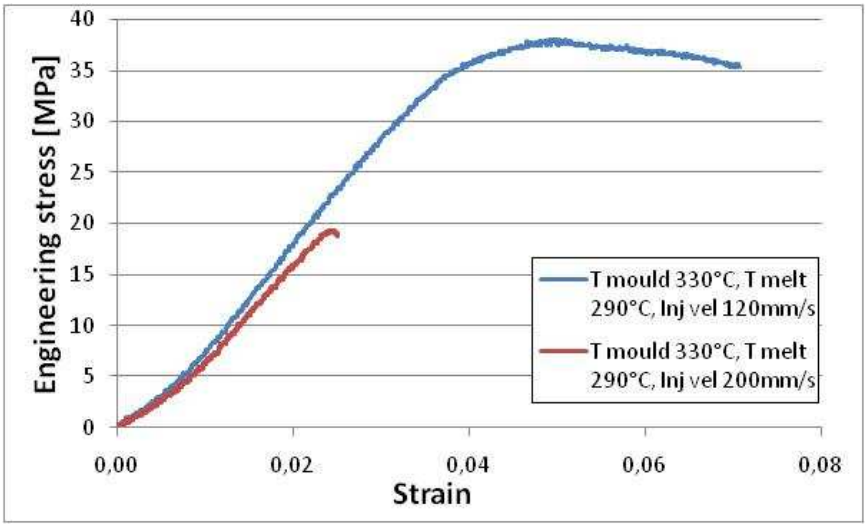

Figure 9.20 - Examples of brittle and ductile weld line failure modes.

Experimental tensile tests were simultaneously captured using the high speed camera apparatus described in section and a polarized lens. This allowed direct observation of the differences between the two failure modes. Images of each failure are shown in Figure 9.21 and Figure 9.22.

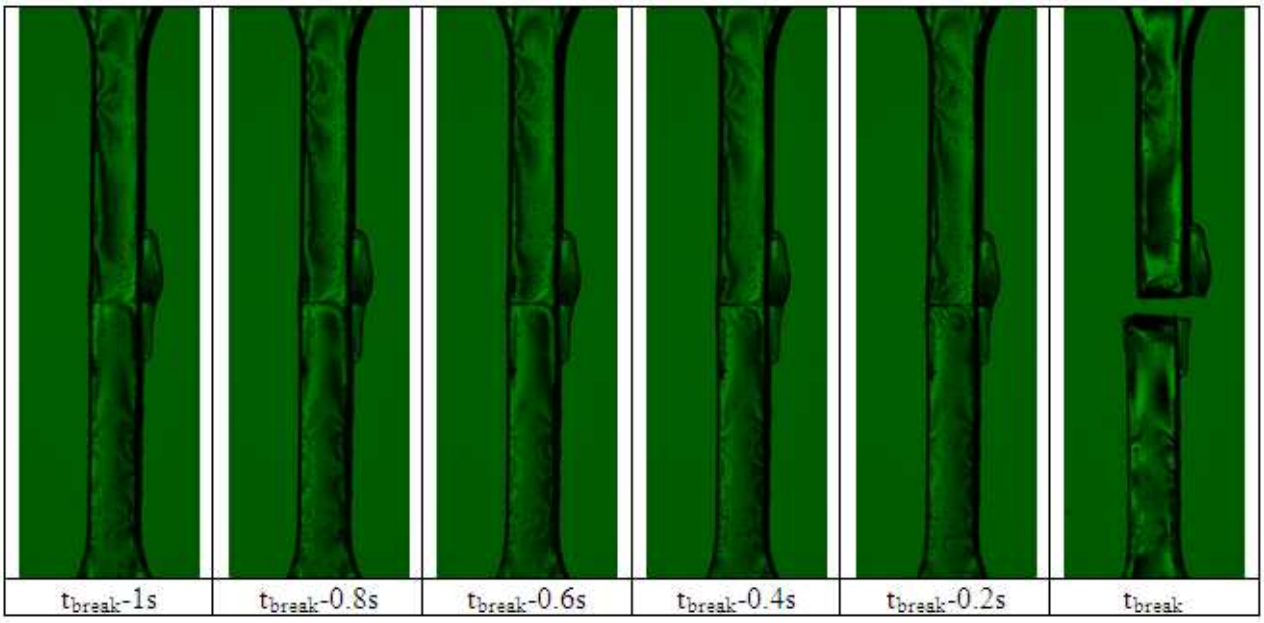

Figure 9.21 - High speed camera images of product failure – brittle failure.

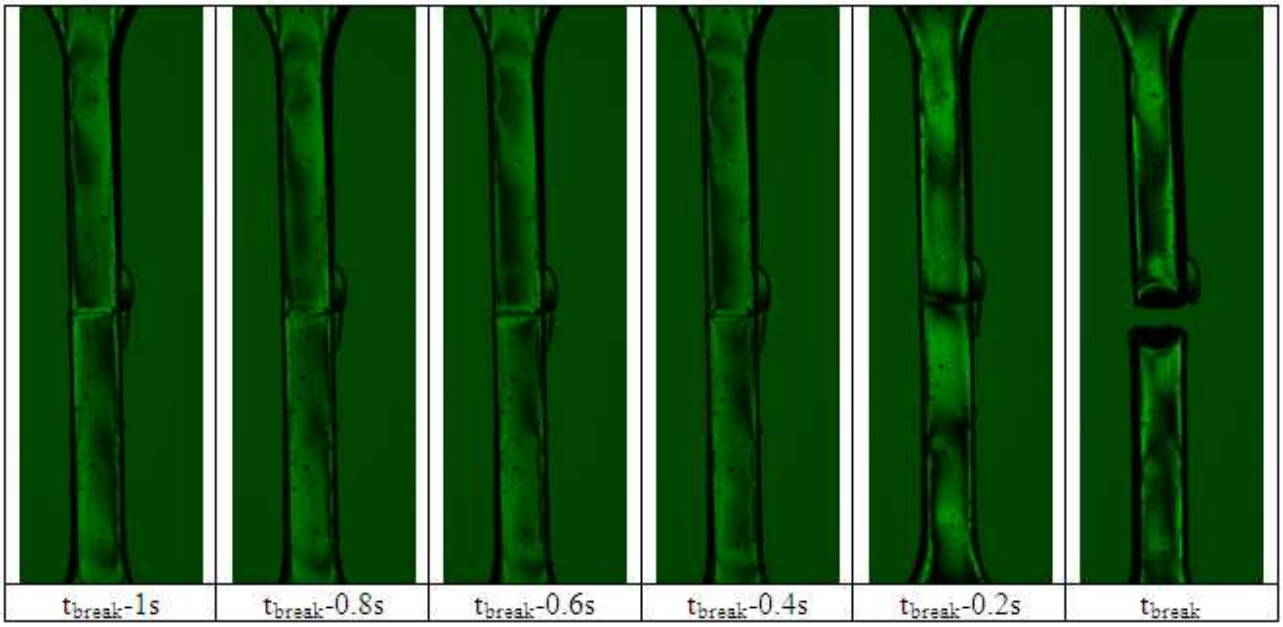

Figure 9.22 - High speed camera images of product failure – ductile failure.

For the brittle failure mode the sample simply pulls apart at the weld line which indicates a very poor knitting of material in this region. For the ductile failure, the polymer is seen to deform quite extensively in the region around the weld line and in some cases crack propagation along the weld line is observed. In the case of mould temperature of 155 °C and injection speed of 120 mm/s, only

the ductile behaviour was observed. This failure would suggest a significantly improved knitting of the material at the flow front has been achieved.

9.5.3 Flow visualization

It is interesting to note that the flow front profile remained pretty much unperturbed between each experiment which shows that it is predominantly cavity geometry dependent, which is in accordance with previous studies. Flow front impingement velocity provided interesting information regarding cavity filling. The impingement velocity correlates with the data generated for the UTS values discussed in the previous section with a correlation factor of 0.52. This suggests the existence of a relationship between impingement velocity and UTS, as it may be expected. Figure 9.23 illustrates this with a plot of impingement velocity variation and UTS as x-y pairs. High impingement velocities are not ideal for optimal weld line formation. Injection speed, melt temperatures and their interactions with the mould temperature affect the impingement velocity (Figure 9.24 and Figure 9.25). This would suggests that also melt temperature affect the weld line strength despite of results of the Section 9.5.2.

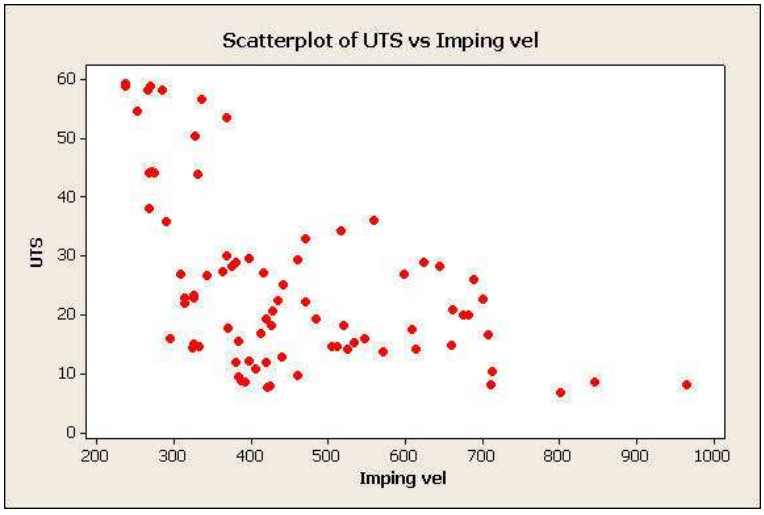

Figure 9.23 - Impingement velocity and UTS values plotted as x-y pairs.

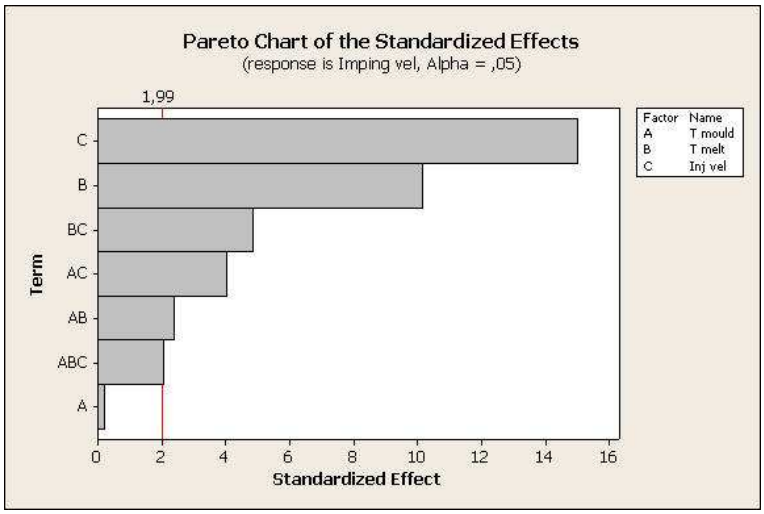

Figure 9.24 - Pareto chart of the standardized effects for impingement velocity.

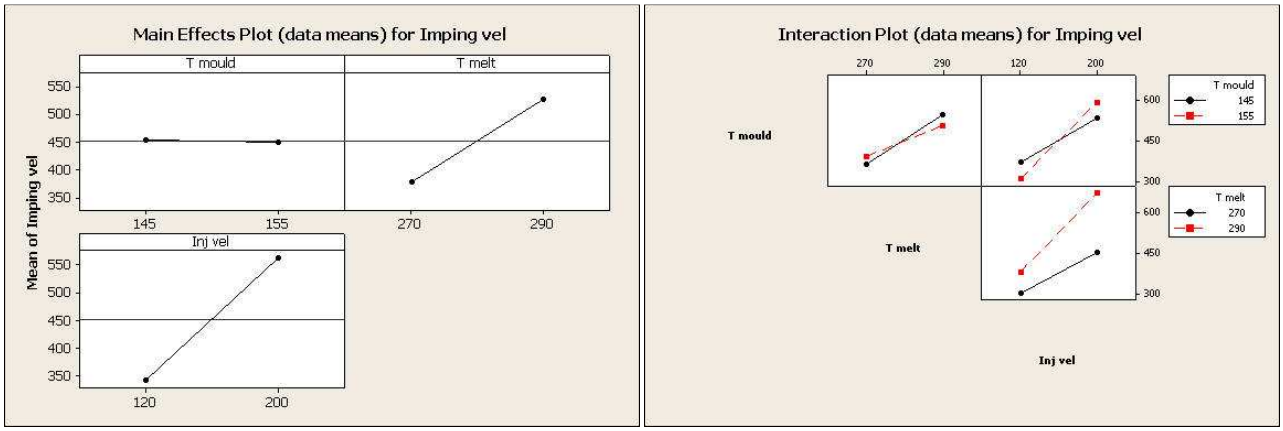

Figure 9.25 - Main effect and interaction plots for impingement velocity.

9.5.4 Cooling time influence

Figure 9.26 and Figure 9.27 summarizes the averaged results for the effect of the cooling time. It can be seen that the cooling time appears to contribute significantly to the surface quality. *Ra* and *Rv* are shown to be inversely proportional the cooling time on the weld line zone for both type of weld line. When the mould temperature at the ejection stage is set at 125 °C, the weld line in some cases is clearly detectable. A reduction of 10 °C in the mould temperature enables to reduce significantly the surface roughness and weld line depth. When the mould temperature is decreased of other 5 °C, *Ra* and *Rv* do not vary significantly. The movement of the surface that causes the reopening of the weld line is not affected from the geometry of the plastic part, but it seems to be related to the viscoelastic properties of the material. There is a significant extensional deformation

at the surface of the advancing flow front which lead to a high orientation of the macromolecules perpendicular to the wall. The results suggest that the polymer stress relaxation at high temperature actually leads to the reopening of the weld line.

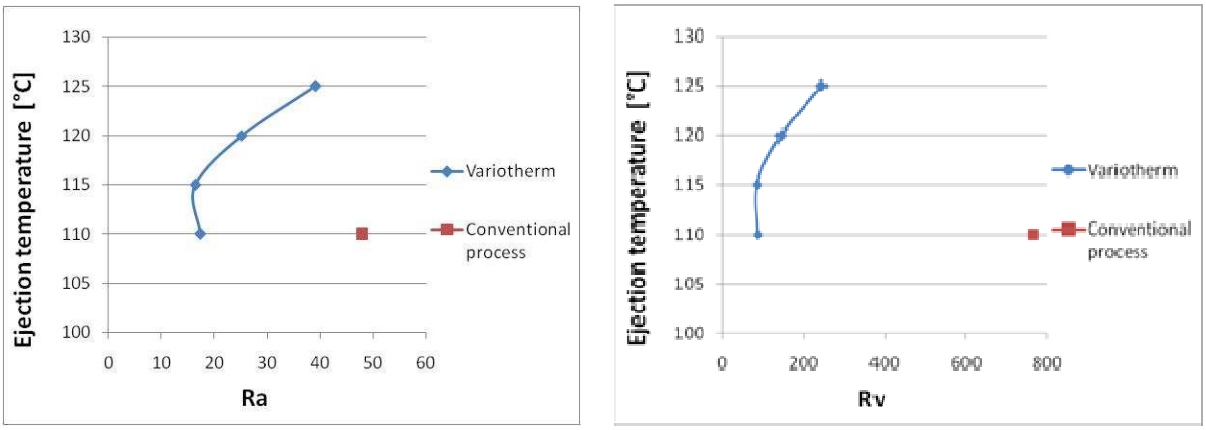

Figure 9.26 - Graphs showing Ra (left) and Rv (right) vs mould temperature at ejection for the flat plate with circular hole.

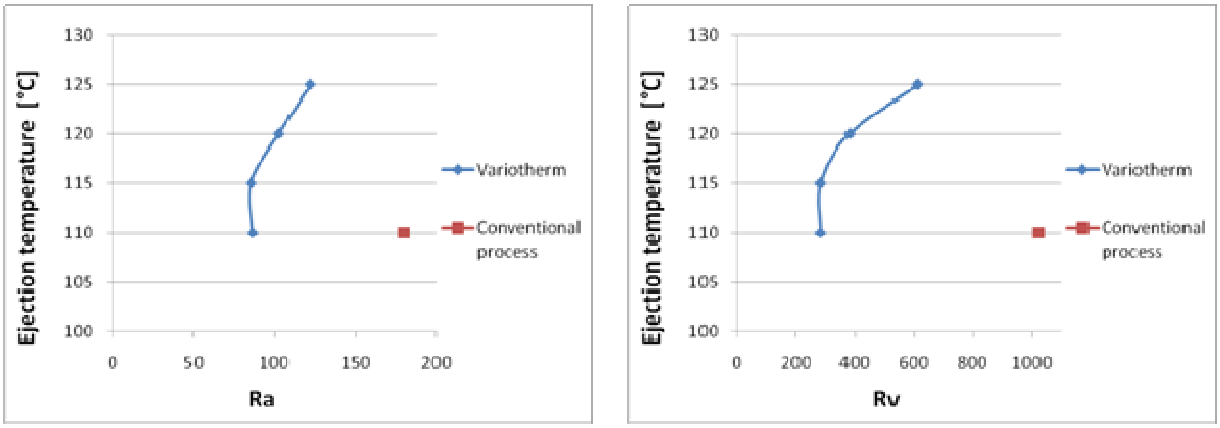

Figure 9.27 - Graphs showing Ra (left) and Rv (right) versus mould temperature at ejection for the tensile specimen.

9.5.5 Surface finish: conventional processing vs. RHCM

In order to perform a comparison between conventional process and RHCM, two main types of weld lines and two different materials were analyzed. PC and PC with 1% of CNT-nanocyl were used for this experiment. Variation is seen between scans and the standard deviation of the mean is tabulated. Table 9.2 summarizes the averaged results.

Table 9.2 - Comparison of surface roughness for conventionally moulded and RHCM parts. Standard deviations of the means are shown in brackets.

		TENSILE SPECIMEN			FLAT PLATE		
		Ra[nm]	**Rq[nm]**	**Rv[nm]**	**Ra[nm]**	**Rq[nm]**	**Rv[nm]**
PC	**Conventional**	134.9 (43)	204 (73)	958.6 (288.7)	40.8 (24.7)	94.5 (56.5)	628.2 (305.8))
	RHCM	78.5 (13.7)	100.5 (19.3)	313.6 (83.6)	16.4 (4.6)	20.7 (5.4)	84.2 (43.1)
	Reduction	*41.8%*	*50.8%*	*67.3%*	*59.9%*	*78.1%*	*86.6%*
PC with 1% CNT-nanocyl	**Conventional**	180 (52.7)	245.8 (64.9)	1020.6 (237.1)	48 (12.8)	104.2 (20.4)	736.6 (275.6)
	RHCM	95 (49.1)	126.7 (65.2)	547.2 (411.6)	20.5 (9)	25.1 (9.8)	88 (41.9)
	Reduction	*47.2%*	*48.5%*	*46.4%*	*57.3%*	*75.9%*	*88.5%*

Both materials show a significant reduction in surface roughness and weld line depth by approximately 50% for all parameters. Major surface improvements were also obtained for flat plate with circular pin by approximately 60% for *R*a, 75% for *Rq* and 85% for weld line depth. The weld line was clearly detectable in the conventional injection moulding process. The typical V-groove of the weld line was removed using RHCM (Figure 9.28 and Figure 9.29).

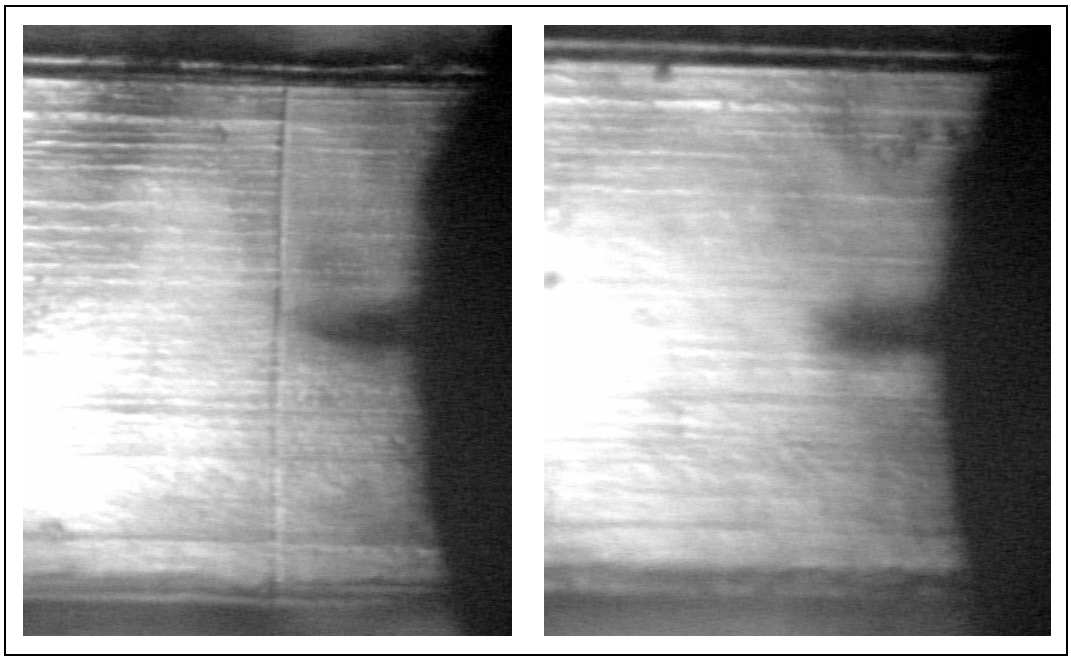

Figure 9.28 - Elimination of weld line for the tensile specimen using RHCM.

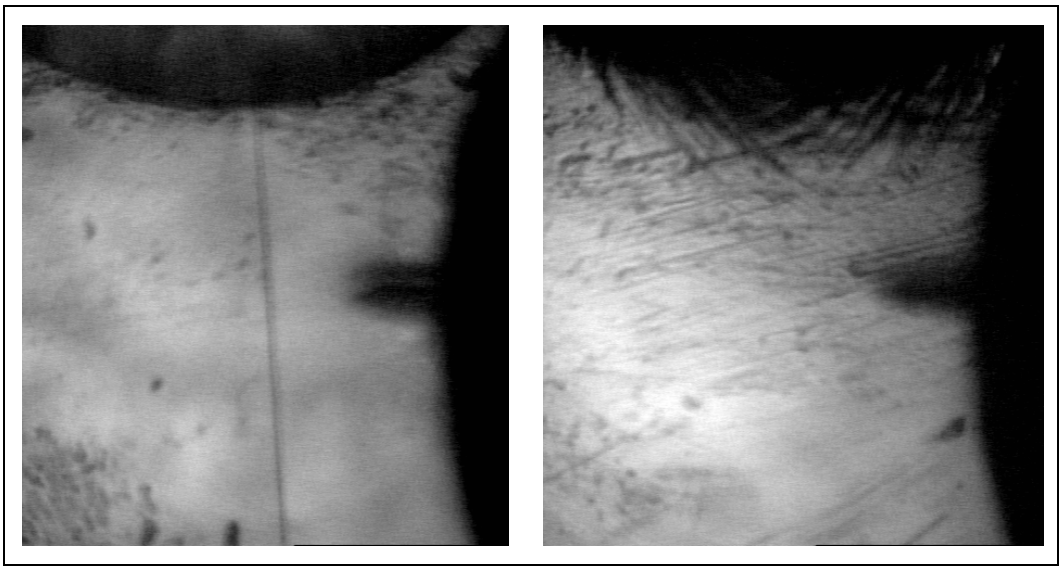

Figure 9.29 - Elimination of weld line for the flat plate with circular pin using RHCM.

Figure 9.31 compares the flow front shape for the conventional injection moulding process and RHCM. This comparison shows very little variation in flow front shape, despite the large difference in mould temperatures. Therefore, visualisation of flow front shape alone is not considered to be a sufficient mechanism to explain the mechanism of the weld line formation, however it can be a useful aid in understanding the filling sequence.

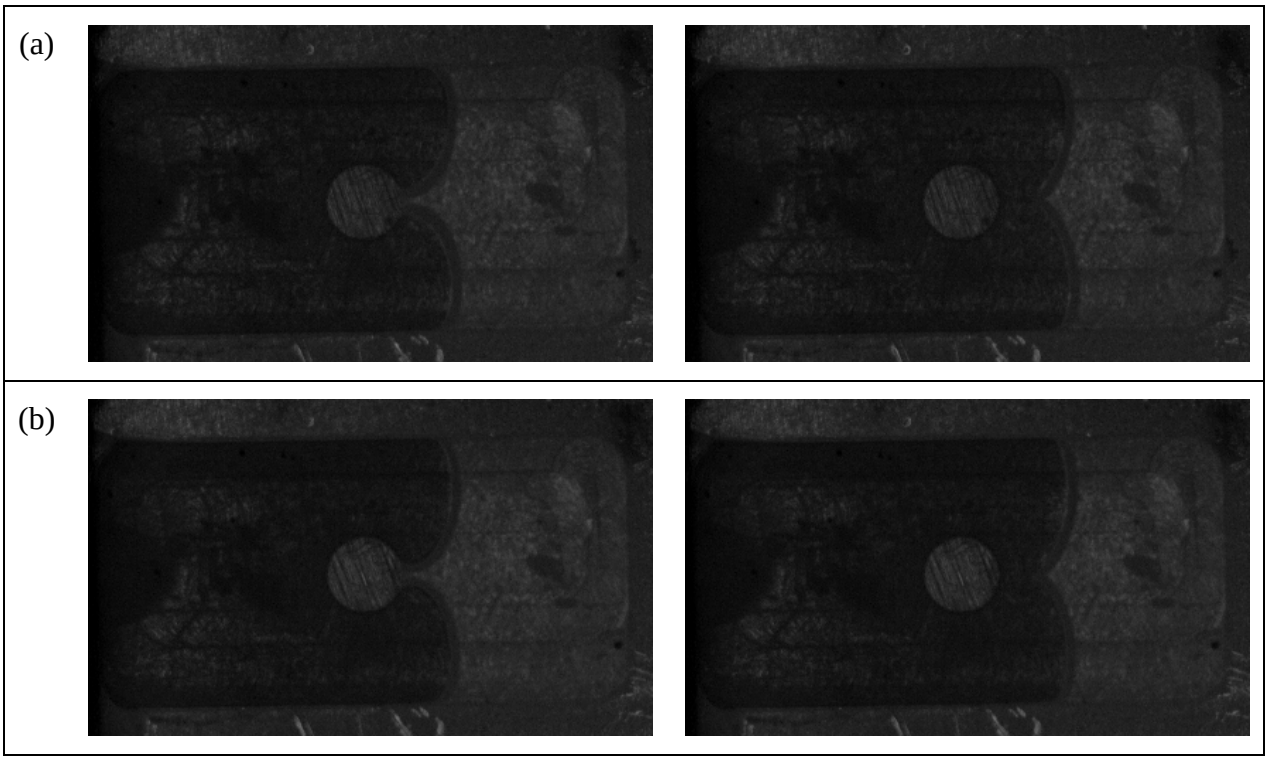

Figure 9.30 - Comparison of flow front shapes: a) Conventional process b) RHCM.

9.5.6 Mechanical properties: conventional processing vs. RHCM

Table 9.3 summarizes the averaged results of the experimental tensile tests. Both PC and PC with 1% CNT-nanocyl show a significant increase in the EAB by approximately 200% between the conventional process and RHCM with the mould at a temperature 10 °C higher than T_g. The variotherm system allows to improve the UTS by 80% for PC and by 50% for PC with nanofillers. The specimen moulded with the conventional process exhibited two modes of failure, both brittle and ductile. Instead only the ductile behaviour was observed for the specimen moulded by RHCM. The variotherm system can therefore be used to significantly improve the knitting of the material at the flow front.

Table 9.3 - Comparison of elongation at break (EAB) and ultimate tensile strength (UTS) for conventionally moulded and RHCM parts. Standard deviations of the means are shown in parentheses.

		0,006 mm/s		0,01 mm/s	
		EAB	**UTS [MPa]**	**EAB**	**UTS [MPa]**
PC	**Conventional**	0.02 (0.01)	23.446 (8.236)	0.03 (0.026)	27.351 (16.062)
	RHCM	0.055 (0.029)	43.281 (17.938)	0.1017 (0.038)	47.504 (12.947)
	Improvement	*183.45%*	*84.6%*	*219.05%*	*73.5%*
PC with 1% CNT-nanocyl	**Conventional**	0.03 (0.025)	36.671 (14.265)	0.035 (0.022)	40.503 (14.265)
	RHCM	0,095 (0.007)	57.784 (1.982)	0,096 (0.038)	54.105 (6.292)
	Improvement	*214.9%*	*57.57%*	*175.04%*	*33.58%*

CHAPTER 10
CONCLUSIONS

In recent years, the requirement for high gloss parts with better mechanical properties is more and more important for the company. There are many difficulties in producing this type of products by conventional injection moulding. Problems such as warpage, flow mark and weld line often appear in plastic parts produced by conventional injection method. As result, the mechanical properties and appearance of the plastic parts cannot meet the requirements of customers. The subsequent reprocessing operations such as spraying and coating have to be employed after injection moulding process in order to improve the part's properties. These operations increase the manufacturing processes of parts and waste raw material and energy.

Consequently, a new injection moulding technology, rapid heat cycle moulding (RHCM), is proposed. Contrasted with traditional injection moulding, in RHCM the mould temperature is increased to a target value, usually higher than the glass transition temperature. Then, after the filling stage is finished, the mould will be cooled with cold water. With the help of the heating process, RHCM technology can significantly eliminate the frozen layer and increase the flow ability of the resin melt to produce perfectly smooth, uniformly finished, thin-walled, complex shaped, and nano structured plastic products with low molecular orientation and residual stress. Besides that, the surface defect such as weld line, flow mark, and floating fibres can be eliminated.

To thermally cycle the mould temperature without a great increase in cycle time and energy consumption, an efficient vario-thermal mould temperature control system, is required. In recent years, a number of innovative approaches for rapidly heating the surface of the mould have been developed, including methods such as resistive heating, induction heating, high-frequency proximity heating, infrared heating, heating and cooling using a volume-controlled variable conductance heat pipe, heating and cooling using thermoelectric Peltier modules, passive heating by the incoming polymer, microwave heating, contact heating, convective heating using hot fluid or condensing vapour forced to flow through conformal channels or bearing ball filled niches, etc. Moreover the mould should have a low thermal mass and exhibit a low inertia to variation of thermal loads. Multilayer mould consisting of insulation layers with a resistance layer can efficiently shorten the moulding cycle time. The aforementioned methods do heat the mould efficiently, but still have a lot of shortcomings to be applied in mass production.

Due to the higher precision and quality requirements of the new plastic parts produced with RHCM process than the ones produced with CIM, the development theory of the moulding problems, like reduced strength weld line, non uniform shrinkage, incomplete filling of micro

structured surfaces etc., are needed to be understood completely. In spite of its industrial relevance, the scientific knowledge of several aspects of this novel process is still very poor.

In this work an innovative RHCM system has been developed to overcome the limitations of the available technologies and it has been used to analyze several aspects of this new manufacturing process.

(i) An innovative RHCM system, based on inserts made of open-cell aluminum foam, has been developed. Both the structural and the thermal behaviour of the system have been modelled to verify that the metallic-foam inserts largely increase the heat exchange rate with respect to the traditional cooling channels while providing the necessary structural support.

(ii) To evaluate the feasibility of the new heating and cooling system, a mould insert with two aluminum foams for a double gated tensile specimen was manufactured and a test production was carried out. A good agreement was obtained between the numerical and experimental results. The test production results indicate that the proposed innovative heating and cooling system can realize high-temperature injection moulding reducing the moulding cycle time with respect to traditional RHCM technique. The use of metallic foam allows a temperature control medium very close to the surface, extremely fast temperature drop and uniform temperature distribution.

(iii) The innovative technology for rapid heating and cooling of injection moulds has been used to analyze the effect of fast variations of the mould temperature on the improvement of micro features replication and mouldings appearance. The new RHCM technology allows to significantly improve the degree of surface micro structure replication, especially for those features characterized by the smallest values of thickness and aspect ratio.

(iv) The effect of fast variation of the mould temperature on the weld line strength of three engineering thermoplastic materials has been investigated. Tensile tests were carried out both on specimens produced by conventional injection moulding and employing the RHCM. A significant improvement in the mechanical properties was obtained for unfilled and reinforced materials using RHCM. By comparing the test results of experiment, it can be concluded that a smaller V notch area relates to a higher ultimate tensile stress of the weld line. system.

(v) A new mould for the production of high gloss cover plates was manufactured. Two different heating/cooling systems, the ball filling and the system based on the use of metal foams, were tested. The obtained results showed how the RHCM system developed in this work allows to reduce the cycle time of about 4 s. The new mould was used to study the effect of RHCM on the surface gloss of plastic parts. ABS shows a significant reduction in the surface gloss between the convectional process and temperature cycle injection moulding with mould temperature higher than T_g was measured. The gloss increases with increasing mould temperature. When the ejection temperature was varied from 60°C to 70°C, a slight improvement of the specular reflectance was observed.

(vi) An RHCM tool with a visualization unit was used to observe the development of a micro scale weld line. The factor having the most important effect on surface roughness and weld line depth is the mould temperature. Mechanical properties in the region of the weld line are influenced by mould temperature and injection speed. High mould temperature and low injection speed contributes to improve weld line strength and ductility. Cooling time affects the roughness and weld line depth of plastic parts. The measurement of the temperature evolution on the surface of plastic parts will be the subject of further works. *Ra* and *Rv* are shown to be inversely proportional the cooling time for both type of weld line. Significant improvements in the elongation at break, ultimate tensile strength and surface finish was obtained for PC and PC filled with nanocyl using RHCM. The obtained results showed how the RHCM can be used to entirely remove the V-groove of weld lines in micro injection moulding. A plastic part with high surface finishing and weld line strength can be obtained with high mould temperatures and low impingement velocity using RHCM.

The work presented in this thesis was carried out mainly at the Te.Si. Laboratory, University of Padua, Italy, from January 2009 to December 2011, under the supervision of prof. Paolo Bariani and of Ing. Giovanni Lucchetta. Part of the research activity was performed at the Centre for Polymer Micro and Nano Technology, University of Bradford, Bradford, UK

REFERENCES

[1] Bolstad L. L., US Patent 2 979 773, 1961.

[2] Yao D., Chen S. C., Kim B. H., *Rapid Thermal Cycling of Injection Molds: An Overiview on Techinical Approaches and Applications*, 2008, 4, 233-255.

[3] Kim B. H., Suh N. P., *Low Thermal Inertial Molding (LTIM.),* Polymer- Plastics Technology and Engineering, 1986, 25, 73–93.

[4] Liou M. J., Suh N. P., *Reducing residual stresses in molded parts,* Polymer Engineering & Science, 1989, 29, 441–447.

[5] Chen S. C., Jong W. R., Chang J. A., *Dynamic Mold Surface Temperature Control Using Induction and Heater Heating Combined with Coolant Cooling,* International Polymer Processing 2006, 21, 457–463.

[6] Jansen K. M. B., Flaman A. A. M., *Construction of fast-response heating elements for injection molding applications,* Polymer Engineering & Science 1994, 34, 894–897.

[7] Tadmor Z., *Machine invention, innovation, and elementary steps*, Advances in Polymer Technology, 2002, 21, 87–97.

[8] Yao D., Kim B., *Development of rapid heating cooling systems for injection molding application*, Polymer Engineering & Science, 2002, 42, 2471–2481.

[9] Yao D., Kimberling T. E., Kim B., *High frequency proximity heating for injection molding application*, Polymer Engineering &Science 2006, 46, 938–945.

[10] Xu X. R., *Conformal Cooling and Rapid Thermal Cycling in Injection Molding with 3D Printed Tools*, Ph.D. Thesis; Massachusetts Institute of Technology: Cambridge, 2002.

[11] Xu X., Sachs E., Allen S., Cima M., SPE Technical Papers, 1999, 509–514.

[12] Au K. M., Yu K. M., *A scaffolding architecture for conformal cooling design in rapid plastic injection moulding*, The International Journal Advanced Manufacturing Technology, 2007, 34, 496–515.

[13] Xu X. R., Sachs E., Allen S., *The design of conformal cooling channels in injection molding tooling*, Polymer Engineering & Science, 2001, 41, 1265– 1279.

[14] Dimla D. E., Camilotto M., Miani F., *Design and optimization of conformal cooling channels in injection moulfing tools*, Journal of Material Processing Technology, 2005, 164, 1294–1300.

[15] Kimberling T. E., Liu W., Kim B. H., Yao D., *Rapid hot embossing of polymer microfeatures*, Microsystem Technologies, 2006, 12, 730–735.

[16] Chen S. C., Chang Y., Chang T. H., Chien R. D., *Influence of using pulsed cooling for mold temperature control on microgroove duplication accuracy and warpage of the Blu-ray Disc*, International Communications in Heat and Mass Transfer, 2008, 35, 130–138.

[17] Yang W., J. US Patent 4 390 485, 1983.

[18] Bleier H., Gornik C., Patent Registration DE-10 136 678, 2003.

[19] Abbott R. C., Magnant G. P., Glenn W. A., US Patent 7 176 420, 2007.

[20] Kim B. M., US Patent 5 176 839, 1993.

[21] Kim B. M., US Patent 5 176 839, 1993.

[22] Baumgartner C. E., Hamly, K. D. US Patent 5 489 410, 1996.

[23] Baumgartner C. E., Gutmann J. M., Hamly K. D., Niemeyer M. F., US Patent 5 535 980, 1996.

[24] Niemeyer M. F., Baumgartner C. E., Hovatter T.W., US Patent 5 897 814, 1999.

[25] Kataoka H., Yamaki H., Umei Y., Katou I., *Blow molding of synthetic resin using heat insulating layer-coated mold: Effect of heat insulating layer characteristics on improvement of transferability of the molded article*, Kobunshi Ronbunshu ,1998, 55, 671–676.

[26] Kim Y., Seong K., Kang S., *Effect of insulation layer on transcribability and birefringence distribution in optical disk substrate*, Optical Engineering, 2002, 41, 2276–2281.

[27] Lee J. S., Park K.W., Lee S.W., Kim J. H., Kim S., *Tech. Dig. Optical Data Storage*, SPIE, 2003, 228–230.

[28] Inoue K., Hayashi K., Kawasaki Y., Ohno E., *Study on 40 Gbits/inch² density molding using heat insulted mold*, Jpn Journal of Applied Physics, 2003, 42, 774–775.

[29] Kim Y., Bae J., Kim H., Kang S., *Modelling of passive heating for replication of sub-micron patterns in optical disk substrate*, Journal of Physics D: Applied Physics, 2004, 37, 1319–1326.

[30] Hiroyuki Iwami, Hiroyuki Hamada, *An Advanced Cavity-Core System Mold for Ultra-Low Pressure Injection Molding (ULPAC MOLD)*, ANTEC 2003,468-472.

[31] Schintlmeister W., Wallgram W., Ganz J., Gigl K., *Cutting tool materials coated chemical vapour deposition*, Wear, 1984, 100, 153–169.

[32] Kopf A., Haubner R., Lux B., *Multilayer containing diamond and other materials on hardmetal substrates*, International Journal of Refractory Metals and Hard Materials, 2002, 20, 107–113.

[33] Yao D., Kim B. J., *Developing rapid heating and cooling systems using pyrolytic graphite*, Applied Thermal Engineering, 2003, 23, 341–352.

[34] Hatch D., Kazmer D., Fan B., *Dynamic cooling design for injection molding*, ANTEC, 2001.

[35] Wada A., Tazaki K., Tahara T., Suzuki H., Mizutani Y., US Patent 4 340 551, 1982.

[36] Weber L., Ehrfeld W., Kunststoffe Plast Eur, 1999, 89, 192– 202.

[37] Benzler T., Piotter V., Hanemann T., Mueller K., Norajitra P., *Innovation in molding technologies for microfabrication*, Proceedings of SPIE, 1999, 3874, 53–60.

[38] Schinkothe W., Walther T., *Reducing cycle times, alternative mould temperature control for microinjection moulding*, Kunststoffe Plast Eur, 2000, 90, 17–19.

[39] Michaeli W., Spennemann A., *Injection moulding microstructured functional surfaces, correct temperature control is half the battle*, Kunststoffe Plast Eur, 2000, 90, 16–17.

[40] Chang J. A., Cin J. C., Yeh C. F., *Dynamic Mold Surface Temperature Control for Assisting Injection Molding of Light-Guide Plate and Improving Optical Performance*, SPE Technical Papers, 2007, 1636– 1640.

[41] Johnson R. J., Pitchumani R., *Enchancement of flow in VARTM using localized induction heating*, Composites Science and Technology, 2003, 63, 2201–2215.

[42] Chen S. C., Jong W. R., Chang Y. J., Chang J. A., Cin, J. C., *Rapid mold temperature variation for assisting the micro injection of high aspect ratio micro-feature parts using induction heating technology*, Journal of micromechanics and microengineering, 2006, 16, 1783–1791.

[43] Kim S., Shiau C. S., Yao D., Kim B. H., *Injection Molding Nanoscale Features with the Aid of Induction Heating*, Polymer-Plastics Technology Engineering, 2007, 46, 1031–1037.

[44] Park K., Choi S., Lee S. J., Kim Y. S., *Injection molding for a ultra thin-wall part using induction heating*, Trans. J. Kor. Soc. Mech. Eng. (A), 2007, 31, 594-600.

[45] Byon S. K., US Patent 5 762 972, 1998.

[46] Huang J.T., Lin L.T., US Patent 20 070 075 463, 2007.

[47] Kim B. H., Yao D., US Patent 6 846 445, 2005.

[48] Brown G. H., *Theory and Application of Radio-Frequency Heating*, D. Van Norstrand Co: New York, 1947.

[49] Akopyan R. L., US Patent 6 984 352, 2006.

[50] Akopyan R. L., US Patent 7 122 146, 2006.

[51] Erwin L., Suh N. P., *A method for the rapid processing of thermoplastic articles*, Polymer Engineering & Science, 1976, 16, 841–846.

[52] Kim B. H., Wadhwa R. R., *A New Approach to Low Thermal Inertia Molding*, Polymer Plastic Technology Engineering, 1987, 26, 1–22.

[53] Whiteside B. R., Martyn M. T., Coates P. D., Allan P. S., Hornsby P. R., Greenway G., *Micromoulding: process characteristics and product properties*, Plastics, Rubber and Composites, 2003, 32, 231–239.

[54] Kim S., Trichur R., Beaucage G., Ahn C.H., Kim B. H., *New Plastic Microinjection Molding Technique for Extremely Tall Plastic Structures using Remote Infrared Radiation Heating Method*, In Proceedings of the 10th Solid-State Sensor, Actuator and Microsystems Workshop, Hilton Head Island, SC, 2002, 206–209.

[55] Kurosaki Y., Satoh I., *A Precision Polymer Injection Molding Process Assisted by Infrared Radiation to Upgrade both Optical Quality and Transcribability*, In Proceedings of the ASPE Spring Topical Meeting on Precision Fabrication and Replication, Chapel Hill, NC, 1999, 46–49.

[56] Kurosaki Y., Sato K., Saito T., *Heat Transfer Aspect to Upgrade the Quality of Plastics*, 15th ASPE, 2000, 156–159.

[57] Saito T., Satoh I., Kurosaki Y., *A new concept of active temperature control for an injection molding process using infrared radiation heating*, Polymer Engineering & Science, 2002, 42, 2418– 2429.

[58] Chang P.C., Hwang S.J., *Experimental Investigation of Infrared Rapid Surface Heating for Injection Molding*, Journal of Applied Polymer Science, 2006, 102, 3704– 3713.

[59] Chang P. C., Hwang S. J., *Simulation of infrared rapid surface heating for injection molding*, International Journal of Heat Mass Transfer ,2006, 49, 3846–3854.

[60] Chang P. C., Hwang S. J., *Geometry influence of reflectors for infrared rapid heating on micro-injection molding*, Material Science Forum, 2006, 505–507, 1261–1266.

[61] Yu M. C., Young W. B., Hsu P. M., *Micro-injection molding with the infrared assisted mold heating system*, Material Science and Engineering, 2007, 460-461, 288–295.

[62] Stumpf H., Schulte K., US Patent 5 824 237, 1998.

[63] Yao D., Yi A. Y., Li L., Nagarajan P., *A Strategy for Rapid Thermal Cycling of Molds in Thermoplastic Processing*, ASME Journal of Manufacturing Science and Engineering, 2006, 128, 837–843.

[64] Lee N., Han J., Lim J., Choi M., Han Y., Hong J., Kang S., *Injection molding of nanopillars for perpendicular patterned magnetic media with metallic nanostamp*, Jpn Journal of Applied Physics, 2008, 47, 1803–1805.

[65] Nussbaum F. J., US Patent 3 763 293, 1973.

[66] Kukla C., Loibl H., Detter H., Hannenheim W., *Micro-injection moulding: the aims of a project partnership*, Kunstoffe, 1998, 88, 1331–1336.

[67] Hanemann T., Heckele M., Piotter V., *Current status of micromolding technology*, Polymer News, 2000, 25, 224–229.

[68] Zhao G., Wang G., Guan Y., Huiping L., *Research and application of a new rapid heat cycle molding with electric heating and coolant cooling to improve the surface quality of large LCD TV panels*, Polymer for Advance Technology, 2009, 22, 476-487.

[69] Wang G., Zhao G., Huiping L., Guan Y., *Research of thermal response simulation and mold structure optimization for rapid heat cycle molding processes, respectively, with steam heating and electric heating*, Materials and Design, 2010, 31, 382–395.

[70] Wang G., Zhao G., Huiping L, Guan Y., *Analysis of thermal cycling efficiency and optimal design of heating/cooling systems for rapid heat cycle injection molding process*, Materials and Design, 2010, 31, 3426-3441.

[71] Ming-Chang Jeng , Shia-Chung Chen, Pham Minh Son, Jen-An Chang, Chia-shen Chung, *Rapid mold temperature control in injection molding by using steam heating*, International Communications in Heat and Mass Transfer, 2010, 37, 1295-1304.

[72] Wang G., Zhao G., Huiping L, Guan Y., *Research on optimization design of the heating/cooling channels for rapid heat cycle molding based on response surface methodology and constrained particle swarm optimization*, Expert Systems with Applications, 2011, 38, 6705–6719.

[73] Wang G., Zhao G., Huiping L, Guan Y., *Multi-objective optimization design of the heating/cooling channels of the steam-heating rapid thermal response mold using particle swarm optimization*, International Journal of Thermal Sciences, 2011, 50 790-802.

[74] Ming-Xing Maa; Xi-Ping Li; Guo-Qun Zhao; Yan-Jin Guan, *Optimal design of heating channels for rapid heating cycle injection mold based on response surface and genetic algorithm*, Materials and Design, 2009, 30, 4317–4323.

[75] Wlodarski P. G., Pittman J. F. T., Sienz J., Crow K., Foad R., *Temperature cycle injection moulding for production of weldline-free, high-gloss parts*, PPS Conference Proceedings 26th PPS, 2010.

[76] Rioux J., Yao D., Kim B., *Characterization of the Weldline Strength in Terms Of Crack Growth Resistance in Injection Molded Thermoplastic Elastomers*, Polymer-Plastics Technology and Engineering, 1998, 37, 369–383.

[77] Xie L., Ziegmann G., *A visual mold with variotherm system for weld line study in micro injection molding*, Microsystem Technology, 2008,14, 809–814.

[78] Xie L., Ziegmann G., *Influence of processing parameters on micro injection molded weld line mechanical properties of polypropylene (PP)*, Microsystem Technology, 2009,15, 1427–1435.

[79] Xie L., Ziegmann G., Jiang B., *Reinforcement of micro injection molded weld line strength with ultrasonic oscillation*, Microsystem Technology, 2009, 15,1427.

[80] Ashby M. F., Evans A., Fleck N. A., Gibson L. J., Hutchinson J. W., Wadley H. N. G., *Metal foams: a design guide*, Butterworth-Heinemann, 2000.

[81] Gibson, L.J. and Ashby, M.F.. *Cellular Solids: Structure and Properties*, 2nd ed. Cambridge University Press, Cambridge, 2007.

[82] Weaire D., Phelan R., *A counter-example to Kelvin's conjecture on minimal surfaces*. Philos. Mag. Lett. , 1994, 69, 107–110.

[83] Harte A.M, Fleck N. A., Ashby M.F., Fatigue failure of an open cell and a closed cell aluminum alloy foam, Acta Materialia, 1999, 47, 2511–2524.

[84] Kruger E., *Die Grundwasserbewegung*, Internationale Mitteilungen für Bodenkunde, 1918, 8, 105.

[85] K. Vafai, C.L. Tien, *Boundary and inertia effects on convective mass transfer in porous media*, International Journal of Heat and Mass Transfer, 1982, 8, 1183–1190.

[86] Amiri A., Vafai K., Kuzay T.M., *Effect of boundary conditions on non-Darcian heat transfer through porous media and experimental comparisons*, Numerical Heat Transfer Journal Part A, 1995, 27, 651–664.

[87] Richardson J.T., Peng Y., Remue D., *Properties of ceramic foam catalyst supports: pressure drop*, Applied catalysis A: General, 2000, 204, 19-32.

[88] Cox W., Merz E., *Correlation of dynamic and steady flow viscosities*, Journal of Polymer Science, 1958, 28, 619 – 622.

[89] Wang R.J., Shang D.G., *Low-cycle fatigue life prediction of spot welds based on hardness distribution and finite element analysis*, International Journal of Fatigue, 2009, 31, 508–514.

[90] E. Debondue, J.-E. Fournier, M.-F. Lacrampe, P. Krawczak, *Weld-Line Sensitivity of Injected Amorphous Polymers*, Journal of Applied Polymer Science, 2004, 93, 644–650.

[91] Fiorotto M., Lucchetta G., *Influence of process parameters on the weld lines formation in rapid heat cycle molding*, AIP Conf. Proc. 1353, 797-802.

[92] Fiorotto M., Lucchetta G., *Application of high porosity metal foams in a heating/colligns system for rapid heat cycle injection molding process*, PPS Conference Proceedings 27th PPS, 2011.

[93] Fiorotto M., Whiteside B., Lucchetta G., *A study on surface finishing and weld line strength in micro injection moulding using a variotherm and visual mould*, PPE 2011.

[94] Bariani P.F., Lucchetta, G., Fiorotto, M., 2011, *Sistema di riscaldamento e raffreddamento rapido di stampi per materiali polimerici*, Italian Patent Application PD2011A000117.

[95] Dawkins E., Engelmann P., Horton K., *Color and gloss - The connection to process conditions. Journal of Injection Molding Technology*, 1998, 1, 1–7.

[96] Edwards S. A., Choudhury N. R., *Variations in Surface Gloss on Rubber-Modified Thermoplastics: Relation to Morphological and Rheological Behavior*, Polymer Engineering & Science, 2004, 44, 96.

[97] Oliveira M. J., Brito A. M., Costa M. C., Costa M. F., *Gloss and Surface Topography of ABS: A Study on the Influence of the Injection Molding Parameters*, Polymer Engineering & Science, 2006, 46, 1394-1401.

[98] ISO - Plastics - Determination of tensile properties - Part 2: Test conditions for moulding and extrusion plastics, ISO 527-2 (1993).